UNIVERSITY OF PISA
Department of Physics

GRADUATE STUDIES IN APPLIED PHYSICS
21st Entrance (2006-2008)

SHEAR ALFVÉN MODES IN THE PRESENCE OF A MAGNETIC ISLAND

Ph.D. student: Alessandro Biancalani

Advisors: Prof. Francesco Pegoraro,
Prof. Liu Chen, Dr. Fulvio Zonca

Referees: Dr. Emanuele Poli, Prof. Sadruddin Benkadda

December, 2010

Contents

Acknowledgments

This work was supported by the Euratom Communities under the contract of Association between EURATOM/ENEA and in part by PRIN 2006. This work was also partially supported by DOE grants DE-FG02-04ER54736 and DE-FC02-04ER54796, by the NSF grant ATM-0335279, and by the "Consorzio di Ricerca per l'Energia e le Applicazioni Tecnologiche dell'Elettromagnetismo" (CREATE).

Discussions with Andreas Bierwage on the numerical methods are gratefully acknowledged. Useful conversations with Claudio Di Troia, Ilija Chavdarovski, Xin Wang, Andrea Cintio, Peter Porazik and Kevin Han Yan are also kindly acknowledged. Greatefully acknowledgments are expressed to the research teams of ENEA-Frascati and of University of California of Irvine, for the warm hospitality in the period when this work was done.

Special thanks to my advisors, Prof. Francesco Pegoraro, Prof. Liu Chen and Dr. Fulvio Zonca, for their teachings and their patience. Thanks also to the referees of this thesis, Dr. Emanuele Poli and Prof. Sadruddin Benkadda, for their important help in cross-checking the content and the form of this work.

To the star-crossed lovers.

Chapter 1

Introduction

1.1 Shear Alfvén waves in fusion plasmas

Fusion plasmas are high temperature ionized gases, heated with the aim of reaching self-sustained nuclear fusion. In particular, we consider here fusion plasmas confined by means of magnetic fields in toroidal chambers named tokamaks. The present generation of tokamak devices has reached the point at which the demonstration of breakeven plasma conditions is feasible and the next step in R&D is the design and construction of a machine with the goal of operating in controlled burning plasma conditions. The International Thermonuclear Experimental Reactor (ITER) is the result of an international collaboration and the expression of the effort in the scientific community to achieve this goal [1].

The success of the fusion research program critically depends on two major issues: first, on the ability of reaching burning plasma conditions; second, on the possibility of having the $3.52MeV$ alpha particles produced by fusion reactions well confined, so that they may thermalize and transfer their energy to the plasma bulk, thereby sustaining fusion without the need of external heating. Hot and dense plasmas must be produced to accomplish the first objective. Efficient plasma heating is then needed to attain core temperatures of $T \sim 40keV$, and, since the plasma resistivity drops as $T^{-3/2}$, alternate options to ohmic heating have been proposed, such as ion cyclotron wave heating (ICH). In this case hot ion 'tails' up to a few MeV are formed.

In addition to the second objective, i.e. the good fusion alpha confinement, a non-inductive current drive system is often desirable to provide a long pulse, steady state operation scenario. A possibility is in the use of Neutral Beam Injectors (NBI), as for ITER, where $1.3MeV$ deuterium

beams have been proposed. The efficiency of this current drive system is influenced by the coherence properties of the beam after ionization. Pitch angle scattering of the injected hot ions, of course, results in a lower net produced current.

Thus, energetic ions in the MeV range are present in ignited plasmas, either as fusion products or because they are produced by auxiliary heating/current drive systems. In any case, the good confinement properties of these particles are of major importance for the success of the fusion research program.

The energetic ions classical (or ' neoclassical') transport due to Coulomb collisions is compatible with all of the above requirements. In order to infer the performance of the present and future tokamak devices, it is then necessary to determine the level of anomalous diffusion caused by collective instabilities and turbulence phenomena induced by wave-particle resonant interactions.

An estimate of the energetic ('hot') particle velocity v_h of the order of the Alfvén speed $v_A \equiv B/\sqrt{4\pi\varrho}$ (ϱ being the mass density), $v_h \sim v_A$, focuses the attention on Alfvénic instabilities induced by shear Alfvén waves (SAW). SAW are magnetohydrodynamic plasma waves propagating with the characteristic Alfvén velocity v_A along the magnetic field lines. At $1MeV$ a deuteron has a speed of $v \sim 10^9\, cm/s$. Furthermore the Alfvén velocity in a 50% DT plasma is $v_A \simeq 10^8 B(T)/\sqrt{n(10^{14}cm^{-3})}\; cm/s$ (n being here the particle density). Thus, for typical parameters, $B \simeq 5T$ and $n \simeq 10^{14}cm^{-3}$, we have $v_A \sim v_h$. Compressional Alfvén waves (CAW), instead, are hardly excited by resonances. To demonstrate this, consider that in a toroidal equilibrium the parallel wave vector is ordered as $k_\parallel \sim 1/R_o$ with R_o being the major radius of the torus; while the perpendicular wavenumber is $k_\perp \sim m/a$ with a being the torus minor radius and m the poloidal mode number. The compressional wave dispersion relation gives then $\omega_{CAW} \simeq k_\perp v_A \gg k_\parallel v_A \simeq k_\parallel v_h \simeq \omega_{SAW}$. Compressional and shear Alfvén waves are, however, weakly coupled because of equilibrium inhomogeneities. The free energy source that can drive instabilities is due to configuration space nonuniformities. In addition, SAW group velocity is directed along the magnetic field line and, therefore, fast ions can stay in resonance and effectively exchange energy with the wave [2, 3].

1.2 Continuous spectrum and continuum modes

SAW in a nonuniform equilibrium experience energy absorption (*continuum damping* [4, 5]), due to singular structures that are formed in the proximity of resonant surfaces. This mechanism can be understood in its simplest form by considering the SAW dynamics in a slab model, namely a magnetic configuration with one direction of nonuniformity.

To this aim, we consider here an incompressible plasma in an equilibrium magnetic field $\boldsymbol{B}_0(x) = \boldsymbol{B}_{0z} + \boldsymbol{B}_{0y}(x)$ varying along a coordinate x. In such a configuration, the plasma moves mainly with the $E \times B$ velocity: $\delta\boldsymbol{v} = c\ \delta\boldsymbol{E} \times \boldsymbol{B}_0/B_0^2$, with c being the speed of light. Consequently, the Faraday's law $(\omega/c)\delta\boldsymbol{B} = -\boldsymbol{\nabla} \times \delta\boldsymbol{E}$, governing the perturbed magnetic field $\delta\boldsymbol{B}$, reads: $\delta\boldsymbol{B} = (\boldsymbol{B}_0 \cdot \boldsymbol{\nabla})\boldsymbol{\xi} - (\boldsymbol{\xi} \cdot \boldsymbol{\nabla})\boldsymbol{B}_0 - \boldsymbol{B}_0(\boldsymbol{\nabla} \cdot \boldsymbol{\xi})$, where the plasma displacement is defined by $\delta\boldsymbol{v} = -i\omega\,\boldsymbol{\xi}$. Substituting Faraday's law in the momentum equation $\varrho\,\omega^2\boldsymbol{\xi} = \boldsymbol{\nabla}\boldsymbol{P} - \boldsymbol{J} \times \boldsymbol{B}/c$, we obtain:

$$\frac{\omega^2}{v_A^2}\boldsymbol{\xi} = k_\parallel^2\boldsymbol{\xi} + \frac{4\pi}{B^2}\boldsymbol{\nabla}\tilde{P} + \frac{\boldsymbol{B}_0}{B_0^2}(\boldsymbol{B}_0 \cdot \boldsymbol{\nabla})(\boldsymbol{\nabla} \cdot \boldsymbol{\xi}) \tag{1.1}$$

where we have used Ampere's law $\boldsymbol{\nabla} \times \boldsymbol{B} = 4\pi\boldsymbol{J}/c$, and $\tilde{P} = P + \boldsymbol{B} \cdot \delta\boldsymbol{B}/(4\pi)$ is the total plasma pressure (kinetic plus magnetic). We use now the hypothesis of plasma incompressibility $\boldsymbol{\nabla} \cdot \boldsymbol{\xi} = ik_\parallel\xi_\parallel + ik_\perp\xi_\perp + d\xi_x/dx = 0$, where the direction denoted as $\perp$ is perpendicular to x and to the magnetic field, and write Eq. 1.1 in components for $\xi_\parallel$, $\xi_\perp$ and ξ_x:

$$\epsilon\xi_\parallel = \frac{4\pi i}{B^2}k_\parallel\tilde{P} \tag{1.2}$$

$$\epsilon\xi_\perp = \frac{4\pi i}{B^2}k_\perp\tilde{P} \tag{1.3}$$

$$\epsilon\xi_x = \frac{4\pi}{B^2}\frac{d\tilde{P}}{dx} \tag{1.4}$$

where $\epsilon(x) = \omega^2/v_A^2 - k_\parallel^2(x)$. Using now the hypothesis that $k_\parallel \ll k_\perp$, we obtain from plasma incompressibility: $\xi_\perp = (i/k_\perp)(d\xi_x/dx)$. Using this relation, and the momentum equation components 1.3 and 1.4, we obtain:

$$\frac{d}{dx}\Big(\epsilon\frac{d\xi_x}{dx}\Big) - \epsilon\,k_\perp^2\,\xi_x = 0 \tag{1.5}$$

Equation 1.5, has been extensively used to describe in general SAW dynamics in slab models and cylindrical geometry [6], and applied to

describe the particular case of singular structures forming near the resonances, where $\epsilon = 0$, and the consequent loss of energy of the wave by continuum damping [4, 5]. The spectrum of resonances, given by $\epsilon(x) = 0$, is named *continuous spectrum*, and the singular structures *continuum modes*. In this dissertation, the general equation analogous to Eq. 1.5 will be studied in Sec. 4.2, for an equilibrium given by a tokamak geometry with magnetic islands.

Here, we show that continuum modes are formed near a continuum resonance, by studying singular properties of the solutions of Eq. 1.5. To this extent, we linearize $\epsilon(x)$ near a fixed position $x = x_0$ as $\epsilon(x) = \alpha(x - x_0)$, α being here a constant, we multiply Eq. 1.5 by $\alpha(x - x_0)$, and change variables with:

$$(x - x_0) \rightarrow s = \ln(\alpha(x - x_0))$$

With this substitution, Eq. 1.5 reads

$$\frac{d^2}{ds^2}\xi_x - k_\perp^2 \exp(2s)\ \xi_x = 0 \tag{1.6}$$

For $x/x_0 \simeq 1$, namely near the resonance, the solution can be approximated as:

$$\xi_x = C_1 + C_2 s = C_1 + C_2 \ln(\alpha(x - x_0)) \tag{1.7}$$

where C_1 and C_2 are two constants depending on the initial values. If the linearization is made near the $\omega^2 = 0$ singular radius, then the two logarithmic singularities coalesce into a $1/(\alpha(x-x_0))$ singularity. We can guess the importance of these latter cases noting that if $\omega^2 = 0$ then also $k_\parallel^2 = 0$ and Alfvén modes will have no more restoring force. According to the energy principle this latter configuration is the most unstable.

We have shown that near a resonance where the frequency of the wave belongs to the continuous spectrum, a singular structure is formed, named continuum mode. Hence, if a surface magnetohydrodynamic wave is excited by an external coupler, the wave will be phase mixed by this resonance and its energy will be dissipated to the plasma. The Alfvén wave absorption can be explained by a mode conversion process. When the singularity in the wave equation is removed by the finite-ion-Larmor-radius and finite-electron-mass corrections, a new branch of the Alfvén wave - the kinetic Alfvén wave - emerges [7]. Then, the energy in the shear Alfvén wave converts into the kinetic Alfvén wave which is an electrostatic wave of very short wavelength easily absorbed by plasma electrons via electron Landau damping or collisional damping.

The existence of Alfvén wave resonance in nonuniform ideal magnetohydrodynamic plasmas as well as its potential application to plasma heating were noted by Grad [8], and expressed with a rigorous theory by Chen and Hasegawa [4, 5]. The continuum damping rate was found to scale as the gradient of the continuous spectrum:

$$W = \frac{\omega B^2}{8k_\perp^2} C_2^2 \left| \frac{d\epsilon}{dx} \right|$$

where W is the damping rate per unit area of antenna, and the wave displacement amplitude C_2 near the resonance is proportional to the external driving force. This means that an instability can grow more easily near a continuum accumulation point (CAP), namely where $d\epsilon/dx = 0$.

Due to nonuniformities along the field lines in toroidal geometry, gaps appear in the SAW continuous spectrum [9]. The mechanism is similar to that which creates forbidden energy bands for an electron traveling in a periodic lattice.

1.3 Shear Alfvén instabilities

Two types of collective shear Alfvén instabilities exist in tokamak plasmas: discrete Alfvén Eigenmodes (AE), with frequency inside SAW continuum gaps [10], and Energetic Particle continuum Modes (EPM) [11], with frequency determined by fast particle characteristic motions.

Several types of AE exist, corresponding to several types of gaps in the continuous spectrum. Toroidicity-induced AE (TAE) exist within a gap, which is produced by the toroidal coupling between the m-th and the (m+1)-th poloidal harmonics. For plasmas with an elliptic cross section, coupling between the m-th and the (m+2)-th poloidal harmonics produces another gap near $\omega = 2\omega_{TAE}$. Eigenmodes with frequencies inside this gap are called ellipticity-induced Alfvén eigenmodes (EAE) [12]. When the plasma cross section has some triangularity, coupling between the mth and the (m + 3)th poloidal harmonics produces another gap near $\omega = 3\omega_{TAE}$, and eigenmodes inside this gap are called non-circular Alfvén eigenmodes (NAE) [13]. The width of the gap becomes progressively narrower for the high-order gaps. At finite plasma β, coupling between acoustic waves and shear Alfvén waves introduces a new β-induced gap at frequencies lower than the TAE gap [14]. The AE with frequency inside the β-induced gap are called Beta-induced AE (BAE).

The inclusion of kinetic effects into the description of TAE in warm plasmas produces the appearance, in the frequency range associated with

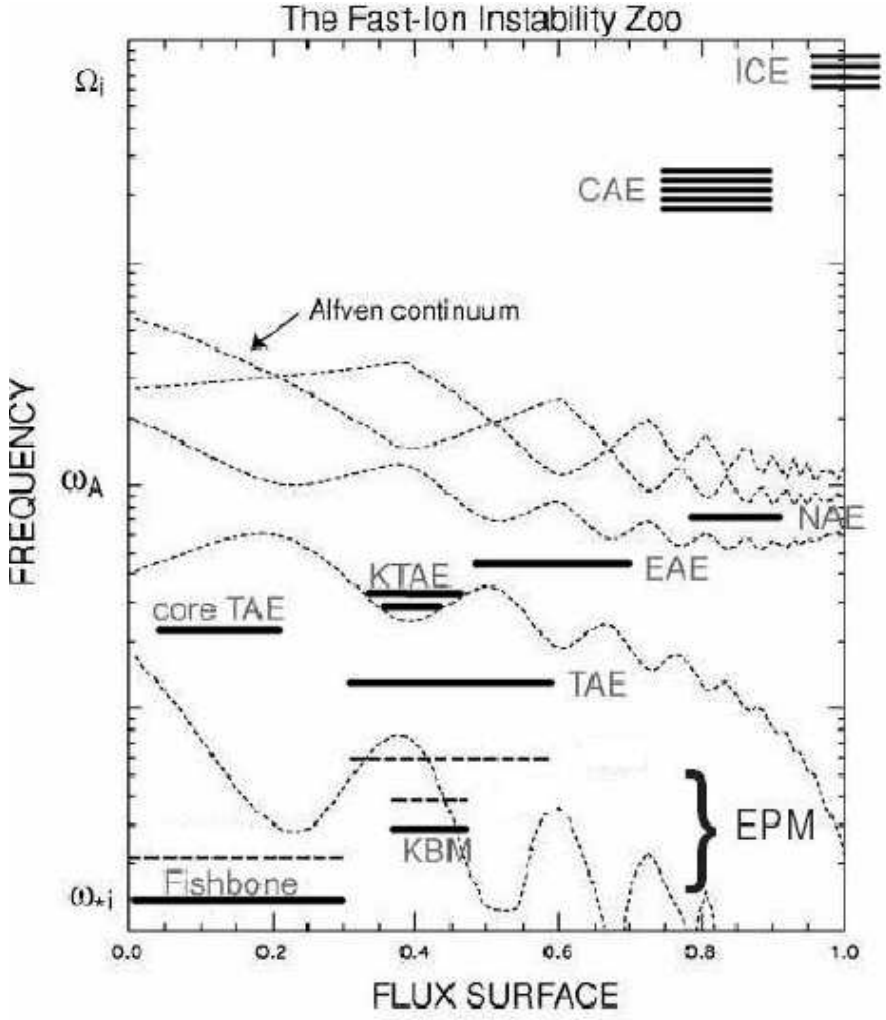

Figure 1.1: Schematic illustration of the approximate frequency, radial location and mode width of observed fast-ion driven normal modes (solid lines) and energetic particle modes (dashed lines) versus poloidal flux for a monotonically increasing q profile [15]. The $n = 3$ shear Alfvén frequency continuum curves (dotted curves) are also shown. Here an axisymmetric tokamak equilibrium is considered, without magnetic islands. From high frequency to low, the acronyms stand for ion cyclotron emission (ICE), compressional Alfvén eigenmode (CAE), triangularity-induced Alfvén eigenmode (NAE), ellipticity-induced Alfvén eigenmode (EAE), kinetic toroidicity-induced Alfvén eigenmode (KTAE), toroidicity-induced Alfvén eigenmode, and kinetic ballooning mode (KBM).

the TAE, of new families of weakly damped discrete modes, the kinetic TAE (KTAE) [16]. As KTAE are intrinsically exempt from radiative damping, with continuum damping replaced by mode coupling between KTAE with frequencies above the TAE gaps, their total damping rates and instability thresholds can be lower than those of the TAE. KTAE can affect fast particle confinement and redistribution. In fact, several KTAE may be associated with every TAE gap. The number of KTAE that can be simultaneously excited can thus be much larger than the number of TAE, and the correspondent anomalous transport and losses of fast particle increased significantly.

Besides the existence of eigenmodes of the thermal plasma, such as TAEs and KTAEs, it has been shown that other instabilities may be spontaneously excited by a sufficiently strong energetic particle drive [11]. These energetic particle modes (EPMs), due to the non-perturbative contribution of particle dynamics in determining mode structures and frequencies, have linear and non-linear behaviors which are different from those of TAEs and KTAEs. In particular, it has been demonstrated that when the particle drive is large enough to exceed the EPM threshold, a strong redistribution in the energetic particle source can take place, yielding potentially large particle losses and eventually mode saturation.

The different damping mechanisms of AE and EPM imply a different instability threshold of these two types of modes. In particular, modes belonging to the AE type have a generally low instability threshold, being practically unaffected by continuum damping [2, 3]. On the other hand, EPM can become unstable provided the drive exceeds a threshold determined by the continuum damping absorption, and therefore have a generally higher instability threshold. In this work, we focus on AE, which are more easily excited. For this reason, the importance of understanding the continuous spectrum structure is clear if one faces the stability problem of a tokamak and its potential impact on reaching the ignition condition.

1.4 Shear Alfvén modes in the presence of a magnetic island

SAW nonlinear dynamics is a research topic with many open issues. In the special case of uniform plasmas a peculiar state exists, called the *Alfvénic state*, which arises whenever we can assume ideal MHD, plasma incompressibility and the validity of the Walén relation ($\delta v/v_A =$

$\pm\delta B/B$, where δv and δB are the perturbed velocity and field) [17, 18, 19, 20]. In such a case, the nonlinear effects due to Maxwell and Reynolds stresses cancel and give a self-consistent nonlinear state (see Sec. 2.2.3). On the other hand, in nonuniform tokamak plasmas, with non-ideal effects such as resistivity or finite plasma compressibility, the Alfvénic state conditions are violated and SAW are characterized by a rich nonlinear dynamics.

The study of the nonlinear interaction of SAW and MHD fluctuations can be of practical interest in realistic tokamak scenarios. In fact, in a tokamak plasma, the SAW continuous spectrum is modified by the interaction with low-frequency MHD fluctuations, such as magnetic islands, which are formed when the original sheared equilibrium magnetic field lines break due to non ideal effects (in particular finite resistivity) and reconnect with different magnetic topology [21]. A modification in position and frequency of the continuum accumulation points is directly related to a modification in the dynamics of global Alfvén modes present in a tokamak, such as beta induced Alfvén Eigenmodes (BAE). BAE are considered in this dissertation as an example of AE in tokamaks, because it will be shown a posteriori that their frequency range is comparable to the nonlinear frequency shift due to the presence of the magnetic island. Therefore, we neglect terms due to toroidicity or ellipticity of the tokamak section, responsible for the existence of TAE or EAE, which are expected to be less modified by the presence of the magnetic island. Moreover, the presence of new gaps in the continuous spectrum can host new Alfvén eigenmodes, induced by the presence of the island.

We derive the fluid theoretical description of the SAW dynamics in the presence of a finite size magnetic island in finite-β plasmas, keeping into account only toroidal effects due to geodesic curvature, which are responsible for the BAE gap in the low frequency part of the SAW continuous spectrum [14, 22, 23]. Since the typical island frequency and growth rate are much lower than the SAW oscillation frequency, we can model the equilibrium magnetic field as the sum of a tokamak axisymmetric part plus a quasi-static helical distortion due to the magnetic island. We adopt a linear ideal MHD model, and we consider:
(a) shear Alfvén modes with the same helicity as the magnetic island [24],
(b) shear Alfvén modes with different helicity from that of the magnetic island [25, 26].

Firstly, we calculate the radial structure of the SAW continuous spectrum in the presence of a magnetic island. In fact, as discussed above, the radial structure of the SAW continuous spectrum is directly related to the tokamak Alfvén eigenmodes dynamics. Therefore, we consider firstly

continuum modes, which are radially localized near the continuum resonance surfaces. In this framework, with an appropriate rotation of the coordinates problem (a) for continuum modes reduces to 2 dimensions. Since continuum modes are characterized by radial singular behaviors, problem (a) can be further reduced to one dimension, and problem (b) to two dimensions. The local differential equation describing the nonlinear SAW continuum structure is solved numerically with a shooting method code in the whole spatial range of interest (both outside and inside the island), and analytically near the O-point and at the island separatrix, where the equilibrium quantities can be approximated in simple form.

As suggested by the magnetic field line helicity behavior [27, 28], in an equilibrium with a magnetic island a generalized safety factor q can be defined for each flux surface, as an appropriate average of the ratio of the magnetic field components along and perpendicular to the magnetic axis. The separatrix flux surface plays an important role, hosting the BAE continuum accumulation point (BAE-CAP), that - without island - was positioned at the rational surface. The BAE-CAP is the upper extremum of the BAE gap. For modes with the same helicity of the magnetic island, the degeneracy in frequency of even and odd continuum modes is removed by inhomogeneities along the field lines, causing a splitting between the continuous spectrum branches with different parities. As a consequence, the BAE-CAP is also split in different frequencies, depending on the mode number and parity of the eigenfunction. Several branches of the nonlinear SAW continuous spectrum stem from the BAE-CAP. Inside the island, they reach continuum accumulation points at the magnetic island O-point (MiO-CAP). These several CAPs at the O-point are peculiar to the presence of the island and have similar radial structures as those generated by reversed magnetic shear [29, 30]. Outside the island and far from the separatrix, they asymptotically approach the typical spatial dependence of the SAW continuum in a sheared magnetic field in the absence of the island. For modes with different helicity from that of the magnetic island, we find that there exists a continuous spectrum very similar to that of tokamak plasmas within a magnetic island, where the coupling of modes with different mode numbers creates frequency gaps. In particular, a wide frequency gap is formed [25], analogous to the ellipticity induced Alfvén Eigenmode [12] (EAE) gap in tokamaks. This is due to the strong eccentricity of the island cross section.

Secondly, we consider global (namely, non radially singular) Alfvén eigenmodes. Inside the magnetic island, we show that new magnetic-island induced Alfvén eigenmodes (MiAE) exist as bound states, with frequency inside the continuum gap induced by ellipticity. The analytic

theory of MiAE is derived in the particular case of small eccentricity magnetic islands. In this case, the theory of MiAE is analogous to the theory of ellipticity induced Alfvén eigenmodes in tokamaks. As a second example of Alfvén eigenmodes, we consider beta induced Alfvén eigenmodes (BAE), which are present in tokamaks even without islands and have frequencies of the order of the thermal ion transit frequency. The dynamics of BAE in the presence of a magnetic island is studied in the framework of a perturbative theory, where the magnetic island acts as a perturbation to the tokamak equilibrium. In this case, a small magnetic island is considered, and we calculate the effect of the presence of the magnetic island in modifying the frequency of the BAE. We show that BAE frequency is dependent on the magnetic island size, and we compare this dependence with experimental observations, finding a good consistency.

These results have potential implications in explaining stability properties of tokamak plasmas in the presence of magnetic islands. In fact, modes in the BAE frequency range have been observed in the Frascati Tokamak Upgrade (FTU) [28, 31] in the presence of an (m, n) = (-2,-1) magnetic island, where m and n are, respectively, the poloidal and toroidal mode number. A theoretical analysis showed that these modes can be interpreted as BAE modes, when thermal ion transit resonances and finite ion Larmor radius effects are accounted for, with good agreement of measured and calculated frequencies in the small magnetic island amplitude limit [32]. In fact, measured frequencies were found to depend on the magnetic island amplitude as well [28], consistently with the dependence of the BAE frequency on the magnetic island size resulting from our theory. The modes were observed only when the magnetic island size was over a certain critical threshold [28]. Later on, similar observations have been reported in other tokamaks (see, for instance, the observations in HL-2A [33]). Moreover, we point out that magnetic-island induced Alfvén eigenmodes (MiAE), could be resonantly excited by energetic particles and grow unstable inside the island, being essentially free of continuum damping. The presence of MiAE inside a magnetic island could modify the equilibrium profiles and nonlinearly affect the magnetic island growth. On the other hand, MiAE could nonlinearly affect energetic particles redistribution in the proximity of the magnetic island rational surface. As a last application of our theory to study of tokamak stability, we point out that, due to the frequency dependence of shear Alfvén modes on mode numbers and the magnetic island size, the possibility of using their frequency scalings as novel magnetic island diagnostic is an attractive option.

Chapter 2

Equilibrium and model equations

2.1 Equilibrium and coordinate system

2.1.1 Coordinates in tokamak and outside the island

We consider a tokamak geometry where R_0 is the major radius of the torus. The equilibrium is made of an axisymmetric tokamak magnetic field with a component B_{tor} in the toroidal direction ζ_T and a component B_{pol} in the poloidal direction θ_T, plus a helical perturbation B_{rad} in the radial direction r_T, generating a magnetic island. The magnetic island lies on a flux surface with a minor radius r_0. The subscripts T denote here the tokamak coordinates. The gradients associated with these coordinates are: $\boldsymbol{\nabla} r_T = \hat{\boldsymbol{r}}_T$, $\boldsymbol{\nabla}\theta_T = \hat{\boldsymbol{\theta}}_T/r_0$ and $\boldsymbol{\nabla}\zeta_T = \hat{\boldsymbol{\zeta}}_T/R_0$.

We consider the region in the proximity of the rational surface of the magnetic island $q_T = q_0 = m_{isl}/n_{isl}$, where m_{isl} and n_{isl} are respectively the poloidal and toroidal mode numbers of the magnetic island perturbation, and $q_T = r_T B_{tor}/(R_0 B_{pol})$ is the safety factor. We adopt a slab model with coordinates (q_T, u, ζ), applying a rotation of the coordinates in the (θ_T, ζ_T) plane, as shown in Fig. 2.1, where u is defined in Eq. 2.1. This is appropriate to describe a sheared field problem, in the proximity of the rational surface, because the rotation is defined in order to have the axisymmetric magnetic field only along $\hat{\boldsymbol{\zeta}}$ at $q_T - q_0 = 0$. In this model, the axisymmetric magnetic field depends on q_T only, and the coordinate $\zeta = (\zeta_T + \varepsilon_0^2\,\theta_T/q_0)/(q_0\gamma^2)$ is the coordinate of translational symmetry, where $\gamma = \sqrt{1+\varepsilon_0^2/q_0^2}$ and $\varepsilon_0 = r_0/R_0$. The gradients associated with

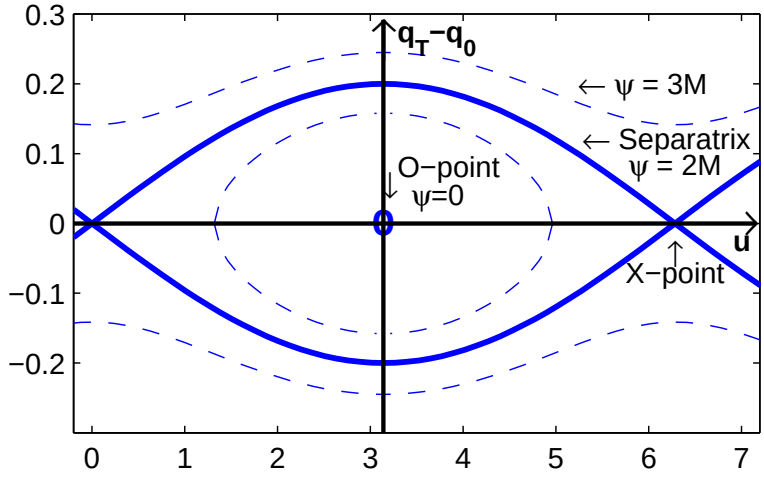

Figure 2.1: Island coordinate system. The horizontal axis $q - q_0 = 0$ is the rational surface of the island. In this example the amplitude of the island is chosen as $M = 10^{-2}$.

these coordinates are: $\boldsymbol{\nabla} q_T = (q_0 s/r_0)\hat{\boldsymbol{r}}_T$, $\boldsymbol{\nabla} u = n_{isl}(\hat{\boldsymbol{\zeta}}_T/R_0 - q_0\hat{\boldsymbol{\theta}}_T/r_0)$ and $\boldsymbol{\nabla}\zeta = (\hat{\boldsymbol{\zeta}}_T + \varepsilon_0\,\hat{\boldsymbol{\theta}}_T/q_0)/(q_0 R_0\gamma)$. The parameter s is the magnetic shear calculated at the rational surface. It is useful to rewrite the gradient of the coordinates u and ζ in the form $\boldsymbol{\nabla} u = \hat{\boldsymbol{u}}/\rho_0$ and $\boldsymbol{\nabla}\zeta = \hat{\boldsymbol{\zeta}}/Z_0$, where $\rho_0 = r_0/(q_0 n_{isl}\gamma)$, and $Z_0 = \gamma q_0 R_0$. In fact, we see that $2\pi\rho_0$ is the actual length of the magnetic island in the u direction and $2\pi Z_0$ is the length of a magnetic field line of the axisymmetric equilibrium at $q = q_0$. In other words, $2\pi Z_0$ is the periodicity length of the magnetic flux tube defined as the region inside the magnetic island separatrix.

The *constant-ψ* approximation is also adopted, assuming that the magnetic island perturbation has the form $B_{rad} = B_{isl}\sin u$, with B_{isl} constant. The flux surfaces of this equilibrium are labeled by ψ, where the coordinates ψ and u are defined by:

$$\begin{aligned} \psi &= (q_T - q_0)^2/2 + M(\cos u + 1) \\ u &= n_{isl}(\zeta_T - q_0\theta_T) \end{aligned} \tag{2.1}$$

The X-points of the magnetic island are at $(q_T - q_0, u) = (0, 0)$ and $(0, 2\pi)$ and the O-point at $(0, \pi)$. M is a constant with value $M = (q_0|s|/n_{isl})(B_{isl}/B_{pol,0})$, determined by the condition $\boldsymbol{\nabla}\psi \cdot \boldsymbol{B} = 0$, where s is the magnetic shear and $B_{pol,0}$ is the poloidal magnetic field evaluated at the rational surface. The topology of the flux surfaces outside

the island is the same as for an equilibrium without islands. This is because the flux surfaces outside the island are not reconnected. Therefore, the set of coordinates (ψ, u, ζ) is well defined to describe the region outside the island. The correspondent differential operators are defined in Appendix 7.1. On the other hand, a further change of coordinates is introduced in the following section, to describe the region inside the island.

2.1.2 Coordinates inside the magnetic island

In our slab model approximation, the plasma inside the magnetic island is a straight flux tube with length $2\pi Z_0$. The magnetic axis of the flux tube, directed along $\hat{\boldsymbol{\zeta}}$, and the O-point of the magnetic island, lie at $\psi = 0$, and the separatrix is labeled by $\psi = \psi_{sx} = 2M$. An appropriate set of cylinder-like coordinates (ρ, θ, ζ) is defined here to describe the region inside the magnetic island, with:

$$\begin{aligned} \rho &= \frac{r_0}{q_0 s}\sqrt{2\psi} \\ \theta &= \arccos(\sqrt{M(\cos u + 1)/\psi}\,) \end{aligned} \tag{2.2}$$

With these definitions, the magnetic axis is at $\rho = 0$ and the separatrix radius is $\rho = \rho_{sx}$, which corresponds to the magnetic island half-width W_{isl}, given by the Rutherford formula [34]:

$$\frac{W_{isl}}{r_0} = 2\sqrt{\frac{B_{isl}}{q_0 s n_{isl} B_{pol,0}}} = \frac{\rho_{sx}}{r_0} = \frac{2}{q_0 \gamma n_{isl}}\sqrt{1-e} \tag{2.3}$$

with e defined below in this section. The angle θ is defined in the domain $(0, \pi/2)$ and extended to $(0, \pi)$ by reflection symmetry w.r.t. $\theta = \pi/2$, with values $0, \pi$ at the rational surface $q = q_0$. Further extension to $(0, 2\pi)$ is obtained by reflection symmetry for $\rho \leftrightarrow -\rho$. With this definition, θ has values $0, \pi$ at the rational surface $q_T = q_0$.

We note that the flux surface's cross section in the (ρ, θ) plane and in the proximity of the O-point is an ellipse:

$$\frac{(q_T - q_0)^2}{a_{q_T}^2} + \frac{(u-\pi)^2}{a_u^2} = 1\,, \quad a_{q_T}^2 = 2\psi\,,\, a_u^2 = \frac{2\psi}{M}$$

We can recognize the geometrical role of the eccentricity near the O-point, calculating the major and minor semi-axes length of the ellipses,

L_u and L_q, which are respectively the semi-length of the ellipse along u and along q:

$$L_u = \frac{a_u}{|\nabla u|} = \sqrt{\frac{2\psi}{M}}\frac{r_0}{q_0 n_{isl}\gamma}\,, \;\; L_q = \frac{a_{q_T}}{|\nabla q_T|} = \sqrt{2\psi}\frac{r_0}{q_0|s|}$$

with these definitions, we can recognize e as the standard geometrical definition of an ellipse's eccentricity:

$$e = 1 - \frac{M n_{isl}^2 \gamma^2}{s^2} \tag{2.4}$$

Although the approximation of the flux surfaces' cross section as ellipses is good only in the proximity of the O-point ($x \ll 1$), the eccentricity can be calculated with the same geometrical definition for all values of $x = \rho/\rho_0$. We obtain:

$$e(x) = \frac{L_u^2 - L_q^2}{L_u^2} = \frac{\big(\arccos(2x^2-1) - \pi\big)^2 - 4(1-e)x^2}{\big(\arccos(2x^2-1) - \pi\big)^2} \tag{2.5}$$

and the value at the O-point is recovered in the limit $x \to 0$, where $e(x) \to e$. This definition of $e(x)$ will be used in the derivation of the global Alfvén Eigenmode dispersion relation, given in Chapter 4. To this extent, it will be useful to note that the eccentricity parameter Δ defined in reference [12], is linked to $e(x)$ by the formula: $e(x) = 4\Delta/\rho$, corresponding to $d\Delta/d\rho = (e(x) + xe'(x))/4$.

Two useful limiting cases are found when the eccentricity goes to one and to zero:

$$e = 1 \;\; \Leftrightarrow \;\; M = 0 \tag{2.6}$$

$$e = 0 \;\; \Leftrightarrow \;\; M = \frac{s^2}{n_{isl}^2\gamma^2} \simeq 1 \tag{2.7}$$

The former is found for vanishing magnetic islands, the latter describes a particular magnetic island amplitude which determines a circular cross section of the magnetic flux tube near the O-point. In the latter case, we can see from Eq. 2.9, that the magnetic field intensity does not depend on θ. This means that the $e = 0$ case has a cylindrical symmetry around the O-point axis ($\psi = 0$), broken only by higher order toroidicity effects, which will not be considered here, because of minor relevance.

Typical magnetic islands in tokamak experiments, have values of eccentricity close to $e \simeq 1$ (see Sec. 5.4 for examples of magnetic islands

detected in tokamaks). The case of zero eccentricity corresponds to an unrealistic value of magnetic island width, which is never encountered in tokamak plasmas because a saturation or a disruption occurs long before the island grows up to these values of width. Nevertheless, in Chapter 3, we calculate the shear Alfvén wave continuous spectrum for the case $e \simeq 0$ too. In fact, this case shows clearly the analogy with the well-known results of continuous spectrum in a tokamak, whose cross section has usually small values of eccentricity. This simplification of small eccentricity of the island cross section will also be used in Chapter 4 for the derivation of the global Eigenmode theory inside magnetic island. The differential operators in this coordinate set are provided in Appendix 7.1.

2.1.3 Equilibrium magnetic field and safety factor

The equilibrium magnetic field is the sum of the axisymmetric equilibrium field and of the magnetic island field. The axisymmetric magnetic field components can be written here in the new coordinates outside and inside the island, by considering that $\hat{\boldsymbol{\zeta}}$ forms an angle $\alpha_0 = \arctan(B_{pol,0}/B_{tor})$ with $\hat{\boldsymbol{\zeta}}_T$. The u and ζ components are easy to obtain as $B_u = B_{tor}\sin\alpha_0 - B_{pol}(q)\cos\alpha_0$ and $B_\zeta = B_{tor}\cos\alpha_0 + B_{pol}(q)\sin\alpha_0$. In the coordinates (ρ, u, ζ), the equilibrium magnetic field is described by the contra-variant physical components:

$$B^\rho_{ph} = 0\ ,\ B^u_{ph} = 2\varepsilon_0 B_0\sqrt{M}P/(q_0^2\gamma^2)\ ,\ B^\zeta_{ph} = B_0 \tag{2.8}$$

Here $P = \sqrt{L^2 + (1-e)(\sin^2 u)/4}$, where $L = \sqrt{x^2 - (\cos u + 1)/2}$, $x = \rho/\rho_{sx}$, and $B_0 = \gamma B_{tor}$. The contra-variant *physical* components of a vector $\boldsymbol{V}$, in a basis $\{\boldsymbol{g}_\rho, \boldsymbol{g}_u, \boldsymbol{g}_\zeta\}$ are defined here as the contra-variant components rescaled with the length of the correspondent basis vector, e.g. $V^\rho_{ph} = V^\rho|\boldsymbol{g}_\rho|$ (see Appendix 7.1 for further explanations). Similarly, in the coordinates defined inside the island we have:

$$B^\rho_{ph} = 0\ ,\ B^\theta_{ph} = 2\varepsilon_0 B_0\sqrt{M}\sqrt{a}\,x/(q_0^2\gamma^2)\ ,\ B^\zeta_{ph} = B_0 \tag{2.9}$$

The function a is defined as $a = \sin^2\theta + \cos^2\theta(1-e)F^2$, with $F = \sqrt{1 - x^2\cos^2\theta}$.

An important parameter describing the equilibrium profile, given the magnetic field, is the safety factor, which is defined for an equilibrium with cylindrical symmetry as: $q = (\rho B_z)/(Z_0 B^\theta_{ph}(\rho))$. The poloidal component (i.e. along θ) has to be written in the contra-variant definition, that is the definition where the radial component is null. Moreover, the *physical* component has to be considered, which is the one that does

not depend on the choice of coordinates, because it is re-scaled with the length of the unitary vector of θ. In the case of an equilibrium with generical flux surface shape, like in the presence of a magnetic island, we use a similar definition of safety factor, but we need to average over the flux surface.

Outside the magnetic island, the topology is conserved by the presence of the magnetic island. Therefore, the safety factor still has the role of measuring the ratio between the magnetic field intensity along the toroidal coordinate, ζ_T, and the poloidal coordinate, θ_T. The additional magnetic field component along the radius r_T gives a modulation to the magnetic flux surfaces. With this modulation, the path measured tangentially to the flux surface, and directed along the poloidal direction, is not given by $r_0\theta_T$, but by a coordinate defined as:

$$y_{out} = \int_0^{\theta_T} r_0 d\theta_T \sqrt{1 + \frac{B_q^2}{B_{pol}^2}} = \int_0^u \gamma\rho_0 du \frac{P_2}{1 - 2\sqrt{M}P/q_0} \tag{2.10}$$

with

$$P_2 = \frac{B_{ph}^{y_{out}}}{B_{pol,0}} = \sqrt{\left(1 - \frac{2\sqrt{M}}{q_0}P\right)^2 + \frac{M^2 n_{isl}^2}{q_0^2 s^2}\sin^2 u}$$

Eq. 2.10 has been obtained by substituting the poloidal component of the magnetic field written in terms of the coordinates x, u: $B_{pol} = B_{ph}^{\theta_T} = B_{pol,0} - \gamma B_{ph}^u = B_{pol,0}(1 - 2\sqrt{M}P/q_0)$. Moreover, we are considering the region in the proximity of the magnetic island rational surface, and therefore we have assumed that the minor radius is constant, consistently with the slab model approximation: $r_T = r_0$. By averaging over y_{out}, we obtain the value of the safety factor outside the island:

$$q_{out} = \oint \frac{dy_{out}}{2\pi R_0}\frac{B_{tor}}{B_{ph}^{y_{out}}} = \frac{1}{2\pi n_{isl}}\int_0^{2\pi q_0 n_{isl}} \frac{du}{(1 - 2\sqrt{M}P/q_0)} \tag{2.11}$$

The radial structure of the safety factor and the magnetic shear outside the island are shown in Fig. 2.2. Far from the separatrix ($x > 1$), the safety factor reaches asymptotically the linear behavior typical of the slab model without island. When the magnetic island amplitude M vanishes, this behavior is recovered for all x. In fact, in this case we have that $2\sqrt{M}P \to (q_T - q_0)$ and therefore $q_{out} \to q_T$. The magnetic shear is calculated as $s_{out} = (r_{min}/q_{out})dq_{out}/dr_{min}$, with $r_{min} = r_0(1 + 4M(x^2 - 1)/q_0)$.

An important result is that the safety factor at the separatrix ($x = 1$) is not q_0, but there is a small difference, proportional to the magnetic island size. This difference is positive on one side of the island, where

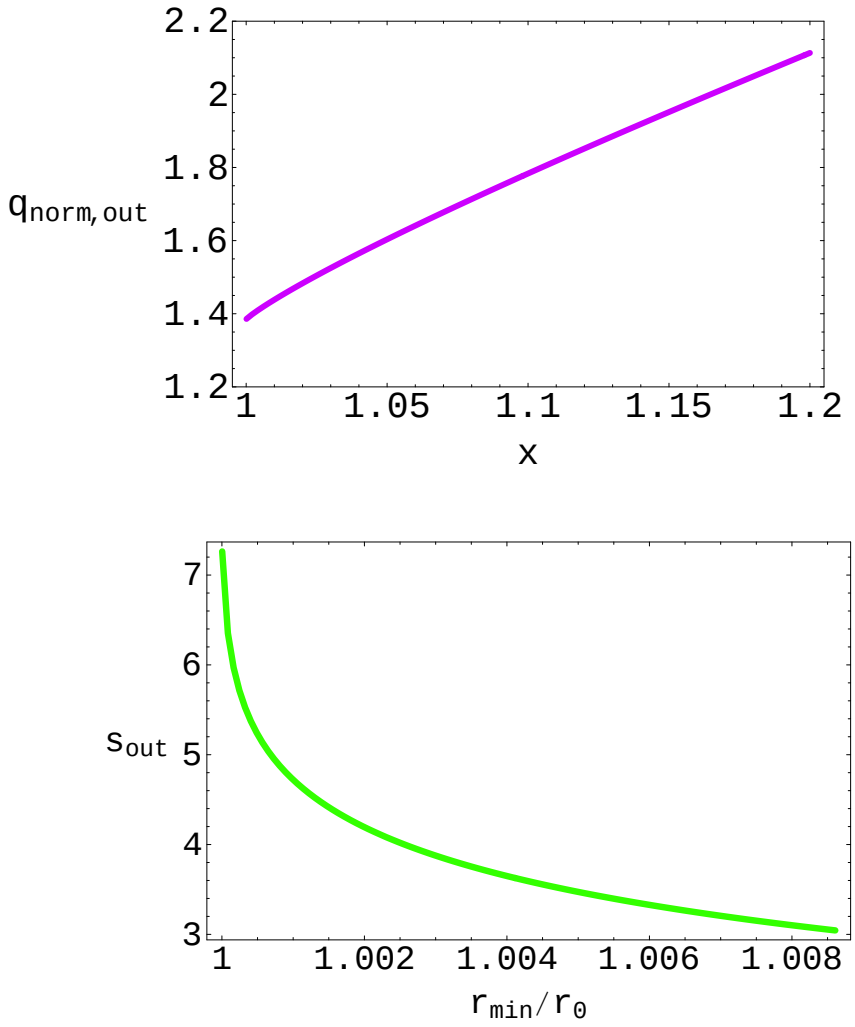

Figure 2.2: Safety factor profile (upper figure) and magnetic shear profile (lower figure) outside a magnetic island. The value of the safety factor reported here is normalized: $q_{norm,out} = (q_{out} - q_0)/(\sqrt{M} n_{isl})$. The magnetic shear is defined as $(r_{min}/q_{out}) dq_{out}/dr_{min}$, with $r_{min} = r_T(u = 0)$ is the minimum tokamak minor radius of a flux surface, which is obtained at $u = 0$ for surfaces with $r_T > r_0$. The radial coordinate x is defined as $x = \rho/\rho_{sx}$.

$q_T > q_0$, and negative on the side where $q_T < q_0$. The absolute value of this difference can be calculated at the separatrix from Eq. 2.11, in the limit $M \ll 1$. We obtain:

$$q_{out,sx} - q_0 = \frac{4\sqrt{M}}{\pi} \simeq 1.27\sqrt{M} \tag{2.12}$$

This result has important implications to the value of the continuous spectrum frequency at the separatrix, as discussed in Chapter 3. In fact, we will see that the BAE continuum accumulation point, which is located at the separatrix, has not the same frequency as without island, but a nonlinearly modified frequency which is proportional to $\sqrt{M}$, consistently with the nonlinearly modified value of the safety factor given by Eq. 2.12.

Now, we define the safety factor inside a magnetic island, using an approach similar to the one used outside the island. Inside the magnetic island, we project the flux surface on the the (ρ, θ) plane, and we call y_{in} the coordinate measuring the path along the flux surface element in this plane, defined by:

$$y_{in} = 2\rho_0 x \int_0^\theta d\theta' \frac{\sqrt{a}}{F} \tag{2.13}$$

The average along y_{in} is used to define the safety factor:

$$q_{in} = \oint \frac{dy_{in}}{2\pi Z_0} \frac{B_z}{B^\theta_{ph}} = \int_0^{2\pi} \frac{d\theta}{2\pi Z_0} \frac{dy_{in}}{d\theta} \frac{B_z}{B^\theta_{ph}} = \int_0^{2\pi} \frac{d\theta}{2\pi Z_0} \frac{B_z}{B^\theta} \tag{2.14}$$

This brings to the evaluation of the safety factor, where the contra-variant component of the poloidal field is $B^\theta = B^\theta_{ph} F\sqrt{1-e}/(\sqrt{a}\,\rho)$. We finally obtain:

$$q_{in} = \frac{2}{\pi} \frac{\gamma}{|s|\sqrt{1-e}} \mathtt{K}(x) = \frac{2}{\pi} \frac{1}{\sqrt{M} n_{isl}} \mathtt{K}(x) \tag{2.15}$$

where we have introduced the complete elliptic integral of the first kind $\mathtt{K}(x) = \int_0^{\pi/2} d\theta/F$. This definition is analogous to the definition used for the axisymmetric tokamak equilibrium. A similar definition for the safety factor was given in Ref. [27], but our result is a factor q_0 smaller. The basic difference of our derivation from that of Ref. [27], is that we take into account that the length of a magnetic island flux tube is $2\pi Z_0 \simeq 2\pi\gamma q_0 R_0$, whereas in Ref. [27] a flux tube with length $2\pi R_0$ is considered, which is the major circumference of the tokamak. In other words, we point out that the magnetic island flux tube performs q_0 loops before closing on itself, and therefore all periodicity boundary conditions have to be imposed in its whole length, and not in the length of the tokamak circumference. This difference enters in particular the definition of the coordinate along

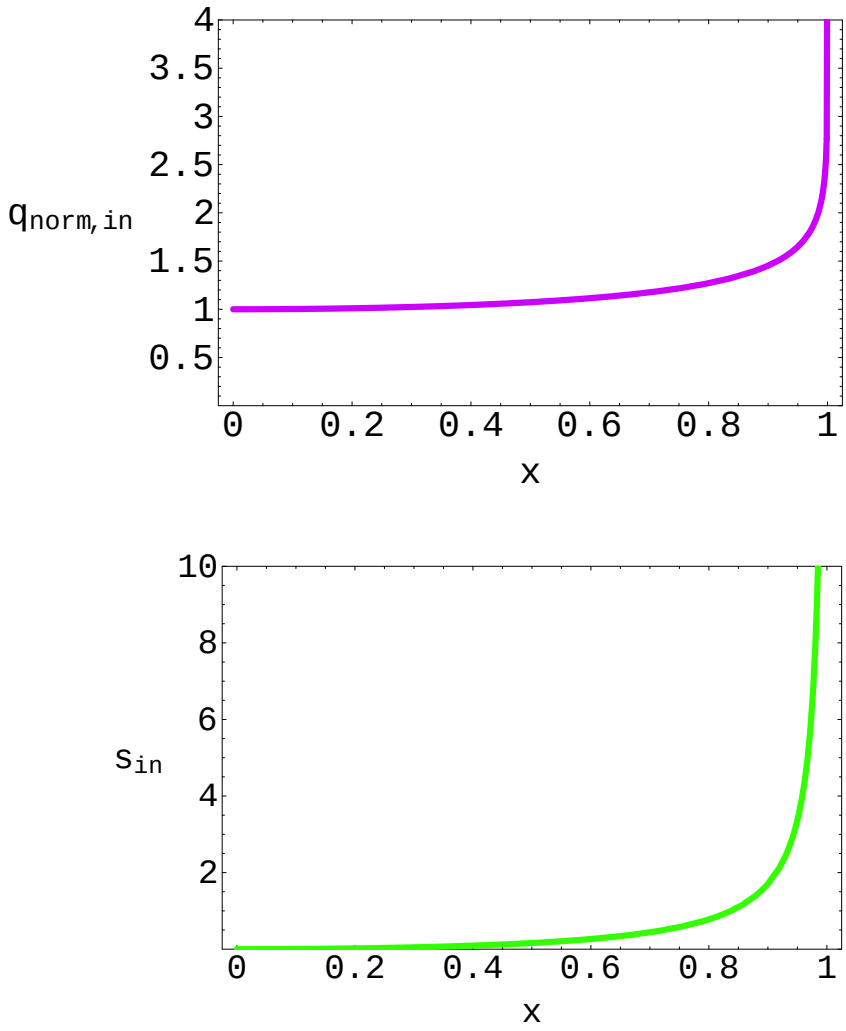

Figure 2.3: Safety factor profile (upper figure) and magnetic shear profile (lower figure) inside a magnetic island. The value of the safety factor reported here is normalized to $q(0) = 1/(\sqrt{M}n_{isl}) = \gamma/(|s|\sqrt{1-e})$. For typical magnetic islands, $1 - e < 10^{-2}$ and we have $q(0) > 10$. On the other hand, the magnetic shear is reported in its whole form, and does not depend on the island size in the model we are using. The radial coordinate x is defined as $x = \rho/\rho_{sx}$.

the axis of the magnetic island flux tube ζ, and approximated in Ref. [27] by the toroidal coordinate ζ_T.

The result, normalized to the minimum value, $q(x=0)$, is shown in Fig. 2.3, normalized with the factor $(\sqrt{M}n_{isl})^{-1}$. We see that, because of the vanishing of B^θ at $\rho = \rho_{sx}$, $\theta = 0, \pi$, we have a singular behavior of the safety factor near the separatrix, $x = 1$. This feature is due to the presence of the X-point, and is found in the safety factor of diverted tokamaks as well. The safety factor is big for small islands and decreases when the island grows. This means that, for a small island, only high values of q are accessible, and more and more values of q become accessible when the island grows. Since the modes with small rational values of q are the most unstable, this fact has important implications in the stability properties of the equilibrium inside a magnetic island. The magnetic shear, defined as $s = (x/q)dq/dx$, is also showed in Fig. 2.3.

It is worthwhile noting that the minimum value of the q profile is obtained at $x = 0$, and depends on the magnetic island size M. We have: $q(0) = (\sqrt{M}n_{isl})^{-1}$. The reason why the safety factor at the O-point is not the same as without magnetic island (although the magnetic island perturbed field vanishes at the O-point) is that the safety factor inside the magnetic island is calculated with respect to the magnetic island flux tube, and not with respect to the tokamak flux tube. Therefore, the periodicity boundary conditions of the modes inside the magnetic island are not the same as those in the tokamak, and the same is valid for the safety factor.

By knowing the minimum value of the safety factor inside the magnetic island, we can formulate the MHD interchange instability condition [35] in terms of the magnetic island size. This is the condition for modes $m/n = 1$ internal to the magnetic island to be unstable, which happens where $q = 1$, and therefore requires: $q(0) < 1$. Substituting the value of the island width W_{isl} into M, using the Rutherford formula, Eq. 2.3, we obtain that a magnetic island is unstable for the interchange instability condition only if the half-width satisfies:

$$\frac{W_{isl}}{r_0} > \frac{2}{q_0|s_0|n_{isl}} \tag{2.16}$$

For typical tokamak plasmas, we have that magnetic islands never reach such amplitudes, usually disrupting much earlier, and the q-profile defined here inside the island never goes below 1. Therefore, the interchange instability is not discussed further in this dissertation, focusing on SAW dynamics in profiles with $q(x) > 1$.

2.2 Model equations

2.2.1 Starting model equations in ideal MHD regime

The ideal magnetohydrodynamic (MHD) equations are used as a starting point for the SAW's fluid treatment, neglecting both resistivity and viscosity:

$$\frac{d\varrho}{dt} = -\varrho \boldsymbol{\nabla} \cdot \boldsymbol{v} \tag{2.17}$$

$$\varrho \frac{d\boldsymbol{v}}{dt} = -\boldsymbol{\nabla} P + \frac{\boldsymbol{J}}{c} \times \boldsymbol{B} \tag{2.18}$$

$$\frac{1}{c}\frac{\partial \boldsymbol{B}}{\partial t} = -\boldsymbol{\nabla} \times \boldsymbol{E} \tag{2.19}$$

$$\frac{dP}{dt} = -\gamma P \boldsymbol{\nabla} \cdot \boldsymbol{v} \tag{2.20}$$

$$\boldsymbol{E} = -\frac{\boldsymbol{v}}{c} \times \boldsymbol{B} \tag{2.21}$$

$$\frac{4\pi}{c}\boldsymbol{J} = \boldsymbol{\nabla} \times \boldsymbol{B} \tag{2.22}$$

$$\boldsymbol{\nabla} \cdot \boldsymbol{B} = 0 \tag{2.23}$$

Here ϱ is the mass density, $\boldsymbol{v}$ the fluid velocity, P the pressure of the bulk plasma, $\boldsymbol{J}$ the plasma current, $\boldsymbol{B}$ and $\boldsymbol{E}$ the magnetic and electric fields and γ the ratio of the specific heats. In this section the symbol c denotes the speed of light. The operator $d/dt = \partial/\partial t + \boldsymbol{v} \cdot \nabla$ is the convective derivative. We neglect resistivity even though we are dealing with tearing modes because their evolution is taken as given here. Moreover, being the typical island frequency and growth rate much lower than the SAW oscillation frequency, we will assume that the equilibrium magnetic field is given by the usual tokamak axisymmetric field plus a quasi-static helical distortion due to the magnetic island.

The frequency range of our interest is given by the typical SAW frequency ($\omega \sim k_\parallel v_A$), above the BAE-CAP frequency. This is the validity range of the fluid theory, where we can neglect the particle resonances in a consistent way. The study of lower frequency dynamics, where transit and trapped particle can resonate with wave, requires the gyro-kinetic theory [2], and is out of the scope of this dissertation.

The balance of pressure and magnetic forces of the axisymmetric equilibrium gives, from Eq. 2.18:

$$\boldsymbol{J}_{\perp 0} = c\frac{\boldsymbol{B}_0}{B^2} \times \boldsymbol{\nabla} P_0$$

The perturbed magnetic field and velocity are expressed respectively in terms of a vector and scalar potential:

$$\delta \boldsymbol{B} = \boldsymbol{\nabla} \times \delta \boldsymbol{A} \tag{2.24}$$

$$\delta \boldsymbol{v}_\perp = \frac{c}{B^2} \boldsymbol{B} \times \boldsymbol{\nabla}_\perp \delta\phi \tag{2.25}$$

where here a perturbed field is always meant to be a SAW perturbation, when not otherwise specified, like for the SAW perturbed magnetic field $\delta \boldsymbol{B}$. The equilibrium is made by the axisymmetric equilibrium plus the island, e.g. $\boldsymbol{B} = \boldsymbol{B}_0 + \delta \boldsymbol{B}_{isl}$.

The governing equations for shear Alfvén modes can be derived from Ohm's law (Eq.2.21), and the quasi-neutrality condition, obtained as the divergence of Ampére's law (Eq.2.22). Quasi-neutrality condition is $\vec{\nabla} \cdot \delta \vec{J} = 0$, i.e.,

$$\vec{\nabla} \cdot \delta \vec{J}_\perp + \vec{B} \cdot \vec{\nabla} \left(\frac{\delta J_\parallel}{B} \right) = 0 \tag{2.26}$$

where $\delta \vec{J}$ is the SAW perturbed current, and $\perp$ and $\parallel$ refer, respectively, to the perpendicular and parallel directions with respect to the equilibrium magnetic field vector (axisymmetric plus island field) $\hat{b} \equiv \vec{B}/B$.

The perpendicular current perturbation is obtained from the perpendicular force balance, i.e.,

$$\begin{aligned} \delta \boldsymbol{J}_\perp \;=\; & \frac{c}{B^2} \boldsymbol{B} \times \varrho \frac{d}{dt} \delta \boldsymbol{v}_\perp + \frac{c}{B^2} \boldsymbol{B} \times \boldsymbol{\nabla} \delta p + \\ & + \frac{J_\parallel}{B} \delta \boldsymbol{B}_\perp - \frac{(\delta B_\parallel B)}{B^2} \boldsymbol{J}_\perp \end{aligned} \tag{2.27}$$

The quasi-neutrality condition, Eq. 2.26, takes the form:

$$\begin{aligned} & -\frac{c^2}{4\pi} \boldsymbol{\nabla} \cdot \Big(\frac{1}{v_A^2} \frac{d}{dt} \boldsymbol{\nabla}_\perp \delta\phi \Big) + \boldsymbol{B} \cdot \boldsymbol{\nabla} \Big(\frac{\delta J_\parallel}{B} \Big) - \frac{\boldsymbol{J}}{B^2} \cdot \boldsymbol{\nabla} \Big(4\pi \delta p + \delta B_\parallel B \Big) \\ & \qquad + 8\pi \frac{\boldsymbol{J}_\parallel}{B^2} \cdot \boldsymbol{\nabla} \delta p + 2c \Big(\frac{\boldsymbol{B}}{B} \times \boldsymbol{\kappa} \Big) \cdot \boldsymbol{\nabla} \delta p \\ & - (\delta B_\parallel B) \boldsymbol{J} \cdot \nabla \Big(\frac{1}{B^2} \Big) + (\boldsymbol{\nabla} \times \delta \boldsymbol{A}) \cdot \boldsymbol{\nabla} \Big(\frac{J_\parallel}{B} \Big) = 0 \end{aligned} \tag{2.28}$$

Here $\boldsymbol{\kappa} = \boldsymbol{b} \cdot \boldsymbol{\nabla} \boldsymbol{b}$ is the curvature of the equilibrium magnetic field, $\boldsymbol{b} = \boldsymbol{B}/B$ being the unit vector. The island perturbed velocity is contained implicitly in the total time derivative d/dt, and the island perturbed field in the total magnetic field $\boldsymbol{B}$ and in the total current $\boldsymbol{J}$. These

nonlinearities will be made explicit in Eq. 2.31. Eq. 2.28 is very general, and describes nonlinearly shear Aflvén waves (SAW), fast magneto-sonic waves (FMS) and slow magneto-sonic waves (SMS). These three wave branches are the only ones predicted by MHD theory. We are not interested in the branch of FMS waves, but only in the compressible SAW, in the presence of a magnetic island. We can neglect the FMS interaction with SAW in our set of equations, using the condition:

$$4\pi\delta p + B\delta B_{\parallel} \;=\; 0 \tag{2.29}$$

which selects only SAW and slow magneto-sonic waves. Moreover, SAW in low-beta plasmas have parallel component of the perturbed magnetic field negligible with respect to the perpendicular component: $\delta B_{\parallel}/\delta B_{\perp} \ll 1$. This reads, in terms of the vector potential: $\delta \boldsymbol{A} \simeq \delta A_{\parallel}\hat{\boldsymbol{b}}$. With this hypothesis, we obtain from the parallel component of Ampére's law (Eq. 2.22):

$$4\pi\delta J_{\parallel} \;= c\,\hat{b}\cdot\vec{\nabla}\times\left(\vec{\nabla}\times\delta\vec{A}\right) \simeq\; -c\,\nabla_{\perp}^{2}\,\delta A_{\parallel} \tag{2.30}$$

Now, we substitute Eqs. 2.29 and 2.30 into Eq. 2.28, and consider modes which are radially localized with respect to equilibrium scales. The forth term in Eq. 2.28 can be neglected with respect to the fifth one, using the hypothesis $k_{\parallel} \ll k_{\perp}$. Moreover, the sixth term can also been neglected because involves only radial derivative corresponding to the equilibrium, while all other terms involve radial derivatives corresponding to the SAW perturbation, which is supposed to be more radially localized. We obtain:

$$\frac{\partial}{\partial t}\boldsymbol{\nabla}\cdot\Big(\frac{c}{v_A^2}\boldsymbol{\nabla}_{\perp}\delta\phi\Big) + (\boldsymbol{v}_{isl}\cdot\boldsymbol{\nabla})\boldsymbol{\nabla}\cdot\Big(\frac{c}{v_A^2}\boldsymbol{\nabla}_{\perp}\delta\phi\Big) + (\boldsymbol{B}_0+\boldsymbol{B}_{isl})\cdot\boldsymbol{\nabla}\Big(\frac{\nabla_{\perp}^2}{B}\delta A_{\parallel}\Big)$$

$$-8\pi\Big(\frac{(\boldsymbol{B}_0+\boldsymbol{B}_{isl})}{B}\times\boldsymbol{\kappa}\Big)\cdot\boldsymbol{\nabla}\delta p - \frac{4\pi}{c}\boldsymbol{\nabla}\Big(\frac{J_{\parallel,0}+J_{\parallel,isl}}{B}\Big)\cdot(\boldsymbol{\nabla}\times\delta\boldsymbol{A}) = 0 \tag{2.31}$$

This is the nonlinear vorticity equation for SAW in low-beta plasmas, which corresponds directly to the linear vorticity equation derived in reference [10], generalized to an equilibrium with a magnetic island. In this way the role of the *geodesic* component (that is the poloidal component of the curvature $\boldsymbol{\kappa}$ in the plane tangent to the magnetic flux surface) is made explicit. When the geodesic curvature goes to zero, such as in the cylindrical limit, there is no more pressure coupling affecting the linear SAW continuous spectrum. That is why, even for non-zero beta, the beta-induced gap in the lower part of the continuous spectrum is not

observed in cylindrical geometry. With respect to reference [10], we have retained here the last term in Eq. 2.28, because it is relevant to derive the Hain-Lüst equation, Eq. 4.3. On the other hand, for continuum modes, which are radially singular in the proximity of the resonance surfaces, the last term in Eq. 2.28 can be neglected.

Here, we are not interested in modeling the magnetic island evolution. Therefore, we study the SAW dynamics with a perturbative theory, assuming that the magnetic island dynamics is not affected by the SAW presence. Therefore, we retain the pressure gradient contribution of the SAW and neglect the contribute of the magnetic island fluctuation, considering the magnetic island as a quasi-static perturbation, which modifies the axisymmetric equilibrium. The nonlinearity in pressure is not expected to change qualitatively the continuous spectrum structure, nor the frequency of the Alfvén eigenmodes in the presence of the magnetic island, and therefore it is reasonable assumption to neglect it. Nevertheless, it is expected to play an important role in the Alfvén mode drive mechanism [36], which is not discussed in this dissertation, and will be faced in a dedicated paper.

Now, give the general definition of the electric field as a function of the scalar and vector potentials:

$$\boldsymbol{E} = -\boldsymbol{\nabla}\phi - \frac{1}{c}\frac{\partial \boldsymbol{A}}{\partial t} \tag{2.32}$$

and we take the parallel component of the nonlinear form, labeling with a δ the quantities referring to the SAW perturbation:

$$\boldsymbol{E}_\parallel = \delta\boldsymbol{E}_\parallel + \boldsymbol{E}_{\parallel isl} = -\frac{\boldsymbol{B}_0\cdot\boldsymbol{\nabla}}{B_0}\delta\phi - \frac{\boldsymbol{B}_{isl}\cdot\boldsymbol{\nabla}}{B_0}\delta\phi - \frac{\boldsymbol{B}_0\cdot\boldsymbol{\nabla}}{B_0}\phi_{isl} -$$
$$- \frac{\delta\boldsymbol{B}\cdot\boldsymbol{\nabla}}{B_0}\phi_{isl} - \frac{1}{c}\frac{\partial\delta A_\parallel}{\partial t} - \frac{1}{c}\frac{\partial A_{\parallel isl}}{\partial t} \tag{2.33}$$

Now we model the SAW perturbation consistently with ideal MHD theory, so that $\delta\boldsymbol{E}_\parallel = 0$, and we model the dynamics of the magnetic island as independent of the SAW perturbation:

$$\boldsymbol{E}_{\parallel isl} = -\frac{\boldsymbol{B}_0\cdot\boldsymbol{\nabla}}{B_0}\phi_{isl} - \frac{1}{c}\frac{\partial A_{\parallel isl}}{\partial t}$$

In the case of the magnetic island, $\boldsymbol{E}_\parallel$ is not zero and, for example, in a resistive MHD theory, is given by $\boldsymbol{E}_{\parallel isl} = \eta\boldsymbol{J}_{\parallel isl}$. We focus now on the SAW perturbation dynamics. After these considerations, and using

$\delta \boldsymbol{B} = -(\boldsymbol{B}_0 \times \boldsymbol{\nabla}\delta A_\parallel)/B_0$ and $\boldsymbol{v}_{isl} = (c\boldsymbol{B}_0 \times \boldsymbol{\nabla}_\perp \phi_{isl})/B_0^2$, Eq. 2.33 can be rewritten as:

$$\frac{1}{c}\frac{\partial \delta A_\parallel}{\partial t} = -\frac{\boldsymbol{B}_0 \cdot \boldsymbol{\nabla}}{B}\delta\phi - \frac{\boldsymbol{B}_{isl} \cdot \boldsymbol{\nabla}}{B}\delta\phi - \frac{\boldsymbol{v}_{isl} \cdot \boldsymbol{\nabla}}{c}\delta A_\parallel \tag{2.34}$$

Equations (2.31) and (2.34) describe the evolution of the SAW vector and scalar potentials in low-beta approximation. The pressure can explicitly be written in terms of $\delta\phi$ assuming an equation of state. In the following sections the linearized form of these equations will be derived for low-frequency SAW modes, corresponding to SAW perturbations in a tokamak equilibrium in the absence of magnetic islands. The reduced nonlinear equations will be also discussed, keeping only the dominant three wave nonlinear couplings. These describe SAW excitations in the presence of finite amplitude magnetic islands.

2.2.2 Limit case of an equilibrium with no islands

Equations (2.20), (2.31), and (2.34), can be linearized with respect to the magnetic island perturbed fields, recovering the equations governing the SAW dynamics in an equilibrium with no magnetic islands. This has been extensively studied in literature and the main results are the radial structure of SAW continuous spectrum, and the theory of Alfvén instabilities, in an axisymmetric tokamak geometry. In this section, we derive the model equations for SAW valid in tokamak geometry, recovering a selected result, namely the existence of a beta-induced gap in the low part of the SAW continuous spectrum. This is the gap where beta-induced AE (BAE) exist.

We start by linearizing the the parallel component of Ohm's law, Eq. 2.34, namely considering a vanishing magnetic island. Moreover, decomposing the perturbation by a temporal Fourier integral we can consider a temporal behavior as parameterized by a frequency ω. We obtain:

$$i\frac{\omega}{c}\,\delta A_\parallel = \frac{(\boldsymbol{B_0} \cdot \boldsymbol{\nabla})}{B_0}\delta\phi \tag{2.35}$$

In the same way, the linearized equation of state, Eq. 2.20 can be put in the form:

$$\begin{aligned} -i\omega p = -\gamma P_0 \boldsymbol{\nabla} \cdot \boldsymbol{v} - \boldsymbol{v} \cdot \boldsymbol{\nabla} P_0 \simeq \\ \simeq -\gamma c P_0 \Big(\boldsymbol{B_0} \times \frac{2\boldsymbol{\kappa}}{B_0^2}\Big) \cdot \boldsymbol{\nabla}_\perp \delta\phi + c\Big(\boldsymbol{B_0} \times \frac{\boldsymbol{\nabla} P_0}{B_0^2}\Big) \cdot \boldsymbol{\nabla}_\perp \delta\phi \end{aligned} \tag{2.36}$$

Now we focus on continuum modes, which are strongly radially localized. This allows us to retain only the relevant terms of Eq. 2.31, namely

the ones containing the highest radial derivatives. With this hypothesis, the SAW vorticity equation, Eq. 2.31, can be cast in the following form:

$$\boldsymbol{\nabla}\cdot\Big(\frac{-ic\omega}{v_A^2}\boldsymbol{\nabla}_\perp\delta\phi\Big)+\boldsymbol{B_0}\cdot\boldsymbol{\nabla}\Big(\frac{\nabla_\perp^2}{B}\delta A_\parallel\Big)-8\pi\Big(\frac{\boldsymbol{B}_0}{B}\times\boldsymbol{\kappa}\Big)\cdot\boldsymbol{\nabla}\delta p=0 \quad (2.37)$$

Substituting the expression of p from Eq. 2.36 into Eq. 2.37, we can obtain an equation for continuum modes in a tokamak geometry, for the scalar potential only:

$$\boldsymbol{\nabla}\cdot\Big(\frac{\omega^2}{v_A^2}\boldsymbol{\nabla}_\perp\delta\phi\Big)+\Big(\boldsymbol{B_0}\cdot\boldsymbol{\nabla}\Big)\Big[\frac{1}{B_0^2}\nabla_\perp^2\Big(\boldsymbol{B_0}\cdot\boldsymbol{\nabla}\Big)\Big]\delta\phi-$$

$$-4\pi\gamma\frac{P_0}{B_0^2}\Big[\Big(\boldsymbol{B_0}\times\frac{2\boldsymbol{\kappa}}{B_0}\Big)\cdot\boldsymbol{\nabla}_\perp\Big]^2\delta\phi+4\pi\Big[\Big(\boldsymbol{B_0}\times\frac{2\boldsymbol{\kappa}}{B_0^2}\Big)\cdot\boldsymbol{\nabla}_\perp\Big]\Big[\Big(\boldsymbol{B_0}\times\frac{\boldsymbol{\nabla}P_0}{B_0^2}\Big)\cdot\boldsymbol{\nabla}_\perp\Big]\delta\phi=0 \quad (2.38)$$

As common to all continuum shear-Alfvén waves, we recognize the first term as the *inertia* term, in which the mass density appears, because of the ideal frozen-in law, and the second one called the *field-line bending* term, describing the restoring force of the magnetic field against perpendicular displacement. The third and the fourth terms are due to pressure. The third one, proportional to β and to the geodesic curvature squared, is the *compressibility* term, becoming important only when we consider low-frequency waves. The fourth one is the *ballooning - interchange* term.

In linear theory, namely in the absence of magnetic islands, magnetic flux surfaces are topologically equivalent to cylindrical nested surfaces. SAW localized perpendicularly with respect to the flux surfaces, have therefore spatial variation mainly in the radial direction, and the velocities have mainly poloidal component. In this case, Eq. 2.38 simplifies further. In fact, the ballooning term is given by the radial component of the velocity and can be neglected. Moreover, here we are not interested in the coupling between different modes due to toroidicity, and therefore we consider v_A as a constant. We can finally write the linearized equation for SAW modes in the low-frequency part of the continuous spectrum [10, 14]:

$$\frac{\omega^2}{v_A^2}\nabla_\perp^2\delta\phi+\frac{B_0}{qR}\frac{\partial}{\partial\hat{\theta}}\Big(\frac{1}{B_0^2}\nabla_\perp^2\frac{B_0}{qR}\frac{\partial}{\partial\hat{\theta}}\Big)\delta\phi-4\pi\gamma\frac{P_0}{B_0^2}\kappa_s^2\,\nabla_\perp^2\delta\phi=0 \quad (2.39)$$

Here $\hat{\theta}$ is the generalized poloidal angle, defined by $\boldsymbol{b}\cdot\boldsymbol{\nabla}=ik_\parallel=(1/qR)\partial/\partial\hat{\theta}$, and $\kappa_s=(2\boldsymbol{b}\times\boldsymbol{\kappa})_s$ is the geodesic curvature, defined as twice the component of the curvature in the plane tangent to the flux

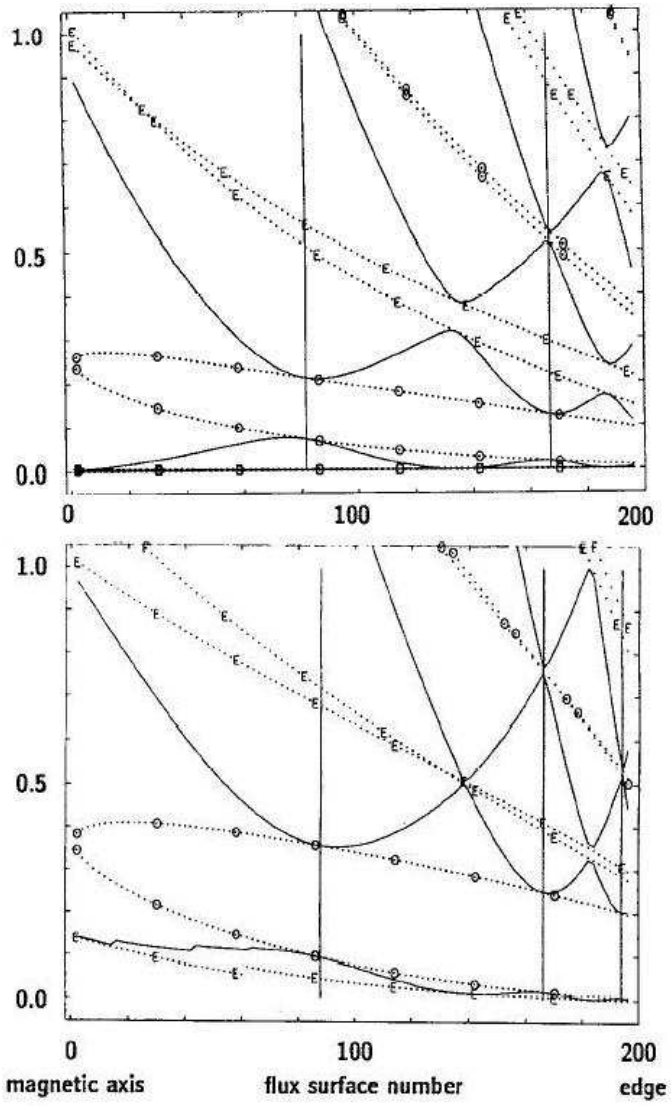

Figure 2.4: Continuous spectrum of shear Alfvén waves in axisymmetric toroidal geometry with $\beta = 0$ (upper figure) and $\beta = 2\%$ (lower figure) [14]. The continuum frequency is plotted as a function of flux surface number. The magnetic axis is at surface number 0, the edge at surface number 197. The dotted curves are the envelopes. Vertical lines mark q values at which the Alfvén wave frequency matches the envelope frequency. The beta-induced gap is present at low frequencies in the $\beta = 2\%$ case, while it is absent in the $\beta = 0$.

surface. We have neglected here the poloidal dependence of the Alfvén velocity, that gives the toroidicity induced gap in an upper part of the continuous spectrum, because out of our treatment. Instead, we have kept the pressure term, whose contribution is important at low frequencies, creating the beta-induced gap.

We can decompose now the mode in Fourier series in the $\hat{\theta}$ space, and average the geodesic curvature $\kappa_s \simeq 2\sin\hat{\theta}/R$ along the magnetic field line:

$$\frac{d}{dr}D(r)\frac{d}{dr}\delta\phi = \frac{d}{dr}\Big(\frac{\omega^2}{v_A^2} - k_\parallel(r)^2 - \frac{\omega^2_{BAE-CAP}}{v_A^2}\Big)\frac{d}{dr}\delta\phi = 0 \qquad (2.40)$$

where

$$\omega^2_{BAE-CAP} = \frac{\gamma\beta}{R^2}v_A^2 \qquad (2.41)$$

is the beta-induced Alfvén Eigenmode continuum accumulation point (BAE-CAP), as derived with the fluid theory [14], and r is a generic radial coordinate, labeling the flux surfaces. Equation 2.40, as shown in the Introduction (Sec. 1.2), has a singular solution near the resonance surface of a given ω, defined as the geometrical location where $D(r) = 0$. In proximity of the resonance surface, the radial group velocity vanishes and the wave energy is absorbed by the plasma at a resonance. Here we have shown that the spectrum of resonances, named continuous spectrum, has a gap in the low-frequency part:

$$\omega^2(r) = k_\parallel^2(r)v_A^2 + \omega^2_{BAE-CAP} \qquad (2.42)$$

Adding higher order terms in ε would give rise to the formation of more complicated structures and gaps in the SAW continuous spectrum due to toroidicity, ellipticity of the tokamak section and other geometrical effects [3].

Moreover, the inclusion of kinetic effects gives a correction in the value of the BAE-CAP frequency (Eq. 2.41), which has the advantage of being *not* dependent on the chosen equation of state and on the relative γ parameter [23]:

$$\omega^2_{BAE-CAP} = \frac{1}{R_0^2}\frac{2T_i}{m_i}\Big(\frac{7}{4} + \frac{T_e}{T_i}\Big) \qquad (2.43)$$

Here T_i and T_e are the ion and electron temperatures and m_i is the ion mass. In the following, we will not need an explicit form of the BAE-CAP frequency, that will be treated linearly as an upward-shift in the continuous spectrum.

2.2.3 Nonlinear case: SAW in the presence of an island

When SAW are excited in the presence of a finite amplitude fluctuation we cannot use anymore the linear treatment in axisymmetric equilibrium. In this case it is necessary to develop a nonlinear treatment, in which the equilibrium, the SAW and the fluctuation coexist. The magnetic island is treated here as a generic fluctuation without entering the nature of its excitation or its dynamics.

Before deriving our model equations for the specific case of an equilibrium with quasi-static magnetic islands in tokamak plasmas, we want here to show a peculiar case that occurs in nonlinear dynamics of SAW. This case, known as *Alfvénic state* [18, 19], is a self-consistent nonlinear state, occurring when the hypothesis of incompressibility is satisfied in uniform plasmas. Under these conditions, the general vorticity equations, Eq. 2.28, and Ohm's law, Eq. 2.34, can be written in the form:

$$\frac{c}{v_A^2}\frac{\partial^2}{\partial t^2}\nabla_\perp^2\delta\phi + \frac{c}{v_A^2}\frac{\partial}{\partial t}\Big(\boldsymbol{v_{isl}}\cdot\boldsymbol{\nabla}\Big)\nabla_\perp^2\delta\phi + \frac{1}{B_0}\frac{\partial}{\partial t}\Big(\boldsymbol{B_0}\cdot\boldsymbol{\nabla}\Big)\nabla_\perp^2\delta A_\parallel +$$

$$+\frac{1}{B_0}\frac{\partial}{\partial t}\Big(\boldsymbol{B_{isl}}\cdot\boldsymbol{\nabla}\Big)\nabla_\perp^2\delta A_\parallel - \frac{4\pi}{c}\boldsymbol{\nabla}\Big(\frac{J_{\parallel 0}+\delta J_{\parallel isl}}{B_0}\Big)\cdot\frac{\partial}{\partial t}\delta\boldsymbol{B}_\perp = 0 \quad (2.44)$$

$$\frac{1}{c}\frac{\partial\delta A_\parallel}{\partial t} + \frac{\boldsymbol{v}_{isl}\cdot\boldsymbol{\nabla}}{c}\delta A_\parallel + \frac{\boldsymbol{B}_0\cdot\boldsymbol{\nabla}}{B}\delta\phi + \frac{\boldsymbol{B}_{isl}\cdot\boldsymbol{\nabla}}{B}\delta\phi = 0 \quad (2.45)$$

where we have neglected SMS waves with the hypothesis of incompressibility, and we have neglected the FMS waves, selecting the polarization $\delta B_\parallel = 0$. A solution of this system is given by:

$$\delta\phi = -\delta A_\parallel \quad (2.46)$$

$$\frac{\delta\boldsymbol{v}_{isl}}{v_A} = -\frac{\delta\boldsymbol{B}_{isl}}{B_0} \quad (2.47)$$

$$\omega = k_\parallel v_A \quad (2.48)$$

propagating along the magnetic field, with $\boldsymbol{k} = k_\parallel\hat{\boldsymbol{b}}$. Eqs. 2.46 and 2.47 are known as the Walén relations on the polarization [17]. This means that, when the island perturbation and the SAW perturbation follow the linear dynamics of pure SAW, then the nonlinear Maxwell and Reynolds stress tensor terms kill each other identically. As a consequence, the dynamics has no effective nonlinear contribution due to the interaction of waves. The fact that two waves can travel without interacting with each

other has practical application in understanding the physics of Alfvén *solitons*, namely self-reinforcing solitary Alfvén waves (wave packets or pulses) which maintain their shape while they travel in the medium.

In tokamaks, the plasma is not uniform and magnetic islands have a dynamics which is not properly described by the Walén relation. In particular, their evolution is much slower than the SAW one, so that for typical frequencies of interest $\omega_{isl} \ll \omega$. This breaks the balance between the Reynolds stress tensor term and the Maxwell stress tensor term, and makes the former negligible. In the particular cases in which the magnetic islands are locked in the plasma, due to the magnetic interaction with the external iron shell asymmetries, the value of v_{isl} is identically zero.

Therefore, in our model we neglect the Reynolds stress tensor term in Eq. 2.31 and the system reduces to an axisymmetric equilibrium with static magnetic islands, described by the equation:

$$\begin{aligned}
&\boldsymbol{\nabla}\cdot\Big(\frac{\omega^2}{v_A^2}\boldsymbol{\nabla}_\perp\delta\phi\Big)+(\boldsymbol{B}\cdot\boldsymbol{\nabla})\Big[\frac{\nabla_\perp^2}{B_0^2}(\boldsymbol{B}\cdot\boldsymbol{\nabla})\delta\phi\Big]- \\
&-\frac{4\pi\gamma P}{B^2}\Big[\Big(\boldsymbol{B}\times\frac{2\boldsymbol{\kappa}_s}{B}\Big)\cdot\boldsymbol{\nabla}_\perp\Big]^2\delta\phi-\frac{4\pi}{c}\boldsymbol{\nabla}\Big(\frac{J_\parallel}{B}\Big)\cdot\big[\boldsymbol{\nabla}\times(\nabla_\parallel\delta\phi)\big]_\perp+ \\
&+4\pi\Big[\Big(\boldsymbol{B}\times\frac{2\boldsymbol{\kappa}_s}{B^2}\Big)\cdot\boldsymbol{\nabla}_\perp\Big]\Big[\Big(\boldsymbol{B}\times\frac{\boldsymbol{\nabla}P}{B^2}\Big)\cdot\boldsymbol{\nabla}_\perp\Big]\delta\phi=0 \qquad (2.49)
\end{aligned}$$

where the equilibrium magnetic field and pressure are referred to the sum of the axisymmetric equilibrium plus the island perturbation. This equation is valid in general for Alfvén Eigenmodes (AE) and continuum modes.

In the case of continuum modes, a further simplification can be made, by considering that the modes are radially localized in a narrow layer, which is much thinner than the equilibrium scales. This allows us to neglect the forth and fifth terms in Eq. 2.49. The result is:

$$\frac{\omega^2}{v_A^2}\nabla_\perp^2\delta\phi+\nabla_\parallel\nabla_\perp^2\nabla_\parallel\delta\phi-\frac{\omega_{BAE-CAP}^2}{v_A^2}\nabla_\perp^2\delta\phi=0 \qquad (2.50)$$

This equation describes the SAW dynamics of continuum modes in the presence of a quasi-static magnetic island. It will be used for the derivation of the continuous spectrum of SAW traveling both inside and outside a magnetic island. Here, $\omega_{BAE-CAP}$ is the frequency of the BAE continuum accumulation point, whose value in fluid theory is given by Eq. 2.41 (see Ref. [14, 22]): $\omega_{BAE-CAP}^2 = \gamma\beta v_A^2/R_0^2$. Here, we adopt the value given by the gyro-kinetic theory [23], expressed in Eq. 2.43. The poloidal

dependence of the Alfvén velocity, causing the toroidicity induced coupling at Alfvénic frequencies, has been neglected in our model equation for continuum modes, Eq. 2.50. Therefore, our model consists of an effective 2D equilibrium, where the only curvature effects are contained in the BAE-CAP frequency. We focus on frequencies in the low-part of the continuous spectrum. We consider the nonlinear contributions coming from the Reynolds stress tensor term $(v_{isl} \cdot \nabla)$ and the Maxwell stress tensor term $(B_{isl} \cdot \nabla)$, while neglecting the pressure nonlinearity contribution. This is justified when studying the real part of the Alfvén mode frequency. On the other hand, the pressure nonlinearity is expected to play an important role in changing the imaginary part of the frequency, by determining the drive mechanism [36].

Chapter 3

Continuous spectrum

As discussed in Sec. 1.2, SAW in a nonuniform equilibrium experience continuum damping, due to singular structures that are formed in the proximity of resonant surfaces. Hence, if a surface magnetohydrodynamic wave is excited by an external coupler, the wave will be phase mixed by this resonance and its energy will be dissipated to the plasma. The resonance frequency spectrum is called *continuous spectrum*. The importance of understanding the continuous spectrum structure is clear if one faces the stability problem of a tokamak and its potential impact on reaching the ignition condition.

The SAW continuous spectrum in an axisymmetric equilibrium can be modified by the interaction with low-frequency MHD fluctuations, such as magnetic islands. In last chapter we have derived our fluid model equations for the SAW continuum modes in the presence of a finite size magnetic island in finite-β plasmas. He keep into account only toroidicity effects due to the geodesic curvature, which are responsible for the BAE gap in the low frequency SAW continuous spectrum. In this chapter, the local differential equation yielding the nonlinear SAW continuum structure is solved numerically, with a shooting method code, in the whole spatial range of interest (both outside and inside the island), and analytically, at the O-point and at the separatrix, where the equilibrium quantities can be approximated in simple form.

New continuum accumulation points are found at the O-point of the magnetic island (MiO-CAP). The beta-induced Alfvén Eigenmodes continuum accumulation point (BAE-CAP) is found to be positioned at the separatrix flux surface. The BAE-CAP frequency is nonlinearly modified by the presence of the magnetic island, with different values depending on the mode numbers and parity of the eigenfunctions. Moreover, we find that a wide frequency gap is formed, analogous to the ellipticity induced

Alfvén Eigenmode (EAE) gap in tokamaks. This is due to the strong eccentricity of the island cross section.

3.1 Continuous spectrum inside the magnetic island

3.1.1 Approximated result from the q-profile

Here, we want to give an approximated evaluation of the continuous spectrum frequency, using the formula that works for a geometry with cylindrical symmetry. The result is not rigorous in general and has differences with the result provided in subsequent sections, obtained solving the rigorous eigenvalue problem. In fact, the regime of validity restricts to $x \ll 1$ and $e \ll 1$, where the magnetic island flux surfaces satisfy the hypothesis of cylindrical symmetry. Nevertheless, it is worthwhile to have an easy formulation which can already give useful hints on the final results, in the whole region of interest $0 < x < 1$, and for all values of e.

In the model used in this section, we approximate the continuous spectrum frequency as:

$$\Omega_A^2 = \frac{(\omega^2 - \omega^2_{BAE-CAP})}{\omega_A^2} = \frac{v_A^2\, k_\parallel^2}{\omega_A^2} = \frac{1}{q^2(x)}\big(\tilde{n}q(x) - j\big)^2 \tag{3.1}$$

with $q(x)$ given in Eq. 2.15, and $\omega_A = v_A/Z_0$. The approximation consists in defining a parallel component of the wave-vector $k_\parallel$, whose definition is valid in the cylindrical theory: $k_\parallel = (\tilde{n}q - j)/(qZ_0)$, with $\tilde{n}$ and j the azimuthal and poloidal number, respectively along the ζ and θ coordinates, in the frame of reference of the flux tube inside the island.

Plots of $\Omega_A^2(x)$ obtained from Eq. 3.1 are shown in Fig. 3.1 and 3.2, for several values of $\tilde{n}$ and j. The first result is that, when a magnetic island with typical size is considered, the continuous spectrum frequencies are very low with respect to the Alfvén frequency (corresponding to $\Omega_A \ll 1$), due to the high value of the safety factor: $\Omega_A \sim 1/q(x) \sim \sqrt{M}$. Moreover, we can see that, close to the cylinder axis, where $q(0) = (\sqrt{M} n_{isl})^{-1}$, the equilibrium profiles are flat and therefore all frequency branches reach constant values. For $\tilde{n} \neq 0$, different branches intersect in different positions and no gaps are created, because of the cylinder symmetry which is assumed when using Eq. 3.1. Nevertheless, when the rigorous eigenvalue problem is solved, then we expect to find gaps in the continuous spectrum in the proximity of the intersections. This is due to the noncircularity

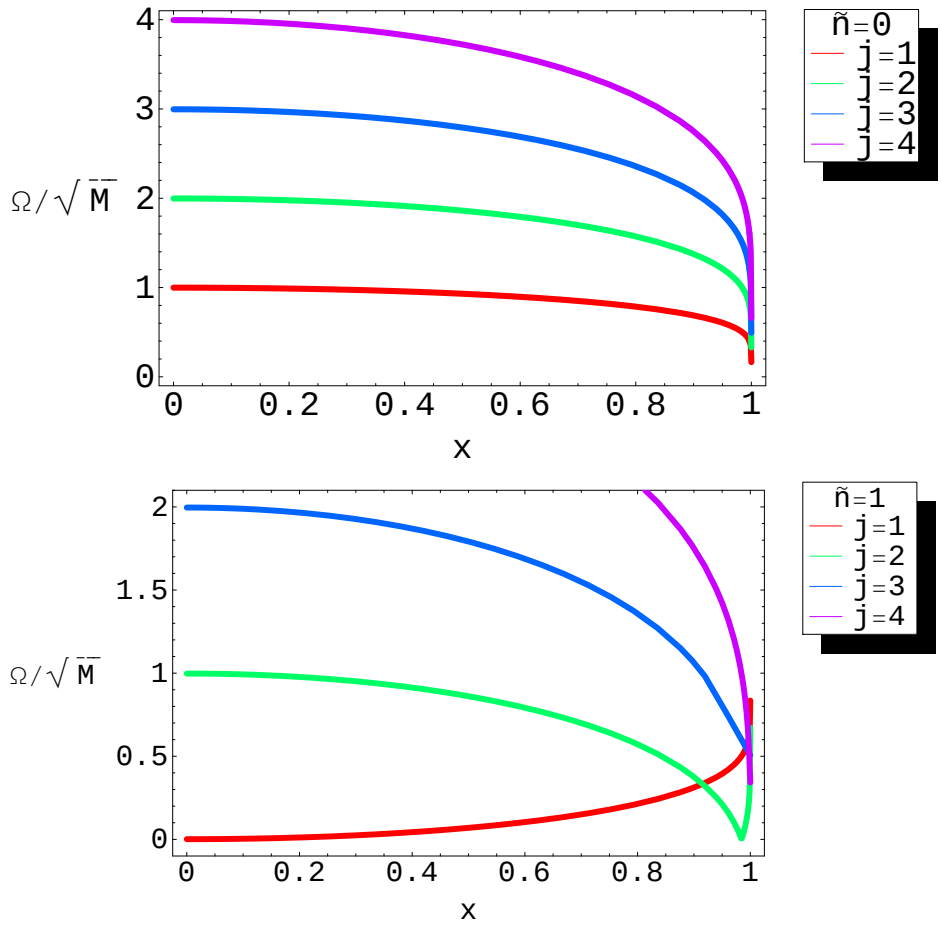

Figure 3.1: Continuous spectrum of SAW inside a magnetic island, $\Omega(x)$, calculated with the approximated formula given in Eq. 3.1, in the limiting case of flux surfaces with circular cross section: $e = 0$. Here $\varepsilon = 0.1$, $q_0 = 2$, $s_0 = 1$. The frequency is normalized to the Alfvén frequency, as in Eq. 3.1, and to the magnetic island amplitude parameter M. The position is labeled by $x = \rho/\rho_{sx}$. We can see that, in this cylinder limit, the various branches intersect without splitting. Here the cases of $\tilde{n} = 0$ and $\tilde{n} = 1$ are considered.

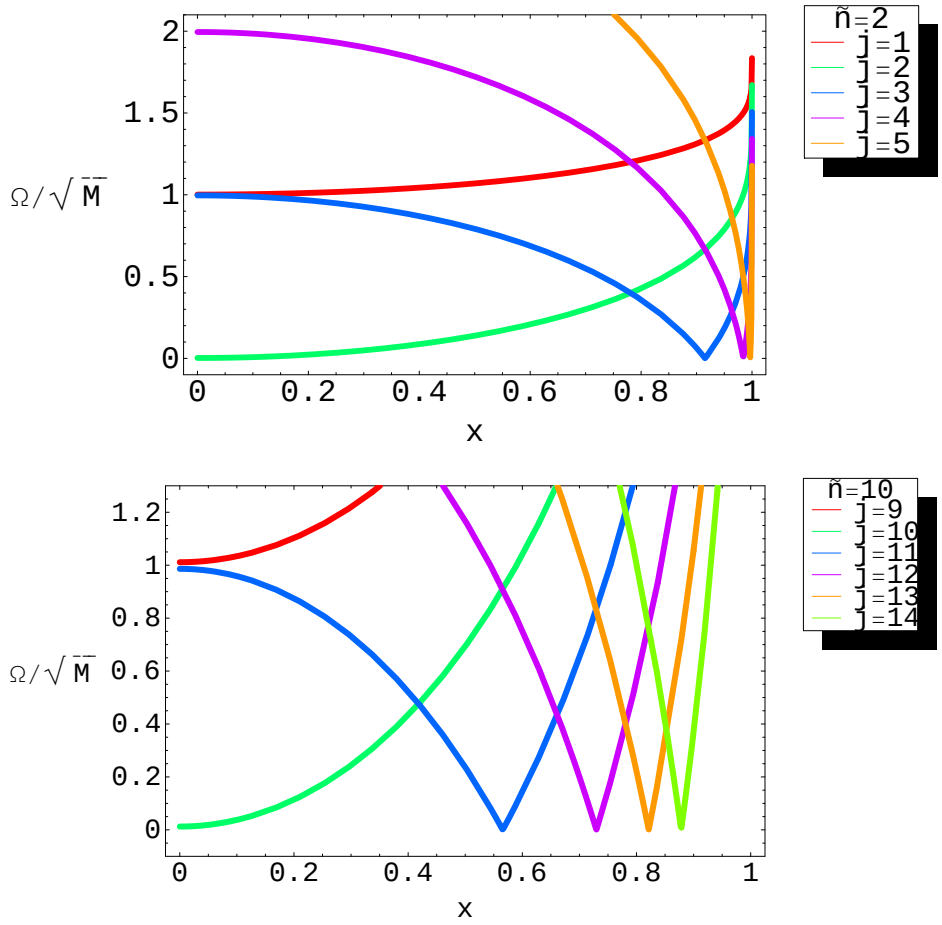

Figure 3.2: Continuous spectrum of SAW inside a magnetic island, $\Omega(x)$, calculated with the approximated formula given in Eq. 3.1, in the limiting case of flux surfaces with circular cross section: $e = 0$. Same parameters as for Fig. 3.1, but here the cases of $\tilde{n} = 2$ and $\tilde{n} = 10$ are considered. Compare these results with the result of the case where the cylinder symmetry approximation is released, and the geometrical effects due to the noncircularity of the flux surface's cross section are retained (Fig. 3.3).

of the flux surfaces, which creates gaps analogously to the continuous spectrum in tokamaks (see Fig. 1.1). At the separatrix, we see that the frequency of the branches with $\tilde{n} = 0$ goes to small values, corresponding to a continuum accumulation point (CAP). The frequency of the CAP is null when calculated with Eq. 3.1. Nevertheless, we will see in next sections, that when the rigorous eigenvalue problem is solved, a nonlinearly modified CAP appears at the separatrix (see Fig. 3.4).

3.1.2 Eigenvalue problem

In section 2.1.2, we have described the region inside a magnetic island flux tube with a cylinder-like set of coordinates, labeling the magnetic flux surfaces with a radial-like coordinate ρ. This magnetic flux tube is assumed here to be the static equilibrium of the problem. In section 3.1.1, we have given an approximate solution of the continuous spectrum problem, by using the formula for the parallel wave-vector $k_{\|}$ which is valid in geometries with cylindrical geometry. Here, we want to solve the rigorous eigenvalue problem. To this extent, we put the equation for radially localized shear Alfvén modes, Eq. 2.50, which is written in a general vectorial form, in an explicit form, using a cylinder-like set of coordinates for a straight flux tube and the differential operators defined in Appendix 7.1. For perpendicularly localized modes, the parallel and perpendicular differential operators have the following form:

$$Z_0 \nabla_{\|} = \sqrt{M} n_{isl} F \frac{\partial}{\partial \theta} + \frac{\partial}{\partial \zeta} \tag{3.2}$$

$$\rho_{sx}^2 \nabla_{\perp}^2 = a \frac{\partial^2}{\partial x^2} \tag{3.3}$$

and the boundary conditions of the problem are periodicity conditions in θ and ζ on 2π circles. Moreover, using the symmetry of the equilibrium in the ζ coordinate, we can write the general solution as $\delta\phi = \hat{\phi}(x,\theta) \exp(-i\tilde{n}\zeta)$, where $\tilde{n}$ is the mode number in the ζ-direction.

For a general $\tilde{n} \neq 0$, the problem we are considering is greatly simplified if we change coordinates from (ρ, θ, ζ) to a field aligned set of coordinates (ρ, θ, ξ), where $\xi = \zeta - \chi(x,\theta)$, and $\chi = (\sqrt{M} n_{isl})^{-1} \int_0^{\theta} d\theta' / F(x,\theta')$ is the normalized incomplete elliptic integral of the first kind. In fact, we have $\boldsymbol{B} \cdot \boldsymbol{\nabla} \xi = 0$ and the parallel derivative takes the simple form $Z_0 \boldsymbol{\nabla}_{\|} = \sqrt{M} n_{isl} F \, \partial / \partial \theta$ (the change of coordinates wouldn't be necessary in the special case of $\tilde{n} = 0$, because the parallel gradient has already this form, due to the vanishing of the derivative along ζ). Finally, Eq. 2.50 is

written in the form of an eigenvalue problem:

$$\Big[\frac{\Omega^2}{Mn_{isl}^2} + \frac{F}{a}\frac{\partial}{\partial\theta}aF\frac{\partial}{\partial\theta}\Big]\tilde{\phi}'' = 0 \tag{3.4}$$

where $\Omega^2 = (\omega^2 - \omega^2_{BAE-CAP})/\omega_A^2$ is the eigenvalue, and $\tilde{\phi}'' = (\partial^2\hat{\phi}/\partial^2 x)\exp(-i\tilde{n}\chi)$ is the eigenfunction. The boundary condition $\hat{\phi}''(\theta = 0) = \hat{\phi}''(\theta = 2\pi)$ reads now $\tilde{\phi}''(\theta = 0) = \tilde{\phi}''(\theta = 2\pi)\exp(2\pi i\tilde{n}q)$, with the safety factor q defined in Eq. 2.15. In Eq. 3.4, plasma inertia and compression are contained in the first term, and magnetic field tension is contained in the second term.

It is useful to write Eq. 3.4 in the form of a Schrödinger equation. The motivation is twofold. Firstly, we can use standard shooting method techniques to solve numerically the problem in the whole range inside the island: $0 < x < 1$. Secondly, we can solve analytically the problem in the proximity of the island O-point, approximating the potential, and benchmark the numerical solution with the analytical one near the O-point. Consider an equation of the form:

$$\frac{d}{dx}g(x)\frac{d}{dx}f(x) + \Omega^2 T(x)f(x) = 0$$

with $f(x)$ the unknown function and $g(x)$ and $T(x)$ known functions. Now implement the substitution $f(x) \to h(x)/\sqrt{g(x)}$. It is straightforward to show that, in the hypothesis of $g(x) \neq 0\ \forall\, x$, this equation can be written in the form:

$$\frac{d^2}{dx^2}h(x) + \Omega^2 A(x)h(x) - V(x)h(x) = 0$$

with $A = T/g$ and $V = (g'' - g'^2/(2g))/(2g)$, g' meaning dg/dx.

In the case of continuum modes inside a magnetic island, the eigenvalue problem takes the form:

$$\frac{\partial^2}{\partial\theta^2}h + \frac{\Omega^2}{Mn_{isl}^2}A_{in}h - V_{in}h = 0 \tag{3.5}$$

with $A_{in} = 1/F^2$, $V_{in} = (g''_{in} - g'^2_{in}/(2g_{in}))/(2g_{in})$, $g_{in} = aF$, and $h = \tilde{\phi}''\sqrt{g_{in}}$. Here for the function g, the prime denotes the θ-derivative, e.g. $g' = \partial g/\partial\theta$.

Eq. 3.5 can be solved treating x as a parameter, $\Omega^2(x)$ as the eigenvalue, that is the continuous spectrum of the problem, and $h(x,\theta)$ as the eigenfunction. The solution can be found numerically in the whole spatial range of interest (in this case $0 < x < 1$, that is inside the separatrix), using a shooting method code.

3.1.3 Results for $\tilde{n} \neq 0$

The equation for SAW continuous spectrum written in the form of an eigenvalue problem in the coordinates (ρ, θ, ξ), Eq. 3.5, is an ordinary differential equation in one variable, θ, where the radial position x is treated as a parameter. It can be solved numerically, with a shooting method code for each position $0 < x < 1$, giving the continuous spectrum $\Omega^2(x)$ as result, for any value of the eccentricity $0 < e < 1$. The result is shown in Fig. 3.3 for $e \ll 1$, and for $e = 0.99$. We note that, in the case of small eccentricity $e \ll 1$, and close to the O-point $x \simeq 0$, we have $a = F = 1$ and Eq. 3.4 reduces to the problem in cylindrical geometry: $\Omega^2 = M n_{isl}^2 (\tilde{n} q - j)^2$, where j is the poloidal mode number.

The case of small eccentricity, corresponding to $M = 1$, is considered firstly. We choose typical values for the equilibrium parameters, $q_0 = 2$, $s = 1$, $n_{isl} = 1$, and consider continuum modes with mode number $\tilde{n} = 10$. In this case, we see that near the O-point, $x \simeq 0$, the result of the cylindrical geometry is recovered, as discussed above. On the other hand, for $0 < x < 1$, the flux surfaces have a non-circular cross section, and therefore the modes with different values of j are coupled. This mechanism creates a gap in the spectrum analogous to the ellipticity induced Alfvén Eigenmode (EAE) gap in tokamaks [12], dubbed here as magnetic island induced AE (MiAE) gap [25, 26]. The closer a flux surface is to the separatrix, the wider is the MiAE gap.

We repeat the calculation for a magnetic island with a reasonable size, with $M = 10^{-2}$, using the same equilibrium parameters. This corresponds to a magnetic island with $W_{isl} \simeq \sqrt{1-e}\, r_0 = 0.1\, r_0$, which is the order of magnitude of a saturated magnetic island in tokamaks. We consider modes with mode number $\tilde{n} = 1$. We find the same structure of continuous spectrum as for $M = 1$, but in this case we obtain a much wider MiAE gap. This is due to the fact that flux surfaces of a reasonable size magnetic island have a high eccentricity, which strongly couples together modes with different values of j. The MiAE gap central frequency is proportional to the magnetic island half-width. The value near the O-point is [25, 26]:

$$\Omega_{MiAE-gap} = \sqrt{M} n_{isl} = \frac{q_0 s n_{isl}}{2} \frac{W_{isl}}{r_0} \tag{3.6}$$

A gap analogous to the toroidicity induced Alfvén eigenmode (TAE) gap [10, 37] is not found here, because we consider a straight flux tube model, neglecting the effect of curvature coupling among different values of j. Nevertheless, such a toroidal MiAE gap is expected to be present

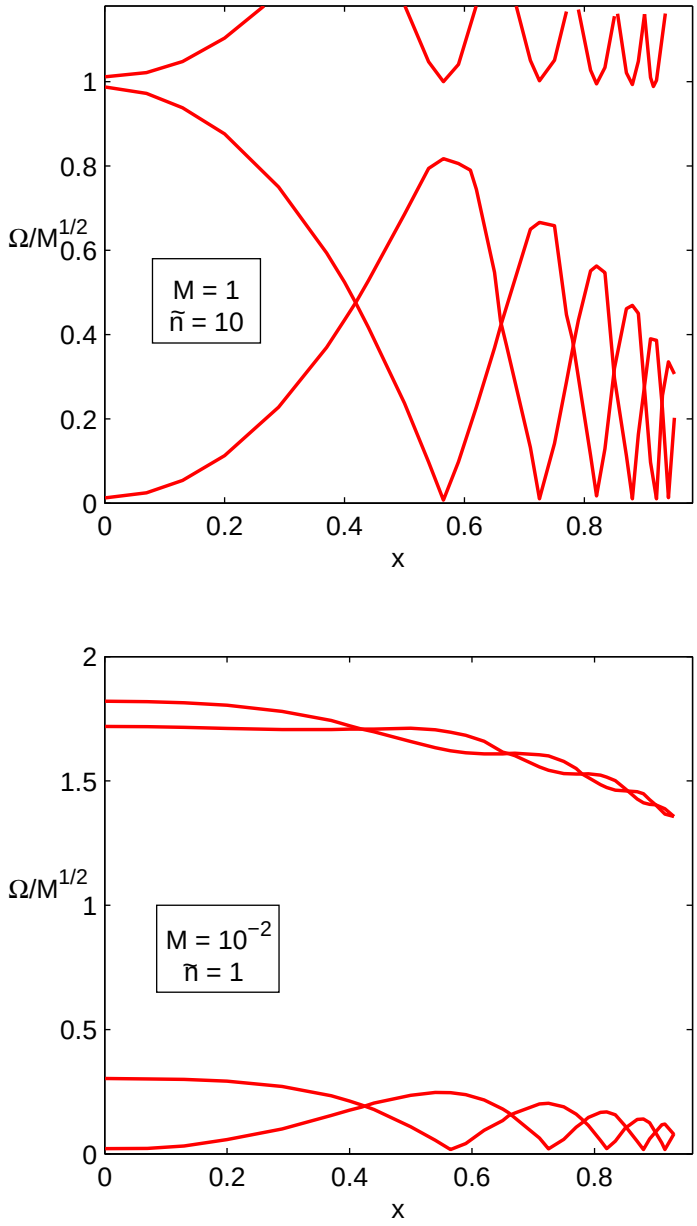

Figure 3.3: Continuous spectrum $\Omega(x)$ plotted versus the radial position inside the island. In the upper figure, the small eccentricity case, $e = 0$, corresponding to $M \simeq 1$ is shown, and modes with $\tilde{n} = 10$ are considered. In the lower figure, a typical size magnetic island is considered: $M = 10^{-2}$, corresponding to an eccentricity of $e \simeq 0.99$, and $\tilde{n} = 1$. Characteristic values of the equilibrium parameters have been chosen, with $n_{isl} = 1$. The O-point is at $x = 0$ and the separatrix at $x = 1$. A MiAE gap is found, centered at frequencies $\Omega^2 \sim M n_{isl}^2$.

inside magnetic islands, at frequencies lower than the frequencies of the ellipticity MiAE gap. Its width can be estimated as $\Delta\Omega^2 \simeq M n_{isl}^2 \varepsilon_0$. The magnetic island has also a modulation in the tokamak toroidal direction, given by the number n_{isl}. This helicity of the flux tube is neglected here and is expected to weakly couple modes of the SAW continuous spectrum with different n, analogously to the case of stellarators. These effects are not expected to qualitatively modify the MiAE gap and will be investigated in a different work as further extension of the present theory.

On the other hand, the BAE gap is considered in our model, resulting in an upward shift in the continuous spectrum of the frequencies ω^2/ω_A^2. For typical tokamak plasma parameters, $\omega_{BAE-CAP}^2/\omega_A^2 \sim \beta q_0^2$, with β denoting the ratio between plasma and magnetic pressures (see Eqs. 2.41 and 2.43). Therefore, finite compression BAE frequency gap and magnetic island induced MiAE gap are of comparable size when $M \sim \beta q_0^2$, i.e. for a typical saturated magnetic island size in tokamaks.

The central frequency of the MiAE gap can be written explicitly from Eq. 3.6, recalling the definition of the normalized frequency Ω, given in Eq. 3.1. We obtain:

$$f_{MiAE-gap} = f_{BAE-CAP}\sqrt{1 + \frac{q_0^2 s^2 n_{isl}^2}{4}\frac{W_{isl}^2}{r_0^2}\frac{f_A^2}{f_{BAE-CAP}^2}} \tag{3.7}$$

Here q_0, s, and W_{isl} are respectively the values of the safety factor and shear calculated at the rational surface of the island, and the magnetic island half-width. The value of $f_{BAE-CAP}$ is obtained from reference [23] (see Eq. 2.43):

$$f_{BAE-CAP} = \frac{1}{2\pi R_0}\sqrt{\frac{2T_i}{m_i}\left(\frac{7}{4} + \frac{T_e}{T_i}\right)} \tag{3.8}$$

For small magnetic islands, the scaling is quadratic with the magnetic island half-width and the approximate value is:

$$f_{MiAE-gap} \simeq f_{BAE-CAP} + \frac{q_0^2 s^2 n_{isl}^2}{8}\frac{W_{isl}^2}{r_0^2}\frac{f_A^2}{f_{BAE-CAP}} \tag{3.9}$$

The regime of validity of the linear approximation is given by:

$$\frac{W_{isl}}{r_0} \ll \frac{2}{q_0|s|n_{isl}}\frac{f_{BAE-CAP}}{f_A} \sim \frac{\sqrt{\beta}}{q_0|s|n_{isl}} \ ,$$

Here we can see explicitly that, in the case of low-β plasmas, the order of magnitude of the MiAE-gap can be comparable with the BAE-CAP

frequency itself. In Sec. 3.2 it will be shown that the nonlinearly modified frequency of the BAE-CAP due to the presence of the island, has the same value of the MiAE-gap central frequency (see Eq. 3.19).

3.1.4 Results for $\tilde{n} = 0$

Here we discuss the solution of Eq. 3.5, calculated numerically with a shooting method code in the range $0 < x < 1$, for any value of the eccentricity $0 < e < 1$. The result is shown in Fig. 3.4 for $e \ll 1$, and in Fig. 3.7 for $e = 0.99$. We choose typical values for the equilibrium parameters, $q_0 = 2$, $s = 1$, $\varepsilon_0 = 0.1$, $n_{isl} = 1$. The periodic boundary condition in θ is satisfied by an infinite set of solutions, labeled by $j = 1, 2, ...$ We find that the presence of magnetic islands modifies the continuous spectrum inside the island in three main ways.
1) The continuous spectrum Ω^2 reaches peaks (continuum accumulation points) at the magnetic island O-point, which are dubbed here MiO-CAP. The frequency of the MiO-CAP depends on the size of the magnetic island. In the particular case of a magnetic island with $e = 0$, the cylindrical limit CAP are recovered.
2) The BAE continuum accumulation point, defined as the position where the continuous spectrum has the minimum in frequency, is displaced from the original position at the rational surface $x = 0$ to the separatrix flux surface $x = 1$. The reason why Alfvén waves traveling in flux surfaces closer and closer to the separatrix have lower and lower resonant frequency is the vanishing of the parallel component of the local wave number ($k_\parallel$) near the X-point. The first odd eigenfunction has frequencies converging to the original BAE-CAP, whose value is the same as in an equilibrium without islands, correspondent to $\Omega^2 = 0$. All other branches converge to a nonlinearly modified BAE-CAP, whose value is $\Omega = M n_{isl}^2$.
3) The magnetic field intensity varies periodically along the field lines in an equilibrium with magnetic islands. The corresponding problem of wave propagation can be described by a periodic potential. Alfvén waves experiencing a variation of the Alfvén velocity along their path respond in different ways if their eigenfunction is even or odd with respect to this potential. This breaks the degeneration of the frequency of even and odd eigenfunctions, splitting the continuous spectrum in two lines corresponding to the two parities.

The solution of Eq. 3.5 can also be found analytically near the O-point and near the separatrix, approximating the potential and obtaining the value of the continuum accumulation points (MiO-CAP and BAE-CAP). The analytical derivation of the MiO-CAP value is shown hereafter, and

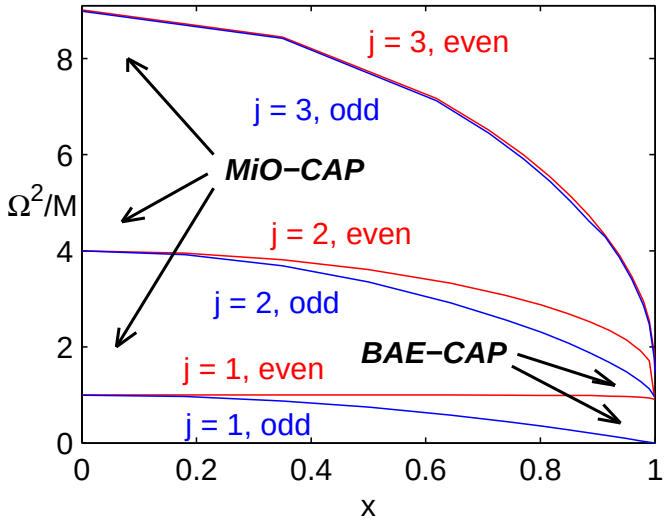

Figure 3.4: Continuous spectrum $\Omega^2(x)$ for the small eccentricity case, $e \ll 1$, corresponding to $M \simeq 1$, plotted versus the radial position inside the island. Typical values of the equilibrium parameters have been chosen and $n_{isl} = 1$. The O-point is at $x = 0$ and the separatrix at $x = 1$. The branches of both even and odd eigenfunctions are shown. At the O-point, the continuum accumulation points (MiO-CAP) recover the value of the cylinder limit. At the separatrix, the first odd frequency branch tends to the original BAE-CAP ($\Omega^2 = 0$) and the others to the nonlinearly modified BAE-CAP ($\Omega^2 = Mn_{isl}^2$).

an estimation of the nonlinearly modified BAE-CAP in Section 3.2.

3.1.5 Analytical treatment near the O-point

The value of the continuum accumulation points at the O-point of the island can be calculated analytically from Eq. (3.5), by approximating the functions A_{in} and V_{in} near the O-point. In this limit, Eq. (3.5) becomes:

$$\frac{\partial^2}{\partial\theta^2}h + \frac{\Omega^2}{Mn_{isl}^2}\,h - V_{in,0}h = 0 \tag{3.10}$$

where the potential is defined by:

$$V_{in,0}(\theta) = e\left(\frac{(1-e)\cos^2\theta}{(1-e\cos^2\theta)^2}(2-e\cos^2\theta)\;-\;1\right) \tag{3.11}$$

Two limiting cases are considered here: $e \ll 1$, corresponding to $M \simeq 1$, and $e \simeq 1$, corresponding to $M \ll 1$. The former describes a magnetic island where the flux surfaces have circular cross section near the O-point. The latter is representative of typical size magnetic islands in tokamak plasmas. In the former case, the function a can be approximated by $a \simeq 1$ and the magnetic field intensity is independent of θ: $B_{ph}^{\theta} \simeq \varepsilon_0|s|B_0\rho/(q_0r_0\gamma^2)$. This means that, in our model, the $e \ll 1$ case has a cylindrical symmetry around the O-point. In this case, the potential $V_{in,0}$ vanishes and Eq. 3.10 has the following eigenvalues (see Fig. 3.4):

$$\Omega^2_{MiO-CAP} = Mn_{isl}^2 j^2 = j^2/q^2(0) \qquad (\text{case } e \ll 1) \tag{3.12}$$

where j is a natural number ($j = 1, 2...$), and $q(0)$ is the safety factor given in Eq. 2.15, calculated at $x = 0$.

On the other hand, in the case of small island amplitude ($e \simeq 1$), the potential can be written as $V_{in,0} \simeq V_0 + \delta V$, where $V_0 = -1$ and $\delta V = V_1\, H(\theta_{eff})$. Here $V_1 = 1/(1-e) = s^2/(Mn_{isl}^2\gamma^2)$ and $H(\theta_{eff})$ is a function with unitary value inside the set $(|\theta| < \theta_{eff}) \bigcup (|\pi - \theta| < \theta_{eff})$ and zero elsewhere, where $\theta_{eff} = 1/2\,(\sqrt{M}/|s|)^{1/2}$. Since the potential $V_{in,0}$ is not constant in θ, in this case the eigenvalue Ω^2 has a different value for even and odd eigenfunctions. However, an approximated value of Ω^2 can be calculated by making some considerations on the potential shape. In fact, having δV a support which is very localized in θ for small amplitude islands, we can neglect its contribution and consider the problem determined by $V_{in,0} = V_0 = -1$. This gives the eigenvalues (see Fig. 3.7):

$$\Omega^2_{MiO-CAP} = Mn_{isl}^2(j^2 - 1) \qquad (\text{case } e \simeq 1) \tag{3.13}$$

We can see that when the island amplitude is vanishing, the frequencies are shifted down by the same quantity Mn_{isl}^2, and therefore the first frequency ($j = 1$) goes close to zero values. These solutions obtained analytically with this approximated potential are very close to the numerical ones. The numerical ones give also the frequency splitting between even and odd eigenfunctions, which are neglected in the approximation of constant potential $V_{in,0} = V_0 = -1$.

3.2 Continuous spectrum outside the magnetic island

3.2.1 Approximated result from the q-profile

Here, we want to give an approximated evaluation of the continuous spectrum frequency outside the island, analogously to what we have done for the region inside the magnetic island, in Sec. 3.1. Although the result is not rigorous in general and has differences with the result provided in subsequent sections, nevertheless it is worthwhile to have an easy formulation which can already give useful hints on the final results, in the whole region of interest $x > 1$. We consider magnetic island with typical size, corresponding to $M \ll 1$, $e \simeq 1$.

We approximate the continuous spectrum frequency analogously to Eq. 3.1, as:

$$\Omega_A^2 = \frac{(\omega^2 - \omega_{BAE-CAP}^2)}{\omega_A^2} = \frac{v_A^2\, k_\parallel^2}{\omega_A^2} = \frac{q_0^2}{q_{out}^2(x)}\big(nq_{out}(x) - m\big)^2 \qquad (3.14)$$

with q_{out} given in Eq. 2.11, and $\omega_A = v_A/Z_0$. Here we are considering the tokamak topology, described by flux surfaces with major radius R_0 and minor radius r_0. The perturbations have toroidal mode number n and poloidal mode number m. The approximated value of the parallel component of the wave-vector $k_\parallel$, is the one taken from the cylindrical symmetry: $k_\parallel = (n\, q_{out} - m)/(q_{out} R_0 \gamma)$. Note that in the limit of vanishing magnetic island, q_{out} tends to q_T (see Eq. 2.11) and the value of $k_\parallel$ in absence of magnetic island is recovered. Moreover, here we restrict to modes with $m/n = q_0$, which are the ones with the same helicity as the magnetic island.

The approximated continuous spectrum $\Omega_A^2(x)$ obtained from Eq. 3.14 is shown in Fig. 3.5, for several values of $j = n/n_{isl}$ and for $M = 10^{-2}$. We note that, far from the separatrix, the frequency branches tend asymp-

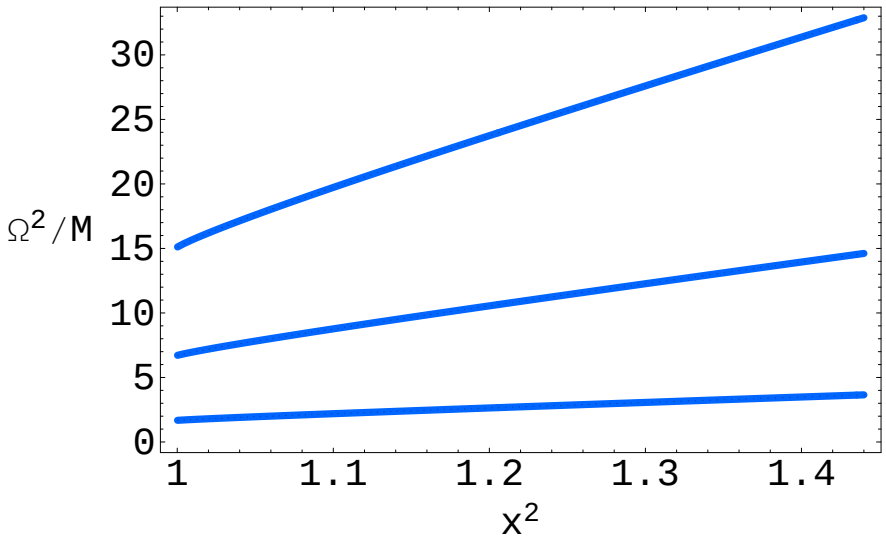

Figure 3.5: Approximated result for the continuous spectrum Ω^2 outside a magnetic island, plotted versus x^2, for $M = 10^{-2}$ and $n_{isl} = 1$. This is calculated with the approximated formula rigorously valid for cylindrical geometries, given in Eq. 3.14, where $x = \rho/\rho_{sx}$. The frequency is normalized to the Alfvén frequency and to M. Modes with $m/n = q_0$ are considered. The lines correspond to modes with $j = n/n_{isl} = 1, 2, 3$, respectively from bottom up. The separatrix is at $x = 1$. Far from the separatrix, the branches tend to the linear asymptotic limit of an equilibrium without islands. At the separatrix, the frequencies tend to a value different from zero. This approximated result can be compared with the rigorous solution shown in Fig. 3.6 and 3.7, where all branches tend to the same value at the separatrix.

totically to the linear behavior in x^2 that characterizes the SAW continuous spectrum without magnetic islands. On the other hand, at the separatrix, the branches tend to finite values, different for each branch number j, named continuum accumulation points (CAP). An estimation of the value of these nonlinearly modified CAP can be given with this approximated model, by using the safety factor value given by Eq. 2.12, approximated in the limit $M \ll 1$. We obtain $\Omega^2/M \simeq 16j^2/\pi^2 \simeq 1.62j^2$.

The eigenvalue problem will be solved rigorously in following sections, showing differences mainly near the separatrix. In fact, the CAP frequency will be found to be the same for all branches, and the value is of the same order of magnitude of the approximated estimation given here, but smaller than that.

3.2.2 Eigenvalue problem

In this section, we face the problem of SAW continuum modes, described by Eq. 2.50, outside the separatrix of a magnetic island, in the coordinate system, (x, u, ζ). The parallel and perpendicular differential operators have the following form:

$$\begin{aligned} Z_0 \nabla_\parallel &= 2\sqrt{M} n_{isl} L \frac{\partial}{\partial u} \\ \rho_{sx}^2 \nabla_\perp^2 &= \frac{P^2}{x^2} \frac{\partial^2}{\partial x^2} \end{aligned}$$

Only continuum modes with $m = q_0 n$ are considered, where m and n are respectively the poloidal and toroidal mode numbers, in the tokamak coordinates θ_T and ζ_T. Those are the modes with the same helicity as the magnetic island: $\partial/\partial\zeta = 0$, and therefore, the problem reduces to 2 dimensions. By applying the differential operators in this explicit form, Eq. 2.50 can be written in the form of an eigenvalue problem:

$$\Big[\frac{\Omega^2}{M n_{isl}^2} + \frac{4L}{P^2} \frac{\partial}{\partial u} L P^2 \frac{\partial}{\partial u}\Big] f = 0 \tag{3.15}$$

where $\Omega^2 = (\omega^2 - \omega^2_{BAE-CAP})/\omega_A^2$ is the eigenvalue, and $f = \partial^2 \delta\phi / \partial^2 x$ is the eigenfunction. Similarly to inside the island, this can be put in the form of a Schrödinger equation. The Schrödinger equation can be solved numerically for $x > 1$ with standard techniques and the numerical solution can be compared with the asymptotic limit, obtained analytically for $x \gg 1$. Moreover, analytical estimations of the frequency can

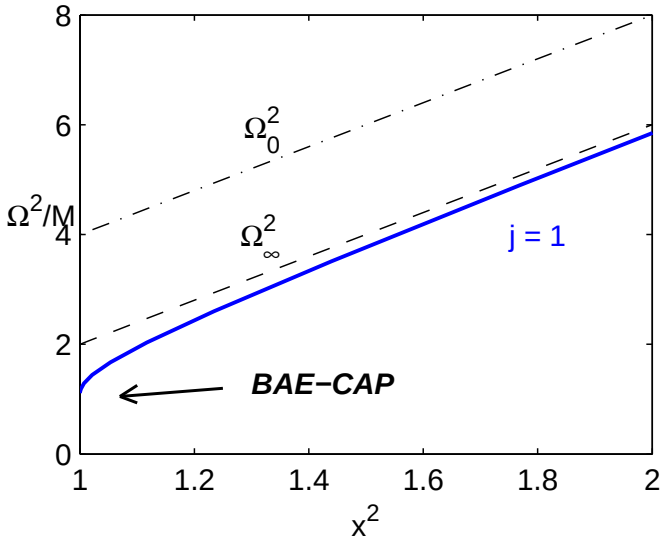

Figure 3.6: Continuous spectrum Ω^2, plotted versus x^2, for $M = 10^{-2}$, corresponding to $e \simeq 0.99$. Typical equilibrium parameters have been chosen, and $n_{isl} = 1$. Outside the magnetic island, all the frequency branches converge to a nonlinearly modified BAE-CAP at the separatrix ($x = 1$), with value $\Omega^2_{BAE-CAP} = M n^2_{isl}$. On the other hand, for $x \gg 1$, the asymptotic limit Ω^2_∞ is approached. In our model, due to the constant-ψ approximation, the solution without magnetic island Ω^2_0 is shifted with respect to the asymptotic limit: $\Omega^2_0 = \Omega^2_\infty + 2M$. Even and odd modes have a negligible difference in frequency, which is two orders of magnitude lower than the continuum frequency, for the chosen equilibrium parameters.

be found near the separatrix. The eigenvalue problem takes the form:

$$\frac{\partial^2}{\partial u^2}h + \frac{\Omega^2}{Mn_{isl}^2}A_{out}h - V_{out}h = 0 \tag{3.16}$$

with $A_{out} = 1/(4L^2)$, $V_{out} = (g''_{out} - g'^2_{out}/(2g_{out}))/(2g_{out})$, $g_{out} = 2LP^2$, and $h = f\sqrt{g_{out}}$.

3.2.3 Results ($\tilde{n} = 0$)

The periodic boundary condition in u is satisfied by an infinite set of solutions, labeled with mode number j (for q_0 integer and $n_{isl} = 1$, $j = n$, with n the toroidal number in the tokamak ζ_T coordinate). The solution of Eq. 3.16 is shown in Fig. 3.6 and Fig. 3.7, for typical island size, $M = 10^{-2}$, and typical values of the equilibrium parameters, $q_0 = 2$, $s = 1$, $\varepsilon_0 = 0.1$, $n_{isl} = 1$. The asymptotic behavior at $x \gg 1$ is depicted in Fig. 3.6 for the case $j = 1$. Three main features describe the continuous spectrum outside the island:
1) The continuous spectrum for $x \gg 1$ reaches the asymptotical limit Ω^2_∞. In this limit, namely for $M \ll 1$, we note that Eq. 3.15 takes the form of a Mathieu equation:

$$\frac{\Omega^2}{n_{isl}^2}f = M\Big(4x^2 - 2(\cos u + 1)\Big)\frac{\partial^2}{\partial u^2}f = \Big((2\psi - 2M) - 2M\cos u\Big)\frac{\partial^2}{\partial u^2}f \tag{3.17}$$

with M playing the role of the modulation coefficient, and the flux-surface coordinate ψ approaching the value $\psi \simeq (q_T - q_0)^2/2$. The asymptotical limit Ω^2_∞ can be calculated from Eq. 3.17, and has a constant difference with the limit of the continuous spectrum in the limit of vanishing island, Ω^2_0:

$$\begin{aligned} \Omega^2_\infty &= n^2 < (q_T - q_0)^2 >_u = Mn_{isl}^2 j^2(4x^2 - 2) \\ \Omega^2_0 &= n^2 \lim_{M\to 0}(q_T - q_0)^2 = Mn_{isl}^2 j^2(4x^2) \end{aligned}$$

This difference is due to the constant-ψ approximation which is made modeling the island field. A more realistic asymptotic behavior can be obtained by abandoning the constant-ψ approximation and considering an improved model where the island field decays with growing $|q_T - q_0|$.
2) Even and odd eigenfunction have different eigenvalues, due to the non-uniformity of the magnetic field intensity along the field line. Inside the island, the frequency difference is of the same order as the frequency value, while outside the island the frequency difference is negligible with

respect to the absolute value. In the case depicted in Fig. 3.6, the frequency difference between odd and even solutions is $\Delta\Omega^2/M \simeq 10^{-2}$.
3) At the separatrix, all continuum frequencies converge to the nonlinearly modified BAE-CAP, whose value is proportional to the magnetic island half-width [24]:

$$\Omega_{nlBAE-CAP} = \sqrt{M} n_{isl} = \frac{q_0 s n_{isl}}{2} \frac{W_{isl}}{r_0} \tag{3.18}$$

In our model, the value of the nonlinearly modified BAE-CAP frequency is the same as the central value of the MiAE gap, Eq. 3.6. In fact, different helicities are considered in the two cases, but they depends on the island size with the same scalings. The reason of the presence of a continuum accumulation point at the separatrix is found in the role of the X-point in lowering the local wavenumber $k_\parallel$. We can write the value of the BAE-CAP frequency ($f = \omega/(2\pi)$), similarly to the central frequency of the MiAE gap (Eq. 3.7), as:

$$f_{nlBAE-CAP} = f_{BAE-CAP} \sqrt{1 + \frac{q_0^2 s^2 n_{isl}^2}{4} \frac{W_{isl}^2}{r_0^2} \frac{f_A^2}{f_{BAE-CAP}^2}} \tag{3.19}$$

Note that we have obtained $f_{nlBAE-CAP} = f_{MiAE-gap}$.

The nonlinear modification of the continuous spectrum and in particular the upward shift in frequency of the BAE-CAP has important implications in the study of the dynamics of global AE in tokamak equilibria in the presence of a magnetic island, as discussed in Sec. 3.3. The dynamics of global AE in tokamaks in the presence of a magnetic island is treated in Chapter 5. The analytical treatment of the continuous spectrum problem near the separatrix is faced in next section.

3.2.4 Analytical treatment near the separatrix

Here, we focus on the region outside the magnetic island, in the proximity of the separatrix. We also consider the limit of $e \simeq 1$, which is the case of a typical size magnetic island in tokamak plasmas. Under these assumptions, the function L and P can be approximated as $L = P = \sqrt{1 - \cos u}/\sqrt{2}$. Consequently, the eigenvalue equation, Eq. 3.16, takes the form:

$$\frac{\partial^2}{\partial u^2} h - W_{\Omega^2} h = 0 \tag{3.20}$$

where the potential W_{Ω^2} is defined as:

$$W_{\Omega^2} = -\frac{9\cos^2 u - (12 + 8\tilde{\Omega}^2)\cos u + (3 + 8\tilde{\Omega}^2)}{16(1 - \cos u)^2}$$

and $\tilde{\Omega}^2 = \Omega^2/(Mn_{isl}^2)$. This equation can be studied as a Schrödinger equation with zero energy. In this framework, we look for values of $\tilde{\Omega}^2$ such that the solution satisfies the boundary conditions of periodicity of u on $(0, 2\pi)$. The potential W_{Ω^2} has positive second derivative, for $\tilde{\Omega}^2 < 3/4$, and negative second derivative for $\tilde{\Omega}^2 > 3/4$. For $\tilde{\Omega}^2 = 3/4$, the potential has a constant value: $W_{\Omega^2} = -(3/4)^2$. For the given boundary conditions, this means that solutions of the problem exist for $\tilde{\Omega}^2 > 3/4$ only. On the other hand, when $\tilde{\Omega}^2 = 4/3$ the potential has maximum value $W_{\Omega^2} = -1$ at $u = \pi$, and therefore does not admit a solution with mode $j = 1$. With these considerations, we can estimate that $3/4 < \tilde{\Omega}^2_{BAE-CAP} < 4/3$ for the first mode number, $j = 1$. Numerically, we find that $\tilde{\Omega}^2 \simeq 1$ for $j = 1$ and that the difference in frequency for other mode numbers and different parities is negligible.

3.3 Summary of the continuous spectrum results

Understanding the radial structure of the SAW continuous spectrum is one of the first steps in facing the MHD stability property of a tokamak equilibrium. In fact, continuum damping is one of the main damping mechanisms of shear Alfvén instabilities, and occurs at the resonant flux surfaces where the mode frequency is resonant with the continuous spectrum frequency. Therefore, a mode is not affected by continuum damping and can more easily grow unstable if its frequency lies in a gap of the continuous spectrum.

The radial structure of the continuous spectrum of SAW has been calculated in this chapter in an equilibrium inside a magnetic island flux tube. The equilibrium is considered to be static, due to the time scale separation between the magnetic island dynamics and the faster SAW dynamics. The flux tube is considered to be straight, in order to focus on the effects of the non-circularity of the cross section. Curvature effects are retained only in the formation of the BAE gap in the low frequency part of the continuous spectrum. A linear, MHD model is adopted for finite-beta tokamak plasmas. A generalized safety factor is defined inside the magnetic island flux tube, giving information on the rational flux surfaces where different modes couple to create gaps in the SAW continuous spectrum. The linearized SAW equation is solved with a shooting method code inside a finite-size magnetic island and the result compared with the SAW continuous spectrum calculated in tokamak equilibria.

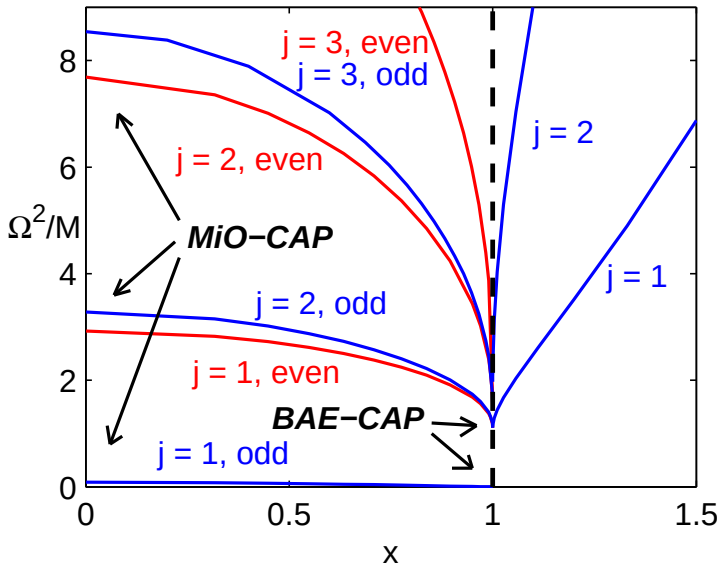

Figure 3.7: Continuous spectrum $\Omega^2(x)$, for $M = 10^{-2}$, corresponding to $e \simeq 0.99$. Typical equilibrium parameters have been chosen, and $n_{isl} = 1$. The region inside the island is at $0 < x < 1$, and the region outside the island at $x > 1$. The MiO-CAP are shown at the O-point ($x = 0$), and the BAE-CAP at the separatrix ($x = 1$).

When considering modes with generic helicity $\tilde{n} \neq 0$, we have found that there exists a SAW continuous spectrum within a magnetic island, similar to that calculated in tokamak equilibria. For the case of small eccentricity of the flux surfaces, modes with different poloidal numbers are not coupled and, therefore, the branches of the continuous spectrum intersect and there is no formation of gaps. This is shown to occur inside a magnetic island with very large (unrealistic) width, near the O-point, where the flux surfaces are nearly circular. On the other hand, a realistic size magnetic island is shown to have wide gaps in the continuous spectrum, due to the strong eccentricity of the flux surfaces. This is analogous to the formation of EAE gaps in tokamaks, but is found here inside the magnetic island equilibrium. Note that MiAE can exist as bound states within the island, essentially free of continuum damping, provided that plasma equilibrium effects and free energy sources can drive and bind them locally. The problem of AE inside the island will be treated in Chapter 4.

We have also considered modes with the same helicity as the magnetic island ($\tilde{n} = 0$). In this framework, the model reduces to 2 dimensions. We have shown that the SAW continuous spectrum of a finite-β tokamak plasma is modified by the presence of a magnetic island. In particular, the BAE continuum accumulation point (BAE-CAP) is shifted in space from the rational surface of the island, to the separatrix flux surface position. Moreover, we have shown that the nonuniformity of the magnetic field intensity along the field lines generates a splitting between the frequency branches of the modes with even and odd (with respect to the potential describing the periodic magnetic field intensity) structures. The frequency of this splitting has a relevant value inside the island, and is negligible outside the island, for typical island sizes. Inside the magnetic island, we have found that the continuum frequency branches converge at the O-point to several magnetic island induced CAP (MiO-CAP). At the separatrix, the frequency of the BAE-CAP is splitted in two values. The continuum branch correspondent to the first odd eigenfunction inside the island, converges to the original BAE-CAP, with same frequency as in absence of a magnetic island, and the other branches converge to a nonlinearly modified BAE-CAP, with a higher frequency, given by Eq. 3.18. Outside the magnetic island, all continuum branches converge at the separatrix to the nonlinearly modified BAE-CAP. Far from the separatrix and outside the magnetic island, the continuum frequency converges asymptotically to the value calculated in an equilibrium with no islands.

Moreover, our results about modes with the same helicity as the magnetic island, $\tilde{n} = 0$, have implications in the study of the dynamics of

Alfvén eigenmodes (AE). In fact, BAE are expected to have an eigenfunction radially peaked in the proximity of the magnetic island separatrix, namely at the BAE-CAP, rather than at the rational surface. The BAE frequency is expected to have higher values when a magnetic island is present, with respect to the values of an equilibrium with no islands, consistently with the BAE-CAP frequency modification described by Eq. 3.18. The problem of nonlinear modification of BAE in the presence of a magnetic island will be treated in Chapter 5.

Chapter 4

Alfvén Eigenmodes inside the island

4.1 Introduction

In the previous chapter we focused on the dynamics of continuum modes, i.e. radially singular modes growing in the proximity of resonance surfaces. The radial localization of the continuum modes has allowed us to separate the perpendicular scale and the parallel scale, resulting in a problem which is characterized by a 1D differential equation. The singularity forming at the resonance surfaces, causes a damping mechanism called continuum damping, and the energy of the mode is therefore absorbed at the resonance surface. We have determined the SAW continuous spectrum of an equilibrium with a magnetic island. This gives the information on where Alfvén instabilities are absorbed by continuum damping.

In this chapter we want to solve the problem for global modes, taking into account the results on the continuous spectrum. We know where the energy of a mode is absorbed, and this gives a boundary condition in space for the global solutions, which must have a negligible amplitude in the proximity of the corresponding resonance surfaces.

We want to focus here on the main mechanisms of global mode formation, peculiar to the magnetic island geometry. Therefore, we keep only the curvature effects in the BAE-CAP frequency and neglect the higher order effects, such as toroidicity induced gap in the SAW continuum. As seen in Eq. 3.1, these curvature effects are retained only in the definition of the normalized frequency Ω, and neglected elsewhere. In this way, the magnetic island flux tube can be assumed to have the

topology of a cylindrical confinement configuration, with a noncircular cross section, and with a large guide field along the axis and a poloidal magnetic field in the plane perpendicular to the axis. In this chapter we consider a large magnetic island, with $e \ll 1$. This corresponds to a magnetic island amplitude which is not typical in tokamaks, but allows us to develop a perturbative theory for the global modes where the smallness parameter is the eccentricity e. Like in Chapter 3, we assume ζ to be the translational symmetry direction, with Z_0 being the characteristic scale length. In this chapter, all parameters - cylinder-like coordinates, safety factor, magnetic shear, et cetera - are intended to describe the configuration inside the magnetic island.

This small but finite eccentricity is responsible for a gap in the continuous spectrum, as shown in Chapter 3, and for the formation of global modes with frequency inside the gap. These are dubbed here magnetic island induce Alfvén eigenmodes (MiAE). These global modes are analogous to ellipticity induced AE (EAE) in tokamaks [12]. The MHD theory of MiAE will be developed in Section 4.2, following the same theoretical scheme of the EAE, namely reference [38]. Moreover, in Section 4.3 we will show that, by adding FLR effects to the MHD theory, a further class of modes is found inside the island. In fact, kinetic Alfvén waves form localized modes inside the islands, analogously to what happens in tokamaks [39].

4.2 Global modes in fluid theory

4.2.1 The model for global Alfvén Eigenmodes

The vorticity equation in nonlinear MHD theory, Eq. 2.31, has been derived in Chapter 2 in the general case of shear Alfvén modes, and describe both global and continuum perturbations. The assumption for the derivation was that the modes are radially localized with respect to the equilibrium scale length. We also consider that for typical tokamak parameters the dynamics of the magnetic island is slow with respect of the SAW dynamics ($\omega_{isl} \ll \omega$), as discussed in Sec. 2.2.3. Therefore, we can neglect the nonlinearity due to the island velocity perturbation and retain only the nonlinearity due to the island magnetic perturbation. Moreover, we consider only modes with frequencies above the BAE-CAP frequency. The study of lower frequency dynamics, where transit and trapped particle can resonate with the wave, is out of the scope of this dissertation. The correspondent kinetic effects can be included in the

framework of the gyro-kinetic theory [2, 40]. The last term of Eq. 2.31 was neglected for continuum modes, and cannot be neglected here for global modes. In fact, it contains only one spatial derivative perpendicular to the equilibrium (tokamak plus island) magnetic flux surfaces, and therefore it is negligible with respect to the other terms only when considering perpendicularly singular modes, such as continuum modes. Consistently with these considerations, Eq. 2.31 can be rewritten in the following form (by applying the operator $(1/c_L)(\partial/\partial t)$ and decomposing in Fourier in time):

$$\frac{\tilde{\omega}^2}{v_A^2}\nabla_\perp^2\delta\phi + i\frac{\omega}{c_L}\boldsymbol{B}\cdot\boldsymbol{\nabla}\Big(\frac{\nabla_\perp^2}{B}\delta A_\parallel\Big) - \frac{4\pi i\omega}{c_L^2}\boldsymbol{\nabla}\Big(\frac{J_\parallel}{B}\Big)\cdot(\boldsymbol{\nabla}\times\delta\boldsymbol{A}) = 0 \quad (4.1)$$

where $\delta\phi$ and δA are respectively the perturbed SAW scalar and vector potentials, and all other quantities refer to the equilibrium. The constant c_L is the speed of light, with label L for differentiating from the metric function c, defined in Appendix 7.1. In ideal MHD, the scalar and vector potentials are linked by the Ohm's law, Eq. 2.34:

$$i\frac{\omega}{c_L}\delta A_\parallel = \frac{\boldsymbol{B}\cdot\boldsymbol{\nabla}}{B}\delta\phi \quad (4.2)$$

Here, $\omega_{BAE-CAP}$ has already been included in the inertia term with the definition of $\tilde{\omega}^2 = \omega^2 - \omega^2_{BAE-CAP}$, consistently with the discussion in Sec. 2.2.2.

The set of Eqs. 4.1 and 4.2 can be cast in a single equation for $\delta\phi$, similarly to what we have done in Eq. 2.38 for continuum modes. We obtain:

$$\frac{\tilde{\omega}^2}{v_A^2}\nabla_\perp^2\delta\phi + \nabla_\parallel\nabla_\perp^2\nabla_\parallel\delta\phi - \frac{4\pi}{c_L}\boldsymbol{\nabla}\Big(\frac{J_\parallel}{B}\Big)\cdot\big[\boldsymbol{\nabla}\times(\nabla_\parallel\delta\phi)\big]_\perp = 0 \quad (4.3)$$

We have adopted the assumption that toroidicity effects are contained in the BAE-CAP frequency to the leading order, and that we can neglect higher order curvature effects. This allows us to consider a geometry where the magnetic island is modeled as a straight flux tube, with non-circular cross section. In Section 2.1, a set of cylinder-like coordinates inside the magnetic island has been defined, named (ρ, θ, ζ), and in Appendix 7.1 the correspondent differential operators are given. For each flux surface inside the magnetic island, labeled by the radial coordinate $x = \rho/\rho_{sx}$, the cross section can be described by an eccentricity $e(x)$, which is given in Eq. 2.5. We note here, that the eccentricity parameter

Δ defined in reference [12], is linked to $e(x)$ by the formula: $e(x) = 4\Delta/\rho$, corresponding to $d\Delta/d\rho = (e(x)+xe'(x))/4$. We study the AE dynamics in the proximity of a rational flux surface x_s, where the eccentricity can be linearized as $e(x) = e(x_s) + e'(x_s)\ (x - x_s)$. With these definitions, we can write the differential operators $\nabla_\parallel$ and $\nabla_\perp$ in the form:

$$\nabla_\parallel = -ik_\parallel + \frac{x}{\rho_{sx}}\frac{B^\theta_{ph}}{B_0}\Big(\frac{d}{dx}\frac{e(x)}{4x}\Big)\cos 2\theta\frac{\partial}{\partial\theta} \tag{4.4}$$

and $\nabla^2_\perp = \nabla^2_0 + \nabla^2_1$, with

$$\rho^2_{sx}\nabla^2_0 = \frac{1}{x}\frac{\partial}{\partial x}x\frac{\partial}{\partial x}+\frac{1}{x^2}\frac{\partial^2}{\partial\theta^2}\ ,\ \ \rho^2_{sx}\nabla^2_1 = -\frac{\big(e(x)+xe'(x)\big)}{2}\cos 2\theta\frac{\partial^2}{\partial x^2} \tag{4.5}$$

with $k_\parallel = (\tilde{n} + (i/q)\partial/\partial\theta)/Z_0$. Here the mode has been written as

$$\delta\phi = \phi(x,\theta)\exp\left(-i\tilde{n}\zeta\right) \tag{4.6}$$

where $\tilde{n}$ is the mode number in the ζ-direction, by using the assumption of translational symmetry along ζ, with $2\pi Z_0$ being the periodicity length (defined in Sec. 2.1.2 as the length of the axisymmetric magnetic field line). In this chapter, the safety factor q is intended to be the safety factor defined inside the magnetic island, given by Eq. 2.15. We have adopted a perturbative theory where the equilibrium flux surfaces have nearly circular cross section, with the eccentricity e being the smallness parameter. In fact, the last terms in Eqs. 4.4 and 4.5 are the corrections of the order of e, and we will see that they are important only in a narrow layer centered at the rational surface x_s. In this layer, modes with different mode number along the θ direction are coupled by eccentricity, allowing discrete modes to exist with frequency inside the ellipticity induced MiAE gaps. Due to the steepness of the solutions near the rational surface x_s, only highest order radial derivatives have been retained in the correction due to eccentricity in Eq. 4.5.

4.2.2 Eigenvalue problem

In this section, we write the MHD equation for global Alfvén Eigenmodes, Eq. 4.3, in the form of an eigenvalue problem inside the magnetic island. We adopt a perturbative theory, where the eccentricity e is the smallness parameter. Consequently, we can start by writing the vorticity equation, Eq. 4.3, in the coordinate system (ρ, θ, ζ), in the form:

$$\big(L_0 + L_1\big)\phi = 0 \tag{4.7}$$

where the operators L_0 and L_1 are defined as:

$$L_0\,\phi = \Omega^2\nabla_0^2\phi - Z_0^2 k_\parallel \nabla_0^2 k_\parallel \phi + \frac{4\pi i}{c_L}\frac{Z_0^2}{\rho}\frac{d}{d\rho}\Big(\frac{J_\parallel}{B}\Big)\,k_\parallel\,\frac{\partial\phi}{\partial\theta} \tag{4.8}$$

$$L_1\phi = -2\Omega^2\frac{(e(x)+xe'(x))}{4}\cos 2\theta\ \phi'' + 2Z_0^2\frac{(e(x)+xe'(x))}{4}k_\parallel\big(\cos 2\theta k_\parallel\phi''\big) + \\ + i\frac{B^\theta_{ph}}{B_0}\frac{\rho Z_0^2}{4}\frac{d}{d\rho}\Big(\frac{e(x)}{\rho}\Big)\Big[\cos 2\theta k_\parallel\frac{\partial\phi''}{\partial\theta} + k_\parallel\big(\cos 2\theta\frac{\partial\phi''}{\partial\theta}\big)\Big] \tag{4.9}$$

where $x = \rho/\rho_{sx}$, $\Omega^2 = Z_0^2\tilde{\omega}^2/v_A^2$ was defined already in Eq. 3.1, and the radial second derivative of ϕ has been denoted as ϕ''. For small values of $e(x)$, the operator L_1 is a higher order correction to L_0, which represents the leading order term of Eq. 4.7.

We remind here that the dependence of the perturbed scalar potential $\delta\phi$ on ζ has already been taken out, in Eq. 4.6. Due to the translational symmetry of our equilibrium along ζ, the Fourier decomposition of modes with the quantum number $\tilde{n}$ is well defined and the modes are uncoupled. Now, we decompose the modes in Fourier series in θ: $\phi(x,\theta) = \sum_j \phi_j(x)\exp(ij\,\theta)$. Due to the small eccentricity, this decomposition describes modes which are weakly coupled. We want to write Eq. 3.4 in the matrix form:

$$D_j\phi_j + D_{j+2}\phi_{j+2} + D_{j-2}\phi_{j-2} = 0 \tag{4.10}$$

The operator D_j can be calculated by considering the case of vanishing eccentricity. In fact, by using the fact that to lowest order in $e(x)$, the safety factor can be written as $q(\rho) = \rho B_\zeta/Z_0 B^\theta_{ph}(\rho)$ (see Eq. 2.14), we write the radial derivative of the current as:

$$\frac{dJ_\parallel}{d\rho} = \frac{c_L}{4\pi}\frac{d}{d\rho}\Big(\frac{1}{\rho}\frac{d}{d\rho}\Big(\frac{\rho B^\theta_{ph}}{B}\Big)\Big) = -\frac{B}{m}\frac{1}{\rho^2}\frac{d}{d\rho}\Big(\rho^3\frac{d}{d\rho}k_\parallel\Big)$$

With these substitutions, D_j can be written in the form of the Hain-Lüst operator [6]:

$$D_j\phi_j = \frac{1}{\rho^3}\frac{d}{d\rho}\rho^3\big(\Omega^2 - Z_0^2k_\parallel^2\big)\frac{d}{d\rho}\Big(\frac{\phi_j}{\rho}\Big) - \frac{j^2-1}{\rho^2}\big(\Omega^2 - Z_0^2k_\parallel^2\big)\Big(\frac{\phi_j}{\rho}\Big) \tag{4.11}$$

For a cylindrical configuration, where $e(x) = 0$, then Eq. 4.7 reduces to the Hain-Lüst equation: $D_j\phi_j = 0$. The contribute of eccentricity in coupling the different modes, is contained in the operators $D_{j\pm2}$, which are written as:

$$D_{j\pm2} = \Big[\frac{(e(x)+xe'(x))}{4}\big(Z_0^2k_{\parallel j}k_{\parallel j\pm2} - \Omega^2\big) -$$

$$- \frac{B^{\theta}_{ph}}{B_0}\frac{\rho Z_0^2}{4}\frac{d}{d\rho}\Big(\frac{e(x)}{\rho}\Big)(j\pm 2)\big(k_{\|j\pm 2}+k_{\|j}\big)\Big]\frac{\partial^2}{\partial\rho^2} \tag{4.12}$$

Equation 4.10, with the operators D_j and $D_{j\pm 2}$ defined in Eqs. 4.11 and 4.12, is the eigenvalue equation describing Alfvén modes inside a magnetic island. It has been written in a matrix form, and we have emphasized the role of ellipticity in coupling the modes j and $j \pm 2$.

Before moving further and solving Eq. 4.10, we want to show here, that with Eq. 4.10 we can also recover the continuous spectrum structure (which was derived in Chapter 3) near the rational surface x_s, where modes j and $j+2$ couple. To this extent, we note that near this rational surface $k_{\|j} \simeq -k_{\|j+2} \simeq 1/(q_s Z_0)$, with $q_s = (j+1)/\tilde{n}$ and $\Omega^2 \simeq \Omega_0^2 = 1/q_s^2$. Note that Ω_0 is the intersection frequency of the continuum branches in absence of ellipticity. Its value is the central frequency of the MiAE gap, and therefore tends to $\Omega_{MiAE-gap}$, defined in Eq. 3.6, near the island O-point, $x = 0$. In the limit of radially singular modes, we can keep only the term with highest radial derivative in Eq. 4.11. With these substitutions, we can describe the continuous spectrum near the rational surface x_s as a set of two equations:

$$\big(\Omega^2 - Z_0^2 k_{\|j}^2\big)\frac{\partial^2}{\partial x^2}\phi_j \quad - \frac{(e(x)+xe'(x))}{2}\Omega^2\frac{\partial^2}{\partial x^2}\phi_{j+2} = 0 \tag{4.13}$$

$$\big(\Omega^2 - Z_0^2 k_{\|j+2}^2\big)\frac{\partial^2}{\partial x^2}\phi_{j+2} - \frac{(e(x)+xe'(x))}{2}\Omega^2\frac{\partial^2}{\partial x^2}\phi_j \quad = 0 \tag{4.14}$$

whose solution is found by setting the determinant of the coefficients to zero. We obtain:

$$\Omega^2_{\pm} = Z_0^2\frac{k^2_{\|j}+k^2_{\|j+2} \pm \sqrt{(k^2_{\|j}-k^2_{\|j+2})^2 + (e(x)+xe'(x))^2 k^2_{\|j}k^2_{\|j+2}}}{2\big(1-(e(x)+xe'(x))^2/4\big)} \tag{4.15}$$

At the rational surface, the difference of the two branches gives the gap width $\Delta\Omega$ in the continuous spectrum:

$$\Delta\Omega = \Omega_+ - \Omega_- \simeq \frac{(e(x)+xe'(x))}{2q} \tag{4.16}$$

This formula explains well the gap formation in the case of small eccentricity $e(x) \ll 1$, and represents the analytical explanation of the numerical results shown in Fig. 3.3, in the regions near the rational surfaces.

4.2.3 Magnetic island induced ellipticity-AE

In this section, we solve the eigenvalue equation for Alfvén modes inside the island, Eq. 4.10, for global Alfvén Eigenmodes (AE), and provide the dispersion relation. We have seen for continuum modes, that the ellipticity has the effect of coupling continuum branches with mode numbers j and $j+2$, with the consequent creation of gaps in the continuous spectrum. We will see here that ellipticity of magnetic island flux surfaces is responsible of the existence of a global mode with discrete frequency inside the gap (MiAE), analogously to ellipticity induced AE (EAE) in tokamaks [12, 13, 38].

We derive the dispersion relation of ellipticity induced MiAE (or magnetic island induced EAE), with a technique of *solution matching*. This perturbative procedure is used in boundary-layer theory to determine analytically the approximate global properties of the solution of a differential equation. This procedure is applied by dividing the region inside the magnetic island in two parts: a narrow layer centered at the rational surface x_s, where the operator D_{j+2} gives a contribute of the same order of magnitude of the operator D_j, and a region outside this layer, where the operator D_{j+2} can be neglected. The inner region, where the coupling due to ellipticity is effective, is named *inertial layer*, and the region outside the inertial layer, where the mode structure is essentially the same as without coupling, is named *external region*. The solutions in the inertial layer and in the external region can be calculated analytically by using appropriate simplifications of the equation in the two different cases. Then, the integration constants are used as free parameters to match the solution values and derivatives at the border between the two regions.

We start by solving Eq. 4.10 in the inertial layer. This can be done analytically by noting that, due to the high derivatives inside the layer, the second term in the operator D_j can be neglected. Moreover, we can linearize all quantities near x_s: $\Omega^2 = \Omega_0^2 + 2\,\delta\Omega^2$, $x = x_s(1+y)$, $1/q = (1-s_s y)/q_s$, $Z_0^2 k_{\|j}^2 = (1+2js_s y)/q_s^2$, $Z_0^2 k_{\|j+2}^2 = (1-2(j+2)s_s y)/q_s^2$, with s_s the shear calculated at the rational surface x_s. With these simplifications, and defining $\xi_j = \phi_j/\rho$, Eq. 4.10 takes the form:

$$\frac{\partial}{\partial y}\Big(\frac{\delta\Omega^2}{\Omega_0^2} - j s_s y\Big)\frac{\partial}{\partial y}\xi_j \quad - \frac{(e(x_s) + x_s e'(x_s))}{4}\frac{\partial^2}{\partial y^2}\xi_{j+2} = 0 \quad (4.17)$$

$$\frac{\partial}{\partial y}\Big(\frac{\delta\Omega^2}{\Omega_0^2} + (j+2) s_s y\Big)\frac{\partial}{\partial y}\xi_{j+2} \quad - \frac{(e(x_s) + x_s e'(x_s))}{4}\frac{\partial^2}{\partial y^2}\xi_j = 0 \quad (4.18)$$

The solutions in the inertial layer are [38]:

$$\xi_j = \frac{1}{\sqrt{j}}\Big(\frac{C_{j+2}+\lambda C_j}{\sqrt{1-\lambda^2}}\alpha - C_j \ln\cos\alpha + A_j\Big) \tag{4.19}$$

$$\xi_{j+2} = \frac{1}{\sqrt{j+2}}\Big(\frac{C_j+\lambda C_{j+2}}{\sqrt{1-\lambda^2}}\alpha + C_{j+2} \ln\cos\alpha + A_{j+2}\Big) \tag{4.20}$$

where A_j, A_{j+2}, C_j and C_{j+2} are four integration constants, λ is defined as $\lambda = 4(j+1)\delta\Omega^2/(\Omega_0^2\sqrt{j(j+2)}(e(x_s)+x_s e'(x_s)))$ and α is defined in:

$$y = \frac{(e(x_s)+x_s e'(x_s))}{4s_s\sqrt{j(j+2)}}\Big(\frac{\lambda}{j+1} + \sqrt{1-\lambda^2}\,\tan\alpha\Big) \tag{4.21}$$

Next, we solve Eq. 4.10 in the external region. In the external region, we can neglect the operator D_{j+2} with respect to D_j, recovering the Hain-Lüst equation for the uncoupled modes:

$$\frac{1}{\rho}\frac{d}{d\rho}\rho^3\epsilon_j\frac{d}{d\rho}\xi_j - (j^2-1)\epsilon_j\xi_j = 0 \tag{4.22}$$

$$\frac{1}{\rho}\frac{d}{d\rho}\rho^3\epsilon_{j+2}\frac{d}{d\rho}\xi_{j+2} - ((j+2)^2-1)\epsilon_{j+2}\xi_{j+2} = 0 \tag{4.23}$$

where $\epsilon_j = \left(\Omega_0^2 - Z_0^2 k_{\|j}^2\right)$. Compare Eq. 4.22 and Eq. 4.23 with the analogous equation defined in the slab model, Eq. 1.5, in Sec. 1.2. Consistently with the perturbative theory procedure, we have assumed here that the frequency of the Eigenmode can be approximated in the external region by the unperturbed frequency Ω_0, namely the intersection frequency of the continuum branches in absence of ellipticity. The solution in the whole region inside the magnetic island can be found numerically by knowing the safety factor profile, $q(x)$, and therefore $k_\|$. Here, we want to calculate analytically the asymptotic limit of the solution near the rational surface x_s. This can be done, by neglecting the second term in Eqs. 4.22 and 4.23, namely keeping only the highest radial derivative terms. By linearizing the function ϵ_j near $x = x_s$, we obtain two equations of the form $d_y\, y\, d_y\, \xi_j = 0$. The solutions for j and $j+2$, on both sides of the inertial layer (labeled here as $+$ and $-$), are:

$$\xi_j^+ = K_j^+\Big(\ln|\epsilon' y| + b_j^+\Big) \quad , \quad \xi_j^- = K_j^-\Big(\ln|\epsilon' y| + b_j^-\Big) \tag{4.24}$$

$$\xi_{j+2}^+ = K_{j+2}^+\Big(\ln|\epsilon' y| + b_{j+2}^+\Big) \, , \quad \xi_{j+2}^- = K_{j+2}^-\Big(\ln|\epsilon' y| + b_{j+2}^-\Big) \tag{4.25}$$

as mentioned also in Sec. 1.2. The integration constants are named $K^\pm$, and the ratio of the constant and logarithmic parts of the solutions is described by the functions $b^\pm$.

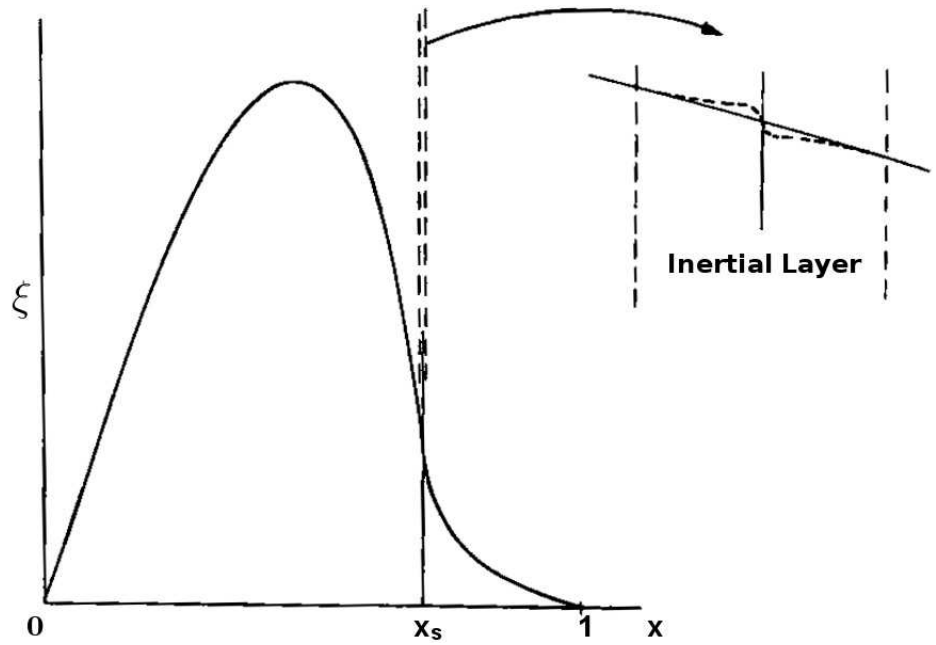

Figure 4.1: Structure of the eigenfunction for the j-th component of the magnetic island induced Alfvén Eigenmodes. The O-point of the island is at $x = 0$ and the separatrix at $x = 1$. The rational surface is at $x = x_s$. In a narrow region centered at the rational surface, called *inertial layer*, the modes with mode number j and $j + 2$ couple due to the finite ellipticity of the magnetic island flux surfaces. In the *external region*, the mode structure is the solution of the Hain-Lüst equation for the modes j and $j + 2$, Eqs. 4.22 and 4.23.

The last step of the procedure of the solution matching is imposing the continuity of the solutions at the two borders between the inertial layer and the external region. We have found 4 integration constants in the inertial layer (A_j, A_{j+2}, C_j and C_{j+2}), and 8 integration constants in the external region ($K_j^{\pm}$, $K_{j+2}^{\pm}$, $b_j^{\pm}$ and $b_{j+2}^{\pm}$) for the solutions corresponding to the mode numbers j and $j+2$, totalling 12 integration constants. Each mode number has 1 equation for the matching of the logarithmic part of the solution and 1 for the constant part of the solution, for each of the two borders, therefore in total the equations are 8 for the two mode numbers. The 4 equations for the matching of the logarithmic terms are:

$$K_j^+ = K_j^- = \frac{C_j}{\sqrt{j}} \quad , \quad K_{j+2}^+ = K_{j+2}^- = -\frac{C_{j+2}}{\sqrt{j+2}} \tag{4.26}$$

and, after having eliminated the coefficients A_j we are left with two equations for the matching of the constant terms:

$$\pi \frac{C_{j+2} + \lambda C_j}{\sqrt{1-\lambda^2}} = C_j (b_j^+ - b_j^-) \tag{4.27}$$

$$\pi \frac{C_j + \lambda C_{j+2}}{\sqrt{1-\lambda^2}} = -C_{j+2} (b_{j+2}^+ - b_{j+2}^-) \tag{4.28}$$

After having applied these equations, the remaining free parameters are 4: $b^{\pm}$. These can be calculated as:

$$b^{\pm} = \lim_{x \to x_s^{\pm}} \Big(\frac{\xi^{\pm}}{y\, \xi'^{\pm}} - \ln |\epsilon' y| \Big) \tag{4.29}$$

by solving numerically Eqs. 4.22 and 4.23, imposing the regularity boundary conditions ($\xi = 0$) at $x = 0$ and $x = 1$.

Finally we can calculate the dispersion relation by setting the determinant of Eqs. 4.27 and 4.28 to zero, and solving for λ. The result is:

$$\Omega_{MiAE} = \frac{1}{q_s} \Big(1 + \frac{\sqrt{j}\sqrt{j+2}}{j+1} \; \frac{e(x_s) + x_s e'(x_s)}{4} \delta \Big) \tag{4.30}$$

where

$$\delta = \frac{(b_j^+ - b_j^-)(b_{j+2}^+ - b_{j+2}^-) + \pi^2}{\pi \big((b_{j+2}^+ - b_{j+2}^-) - (b_j^+ - b_j^-) \big)} \tag{4.31}$$

In the limit of small eccentricity, $e(x) \ll 1$, the gap width is very small and the frequency of MiAE is in the proximity of the intersection frequency of the continuum branches: $\Omega_{MiAE} \simeq \Omega_0$. Close to the O-point, the intersection frequency of the continuum branches is the central frequency of the MiAE-gap defined in Eq. 3.6: $\Omega_0(x \simeq 0) = \Omega_{MiAE-gap}$.

4.3 Global modes with kinetic effects

4.3.1 Eigenvalue problem with kinetic effects

In this section, we face the problem of shear Alfvén mode stability inside a magnetic island, with a fluid model where we add also kinetic effects, in particular effects of finite Larmor radius (FLR). These are shown to be crucial to determine the dynamics of the modes in a plasma where the factor $k_\perp \varrho_i$ is not negligible, giving rise to a class or modes which take the name of Kinetic Alfvén Eigenmodes (KAE). Here the ion Larmor radius is defined as $\varrho_i = v_{ti}/\sqrt{2}\,\omega_{ci}$, where $v_{ti} = \sqrt{2T/m_i}$ is the thermal velocity and $\omega_{ci} = eB/m_i c$ is the ion gyro-frequency. The model equations we adopted in the previous sections, are the equations of ideal MHD, namely fluid equations where (ion) Larmor radius effects are neglected, under the assumption they are much smaller than the length scales of the modes, and therefore they don't enter the mode dynamics. We have seen ellipticity induced MiAE exist with frequency inside the continuum gap, and we will show here that, by adding kinetic effects, another solution of the eigenvalue problem can be found, with frequency outside the continuum gap. This means that a necessary boundary condition for such a mode, is to be vanishing at the flux surface where continuum damping occurs.

The model equations we adopt here, are the vorticity equation, Eq. 4.1 and the Ohm's law, Eq. 4.2, modified in order to take into account of the finite, but small value of $k_\perp \varrho_i$. The kinetic terms are added to the model equations following the conceptual scheme given by Rosenbluth and Rutherford [39]. Vorticity equation and Ohm's law are written in the starting form:

$$\Big(1 + \frac{3}{4}\varrho_i^2(1 + q^2\delta_{kin})\nabla_\perp^2\Big)\frac{\tilde{\omega}^2}{v_A^2}\nabla_\perp^2\phi + i\frac{\omega}{c_L}\,\boldsymbol{B}\cdot\boldsymbol{\nabla}\Big(\frac{\nabla_\perp^2}{B}A_\parallel\Big) - \\ - \frac{4\pi i\omega}{c_L^2}\boldsymbol{\nabla}\Big(\frac{J_\parallel}{B}\Big)\cdot(\boldsymbol{\nabla}\times\boldsymbol{A}) = 0 \tag{4.32}$$

$$E_\parallel = -\frac{\boldsymbol{B}\cdot\boldsymbol{\nabla}}{B}\phi + i\frac{\omega}{c_L}A_\parallel = E_{\parallel kin} \tag{4.33}$$

where, with respect to Eq. 4.1 and Eq. 4.2, a term proportional to $(3/4)\varrho_i^2(1+q^2\delta_{kin})\nabla_\perp^2$ has been added to the inertia term of the vorticity equation, and a term $E_{\parallel kin}$ to the Ohm's law. Note that the parallel component of the electric field is zero only in ideal MHD, but is nonzero when kinetic effects are considered. The form of δ_{kin} and $E_{\parallel kin}$ has been left implicit on purpose, and an explicit form will be given once the

eigenvalue problem is set. Now we write the differential operators as in Section 4.2.1, namely $\nabla_\perp^2 = (1/\rho)d_\rho \rho\, d_\rho - j^2/\rho^2$ and $(B\cdot\nabla)/B = ik_\parallel(\rho)$, where $d_\rho = d/d\rho$, and substitute the perturbed vector potential $A_\parallel$ in Eq. 4.32 in terms of the perturbed scalar potential ϕ, from Eq. 4.33. We obtain:

$$\frac{1}{\rho^3}\frac{d}{d\rho}\rho^3\big(\Omega^2 - Z_0^2k_\parallel^2\big)\frac{d}{d\rho}\xi - \frac{j^2-1}{\rho^2}\big(\Omega^2 - Z_0^2k_\parallel^2\big)\xi$$
$$+\frac{3}{4}\varrho_i^2(1+q^2\delta_{kin})\Omega^2\Big(\frac{1}{\rho^3}\frac{d}{d\rho}\rho^3\frac{d}{d\rho} - \frac{j^2-1}{\rho^2}\Big)\Big(\frac{1}{\rho^3}\frac{d}{d\rho}\rho^3\frac{d}{d\rho} - \frac{j^2-1}{\rho^2}\Big)\xi +$$
$$+ i\Big[\frac{1}{\rho^3}\frac{d}{d\rho}\rho^3 Z_0^2k_\parallel^2\frac{d}{d\rho}\Big(\frac{E_{\parallel kin}}{\rho k_\parallel}\Big) - \frac{j^2-1}{\rho^2}Z_0^2k_\parallel^2\Big(\frac{E_{\parallel kin}}{\rho k_\parallel}\Big)\Big] = 0 \qquad (4.34)$$

where $\xi = \phi/\rho$. We note that Eq. 4.34 is a generalization of the Hain-Lüst equation, defined in the operator in Eq. 4.11, that can be recovered here in the limit $\varrho_i\, d/d\rho \to 0$ (and neglecting $E_{\parallel kin}$, that will be shown to be proportional to $\varrho_i^2\, d^2/d\rho^2$ as well), namely using the hypothesis of validity of the ideal MHD regime. On the other hand, if FLR effects are retained, we note that higher order radial derivatives have been added to the Hain-Lüst equation. The smallness parameter ϱ_i defines a new scale of the system, that modifies substantially the dynamics when the mode length scale is comparable with ϱ_i, i.e. when $\varrho_i\, d/d\rho$ is not negligible. This separation of scales is common not only in plasma physics, where it can be given by non-ideal effects such as kinetic effects, resistivity or finite electron inertia, but it is common more generally in fluid physics, the most famous representative equation being the Navier-Stokes equation. In the Navier-Stokes equation, the smallness parameter is the viscosity η, that determines the separation of scales between the ideal region, where $\eta\, d/d\rho$ is negligible and the system is described by the Euler equation, and the non-ideal region, a narrow boundary layer where $\eta\, d/d\rho$ is not negligible. In the following, we will focus on modes where $\varrho_i\, d/d\rho$ is not negligible.

Here, if we make the assumptions that $\rho\, d/d\rho \gg 1$ and $\varrho_i\, d/d\rho \leq 1$, namely focusing on modes with short characteristic length scales, Eq. 4.34 is greatly simplified:

$$\frac{3}{4}\varrho_i^2(1+q^2\delta_{kin})\Omega^2\frac{d^4}{d\rho^4}\xi + \big(\Omega^2 - Z_0^2k_\parallel^2\big)\frac{d^2}{d\rho^2}\xi + iZ_0^2k_\parallel^2\frac{d^2}{d\rho^2}\Big(\frac{E_{\parallel kin}}{\rho k_\parallel}\Big) = 0 \quad (4.35)$$

In the next Section, an explicit form of δ_{kin} and $E_{\parallel kin}$ in terms of the

equilibrium plasma parameters and of the perturbed function ξ is given, and the eigenvalue problem is studied.

4.3.2 Magnetic island induced kinetic-AE

Here, we give an explicit form of the eigenvalue equation, Eq. 4.35, substituting the values of the kinetic terms as suggested in reference [41]. The existence of the solutions is studied by imposing as boundary conditions that the values vanish where the continuum damping acts. These solutions correspond to KAE located inside the magnetic island. The eigenvalue equation, Eq. 4.35, is written as:

$$\varrho_i^2\Big(\frac{3}{4}+\frac{q^2}{\hat{\omega}}S_0(\hat{\omega})\Big)\Omega^2\frac{d^4}{d\rho^4}\xi+\big(\Omega^2-Z_0^2k_\parallel^2\big)\frac{d^2}{d\rho^2}\xi=0 \tag{4.36}$$

where

$$S_0(\hat{\omega})=\frac{q^2}{2\hat{\omega}^2}\Big[L(\hat{\omega})-2L(\frac{\hat{\omega}}{2})-\frac{2N(\hat{\omega})}{D(\hat{\omega})}\Big(H(\hat{\omega})-2H(\frac{\hat{\omega}}{2})\Big)+$$

$$+\frac{N^2(\hat{\omega})}{D^2(\hat{\omega})}\Big(F(\hat{\omega})-2F(\frac{\hat{\omega}}{2})\Big)\Big]+T(\hat{\omega})-\frac{2N(\hat{\omega})}{D(\hat{\omega})}V(\hat{\omega})+\frac{N^2(\hat{\omega})}{D^2(\hat{\omega})}Z(\hat{\omega})+$$

$$+\frac{q^2}{\hat{\omega}^2D(\hat{\omega}/2)}\Big[F(\frac{\hat{\omega}}{2})-F(\hat{\omega})-\frac{N(\hat{\omega})}{D(\hat{\omega})}\Big(N(\frac{\hat{\omega}}{2})-N(\hat{\omega})\Big)\Big]^2 \tag{4.37}$$

Here $\hat{\omega}=\omega/\omega_{ti}$ and $\omega_{ti}=v_{ti}/qZ_0$ is the transit frequency. The functions used in Eq. 4.37 are defined in Sec. 7.2. The function $Z(\hat{\omega})$ is the plasma Z-function [42]. In the limit $\hat{\omega}\gg 1$ (i.e. far from the BAE-CAP), from the expression of $S_0(\hat{\omega})$, assuming $(q^2(7/4+\tau)\gg 1)$ with $\tau=T_e/T_i$, one can show:

$$\mathrm{Re}\Big(\frac{3}{4}+\frac{q^2}{\hat{\omega}}S_0(\hat{\omega})\Big)\simeq\frac{3}{4}-\frac{q^2}{\hat{\omega}^2}\Big(\frac{13}{4}+3\tau+\tau^2\Big)+\frac{q^4}{\hat{\omega}^4}\Big(\frac{747}{32}+\frac{481}{32}\tau+\frac{35}{8}\tau^2+\frac{1}{2}\tau^3\Big) \tag{4.38}$$

The eigenvalue equation, Eq. 4.36, can be put in the form of a Schrödinger equation, introducing the plasma displacement $\xi'=d\xi/d\rho$ and integrating the whole equation over ρ:

$$\frac{d^2}{d\rho^2}\,\xi'(\rho)+\frac{(\Omega^2-Z_0^2\,k_\parallel^2(\rho))}{\varrho_i^2\Omega^2(3/4+q^2S_0(\hat{\omega})/\hat{\omega})}\,\xi'(\rho)=\text{const.}=0 \tag{4.39}$$

The value of the constant at the RHS can be set to zero here, because we are looking for localized solutions, namely solutions decaying exponentially far from the peak position. In fact, the constant at the RHS is

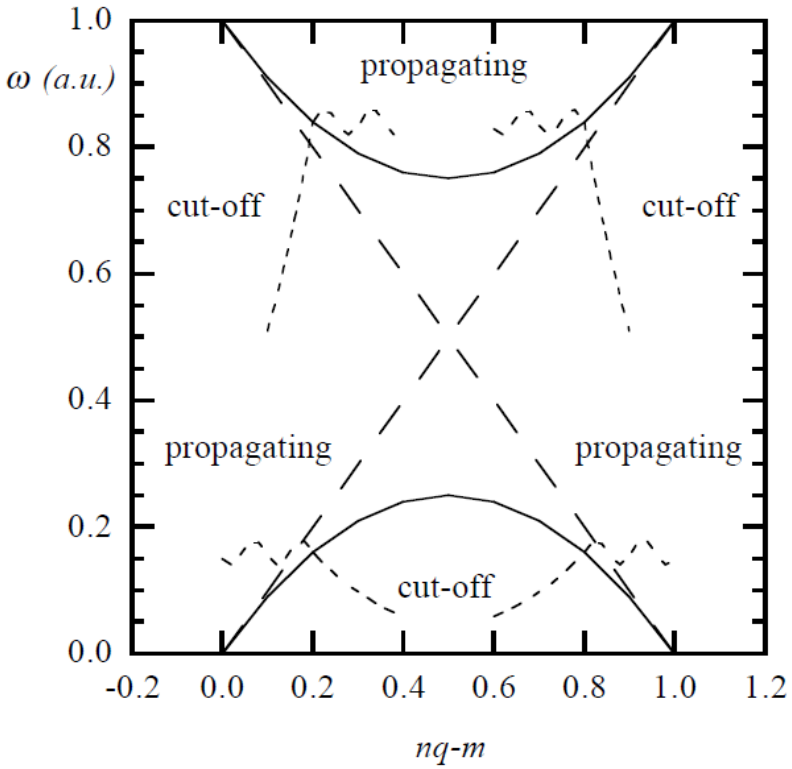

Figure 4.2: Kinetic Alfvén Eigenmodes (dotted lines) induced inside a magnetic island in the proximity of the ellipticity induced MiAE gap. The SAW continuous spectrum, calculated in Chapter 3, is also shown as a continuous line. These modes are the analogous of kinetic Alfvén Eigenmodes in tokamaks [43], where the only difference is the structure of the equilibrium inside the magnetic island, which is described by the structure of the continuous spectrum.

again a term determined by the equilibrium profiles, and it is important to study the MHD solutions, which are not considered in this section.

Looking at Eq. 4.39, we can see that, if the denominator of the potential function is positive, then the solution $\xi'(\rho)$ is oscillating when the numerator is positive and is exponentially decaying or growing when the numerator is negative. We look for a localized solution inside the magnetic island. This means that a physical solution of our problem has to be oscillating in a localized region, to be vanishing at the continuum damping location, and to be exponentially decaying outside this region, in order not to approach the magnetic island separatrix. It has been proved that the value of $\mathrm{Re}(3/4 + (q^2/\hat{\omega})S_0)$ can be negative only for $q < 2.6$ (see Reference [41]). On the other hand, we have seen in Sec. 2.1 (see Fig. 2.3), that for typical magnetic island size, we have $q > 2.6$, and therefore the denominator is always positive. Therefore, for typical values of plasma parameters, corresponding to a positive denominator, a physical solution (i.e. a solution whose eifenfunction is vanishing at $\pm\infty$) has frequency which is above the MiAE-gap, as shown in Fig. 4.2 and 4.3.

4.4 Summary

In this chapter, we have studied the existence of global Alfvén Eigenmodes (AE), namely AE with a discrete frequency and a finite radial width, inside the magnetic island. We have adopted a model for the equilibrium, where the tokamak curvature is contained only in the definition of the normalized frequency. In other words, the equilibrium has been chosen as a straight flux tube, modeling the region inside the magnetic island. This allows us to focus on the main mechanism of formation of AE inside the island: namely eccentricity of the flux surfaces. Moreover, we have studied the existence AE due to the effect of finite Larmor radius. The case of small eccentricity of the flux surfaces has been considered in this chapter, for this is the case affordable with analytical techniques.

The first result has been that MHD theory predicts the existence of global AE with frequency inside the continuum gap described in Sec. 3.1. This means that these modes are practically unaffected by continuum damping. In fact, the equilibrium magnetic field profile inside a magnetic island hosts potential wells where AE can grow unstable. The eigenvalue equation has been derived and solved analytically with a techinque of solution matching. As a result, we provide the dispersion relation of ellipticity induced MiAE (or MiEAE).

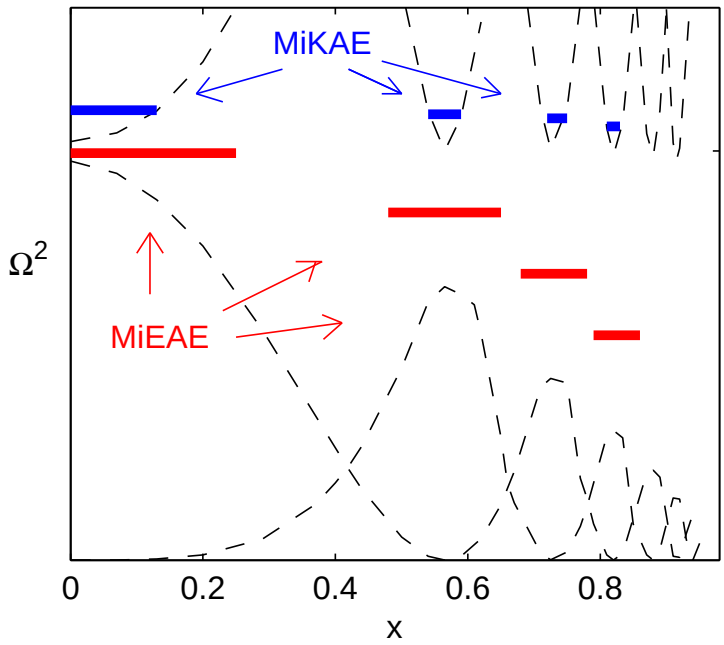

Figure 4.3: Schematic picture of Alfvén Eigenmodes inside a magnetic island. Kinetic AE are depicted in blue and ellipticity induced AE in red. The continuous spectrum is also shown, as a dotted line (compare with Fig. 3.3).

Moreover, the contribution of FLR terms was found to be crucial to create another potential well for AE. The theoretical model adopted to study AE taking into account FLR effects, is found in references [39, 41]. These modes with characteristic length scale is of the order of the ion Larmor radius, have been identified as kinetic MiAE (or MiKAE). Their frequency is predicted to be above the MiAE ellipticity gap. They have been described as localized in a region close to the rational surface, and their perturbed field is predicted to be vanishing outside this region.

In order to calculate the growth rate of MiEAE and MiKAE inside a magnetic island in a tokamak, a further study of driving and damping mechanisms is required, taking into account of resonances with thermal and energetic particles, which is out of the scope of this dissertation. We expect the driving mechanism to be given mainly by energetic particles radial nonuniformities. On the other hand, MiAE could nonlinearly interact with energetic particles and affect their redistribution in the proximity of the magnetic island rational surface.

Chapter 5

Beta induced AE in the presence of an island

5.1 Introduction

The radial structure of the SAW continuous spectrum in the presence of a magnetic island has been studied in Chapter 3, both inside and outside the magnetic island. The structure of the continuous spectrum has given us information on where global instabilities can grow, free of continuum damping. Inside the magnetic island, we have found gaps in the continuous spectrum breaking the intersection of the continuum branches of modes with different poloidal mode number j. In particular, large gaps are found at the intersection between modes with j and $j+2$, induced by ellipticity of the flux surfaces. These gaps in the continuous spectrum make the existence of ellipticity induced MiAE inside the island possible.

Global instabilities can grow also at frequencies lower than the beta-induced Alfvén Eigenmode continuum accumulation point (BAE-CAP). In fact, in our fluid model, continuous spectrum has frequencies only above the BAE-CAP. This means that Alfvénic instabilities with frequencies below the BAE-CAP are not affected by continuum damping. The main instability with frequencies below the BAE-CAP, is the beta induced Alfvén Eigenmode (BAE) [15, 22, 23]. In this chapter, we discuss the nonlinear modification of the BAE frequency, due to the presence of a magnetic island.

In the first section, the main characteristics of BAE are recalled, and the linear dispersion relation is provided, as a result of the gyro-kinetic analysis. In the second section, we provide the nonlinear modification

of the BAE frequency as a result of the upward shift in the BAE-CAP, discussed in Sec. 3.2. In the third section we discuss experimental observations of BAE in the FTU tokamak. Finally, the last section is devoted to a comparison between our theoretical predictions, and the experimental data.

5.2 Beta induced Alfvén Eigenmodes

Beta induced Alfvén Eigenmodes (BAE) are Alfvénic instabilities growing in tokamak plasmas [14, 22, 23]. The BAE frequency lies in the BAE gap in the lower frequency part of the continuous spectrum. This gap is due to a coupled effect of curvature and compressibility, where compressibility is expressed by a finite β, β being the ratio of thermodynamic and magnetic pressures. The upper extremum of the BAE gap is named BAE continuum accumulation point (BAE-CAP). The value of the BAE-CAP calculated in fluid theory [14] was given in Eq. 2.41 and the value calculated in gyro-kinetic theory [23], was given in Eq. 2.43.

BAE are known to interact nonlinearly with the fast particle population. In particular, they can cause energetic ion losses, and therefore, they are as problematic as the toroidicity induced Alfvén Eigenmodes with respect to alpha particle confinement in fusion devices. They are known to be driven by fast ions during neutral beam injection heating, but they were found recently also in purely ohmic heated plasmas, in the Frascati Tokamak Upgrade (FTU) [28, 32]. These observations, showed a clear empirical correlation between the dynamics of BAE and magnetic islands. In particular, the BAE frequency was found to depend on the magnetic island amplitude [31], and BAE were seen only when the magnetic island amplitude was over a certain threshold. This empirical evidence was the basis for conjecturing that, in fact, BAE can be driven by nonlinear coupling with magnetic islands.

In this section, we recall the results obtained in the framework of gyro-kinetic theory, about the BAE dispersion relation, in the limit of vanishing magnetic islands [32, 44], whereas in the next section we provide the nonlinear frequency modification due to the presence of the magnetic island. The dispersion relation of BAE can be derived by matching asymptotically the solution obtained in a narrow inertial layer centered at the rational surface, where kinetic effects are important [44], and the solution obtained in the so-called ideal region, namely far from the inertial layer, where kinetic effects can be neglected [45]. Since we want to study modes interacting with a magnetic island, we consider BAE with

tearing symmetry, namely with odd parallel component of the vector potential $\delta A_\parallel$. The result, taking into account toroidicity, finite Larmor radius (FLR) effects and finite banana orbit width (FOW) effects, is [32]:

$$-2\sqrt{\tilde{Q}}\frac{\Gamma\left(\frac{3}{4}-\frac{\Lambda^2}{4\tilde{Q}}\right)}{\Gamma\left(\frac{1}{4}-\frac{\Lambda^2}{4\tilde{Q}}\right)}=\frac{|\hat{s}m|\pi}{\Delta'} \tag{5.1}$$

where Γ is the complex Gamma function [46], $\hat{s}$ is the magnetic shear, $\Delta' = r_0[d\ln\delta A_\parallel/dr]_{r_0^-}^{r_0^+}$ is the jump in the radial derivative of the radial magnetic field fluctuation at the rational surface $r_T = r_0$, and the functions Λ and $\tilde{Q}$ are defined as:

$$\Lambda^2(\omega)=\frac{\omega^2}{\omega_A^2}\left(1-\frac{\omega_{*pi}}{\omega}\right)+$$

$$+q^2\frac{\omega\omega_{ti}}{\omega_A^2}\left[\left(1-\frac{\omega_{*ni}}{\omega}\right)F_{BAE}(\omega/\omega_{ti})-\frac{\omega_{*Ti}}{\omega}G_{BAE}(\omega/\omega_{ti})-\frac{N_{BAE}^2(\omega/\omega_{ti})}{D_{BAE}^2(\omega/\omega_{ti})}\right] \tag{5.2}$$

$$\tilde{Q}^2(\omega)=\hat{s}^2k_\theta^2\varrho_i^2\frac{\omega^2}{\omega_A^2}\left[\frac{3}{4}\left(1-\frac{\omega_{*pi}}{\omega}-\frac{\omega_{*Ti}}{\omega}\right)-q^2\frac{\omega_{ti}}{\omega}S_{BAE}(\omega)+\frac{\omega_A^4}{\omega^4}\frac{T_e}{T_i}\frac{\Lambda^4}{\left(1-\frac{\omega_{*ni}}{\omega}\right)}\right] \tag{5.3}$$

Here the characteristic frequencies are $\omega_{*ns} = [(T_s c)/(e_s B)](\boldsymbol{k}\times\boldsymbol{b})\cdot(\boldsymbol{\nabla}n)/n$, $\omega_{*Ts} = [(T_s c)/(e_s B)](\boldsymbol{k}\times\boldsymbol{b})\cdot(\boldsymbol{\nabla}T_s)/T_s$, $n_i = n$ is the ion density, $\omega_{*ps} = \omega_{*ns} + \omega_{*Ts}$, $\omega_{ti} = \sqrt{2T_i/m_i}/(qR_0)$, and F_{BAE}, G_{BAE}, N_{BAE}, D_{BAE} and S_{BAE} are defined in Appendix 7.2. The subscript s stands for a particle species index (s=i for ions and s=e for electrons). The term proportional to ω^2/ω_A^2 in Λ is the usual polarization current contribution, whereas the other term is due to geodesic curvature coupling; in $\tilde{Q}^2$ the term proportional to 3/4 represents the FLR effects, the second term contains the FOW effects and the third term reproduces the known result for KAW [5], i.e. $\tilde{Q}^2 = (3/4 + T_e/T_i)(\omega/\omega_A)^2\hat{s}^2k_\theta^2\varrho_i^2$, in the limit $\omega_{ti}/\omega \to 0$, $\omega_{*pi}/\omega \to 0$.

5.3 Nonlinear modification of the BAE frequency

The dispersion relation given in Eq. 5.1, was obtained in the framework of linear gyro-kinetic theory, and describes BAE in an equilibrium without magnetic islands. In this section, we derive the nonlinear modification with a perturbative theory approach. Then in next sections, knowing the linear dispersion relation and the nonlinear shift in frequency due to the presence of the island, we can compare the theoretical frequency scalings with the experimental data.

We want to study the BAE nonlinear dynamics by adopting a perturbative theory. This means that, in our model, we consider BAE as Alfvénic instabilities with an eigenfunction peaked around the rational surface, and with a characteristic radial size which is supposed to be much larger than the magnetic island's width. We want to derive the modification in the BAE frequency, due to the presence of the magnetic island, in this framework. The BAE frequency in linear theory, named here $f_{BAE,0}$, has been given in Eq. 5.1, and the result is a value which lies below the BAE-CAP value, given by Eq. 2.43 in normalized frequencies Ω (and by Eq. 3.8 in non-normalized frequencies $f = \omega/(2\pi)$).

In chapter 3, we have seen that the change in the equilibrium magnetic field, due to the presence of the magnetic island, results in a change in the structure of the continuous spectrum. In particular, inside the island a structure similar to the continuous spectrum in tokamaks is formed, and outside the island an upward shift in the continuum accumulation point is found, resulting in a nonlinearly modified BAE-CAP, expressed by Eq. 3.18. The value of the nonlinearly modified BAE-CAP frequency can be also written in non-normalized frequencies f as in Eq. 3.19, that is repeated here for convenience:

$$f_{nlBAE-CAP} = f_{BAE-CAP}\sqrt{1 + \frac{q_0^2 s^2 n_{isl}^2}{4}\frac{W_{isl}^2}{r_0^2}\frac{f_A^2}{f_{BAE-CAP}^2}} \tag{5.4}$$

Where all parameters are calculated at the rational surface, and W_{isl} is the magnetic island half width.

Now, we assume that the contribute of the continuous spectrum modification inside the magnetic island is negligible with respect to the contribute outside the magnetic island, in modifying the BAE dispersion relation. This is consistent with the perturbative theory approximation, where the magnetic island is small with respect to the BAE radial size.

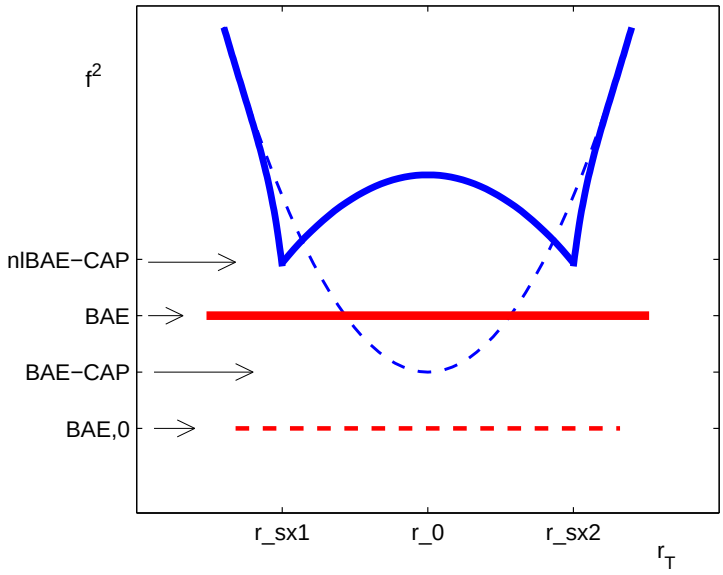

Figure 5.1: Schematic picture of the continuous spectrum $f^2(r_T)$ of modes with the same helicity as the magnetic island. Here a tokamak equilibrium is considered, with and without magnetic island. In an equilibrium without magnetic island the continuous spectrum is depicted by the dotted parabola, the frequency of the BAE-CAP (positioned at the rational surface r_0) is given by Eq. 2.43, and the BAE is depicted by a horizontal dotted line, labeled BAE,0. In an equilibrium with a magnetic island, the BAE-CAP splits in two nonlinear modified BAE-CAPs, and the BAE is expected to have a higher frequency, given by Eq. 5.5. The separatrix positions are labeled by r_sx1 and r_sx2, and the magnetic island half-width is given by $W_{isl} = |r\_sx - r_0|$.

Outside the island, we have shown in Chapter 3 that the main modification of the continuous spectrum due to the presence of the island is the upward shift in frequency of the BAE-CAP, resulting in the nonlinearly modified BAE-CAP described by Eq. 5.4. We can reasonably assume that the shift in frequency of the BAE due to the presence of the island follows linearly the modification of the equilibrium, which results in the shift in frequency of the BAE-CAP. Therefore, by assuming a perturbatively small magnetic island, we can finally obtain the value of the BAE frequency as a function of the magnetic island width:

$$f_{BAE} = f_{BAE,0}\sqrt{1 + \frac{q_0^2 s^2 n_{isl}^2}{4}\frac{W_{isl}^2}{r_0^2}\frac{f_A^2}{f_{BAE-CAP}^2}} \tag{5.5}$$

where $f_{BAE,0}$ is the frequency of BAE for a vanishing magnetic island, obtained by solving Eq. 5.1, and $f_{BAE-CAP}$ is given in Eq. 3.8. In Fig. 5.1, a schematic picture of the continuous spectrum of modes with the same helicity as the magnetic island is shown, and the BAE is shown, with frequency below the nonlinearly modified BAE-CAP.

One can further simplify Eq. 5.5, by linearizing it in the magnetic island amplitude, as done for the central frequency of the MiAE gap (Eq. 3.7), obtaining an approximate value:

$$f_{BAE} \simeq f_{BAE,0} + \frac{q_0^2 s^2 n_{isl}^2}{8}\frac{W_{isl}^2}{r_0^2}\frac{f_A^2}{f_{BAE-CAP}} \tag{5.6}$$

Again, the regime of validity of the linear approximation is given by:

$$\frac{W_{isl}}{r_0} \ll \frac{2}{q_0|s|n_{isl}}\frac{f_{BAE-CAP}}{f_A} \sim \frac{\sqrt{\beta}}{q_0|s|n_{isl}}$$

Where, even for low-beta plasmas, the order of magnitude of the island-induced frequency shift in the BAE-CAP frequency can be comparable with the BAE-CAP frequency itself.

In the following sections, we will discuss experimental observations of BAE in FTU tokamak, and we will compare the experimental frequency scaling with our theoretical prediction.

5.4 Experimental observations

FIG. 5.2 shows a spectrogram from Mirnov coils for FTU shot #25877 (see Ref. [47]). The lower lines ($0 \leq f_{\rm exp} \leq 10$ kHz) represent an $(m_{isl}, n_{isl}) = (-2, -1)$ magnetic island that forms, then locks and unlocks several times. The loching and unlocking of the magnetic island is due to the interaction with the metal external arms of the tokamak vessel, which is stronger the wider the magnetic island is. The lines at higher frequencies (30 kHz $\leq f_{\rm exp} \leq$ 65 kHz) have been interpreted as BAE in a previous work [32] based on linear kinetic analysis neglecting the magnetic island induced frequency shift. Several harmonics of the same BAE mode are found, the dominant one having a frequency of 40-50 KHz. The observed frequency splitting of the mode is due to the Doppler shift (for the BAE propagate with the same velocity in opposite directions in the frame of reference of the magnetic island) and vanishes when the island locks [28, 32]. In the interval 0.20 s $\leq t \leq$ 0.25 s $f_{\rm exp}$ increases, the same phenomenology appearing after each mode unlocking. The magnetic island width can be measured with a soft X-Ray diagnostic. FIG. 5.2 shows a soft X-ray tomographic reconstruction of the plasma displacement Δ measured at various radial positions and times in FTU shot #25877. The displacement at $q = 2$ ($r = 14\,cm$) corresponds to a saturated magnetic island. The island width oscillates in time around a saturated value of $\Delta \simeq 3cm$, corresponding to an half width of $W_{isl} \simeq 1.5\,cm$.

Looking closely at the first $f_{\rm exp}$ increase in FIG. 5.2, it is possible to plot the frequency versus the island magnetic field fluctuation for the strongest mode, i.e. the one with $f_{\rm exp} \sim 45$ kHz. The actual mode frequency is approximately the average of the two branches. FIG. 5.3 shows $f_{\rm exp}$ versus $B_{isl}/B_{pol,0}$, from which a linear scaling is clearly seen for small values of the island width. In this plot the value of $B_{isl}/B_{pol,0}$ is obtained by appropriate rescaling of Mirnov coil measurements, consistently with the direct measurement of the island width from soft X-Rays tomographic data presented in FIG. 5.2. In section 5.5 we compare the experimental data shown in FIG. 5.3 with the theoretical BAE frequency given by Eq. 5.5. Most of the quantities can be taken directly from the experimental observations. On the other hand, the ion temperature T_i and the magnetic shear s cannot be measured directly. An approximate value can be estimated by predictive simulations with the JETTO code [48]. The uncertainty remaining in the value of T_i and s is used here as a free parameter in the small domain of allowed values given by the JETTO code, in order to achieve a better agreement between theoretical predictions and experimental observations (see Fig. 5.3).

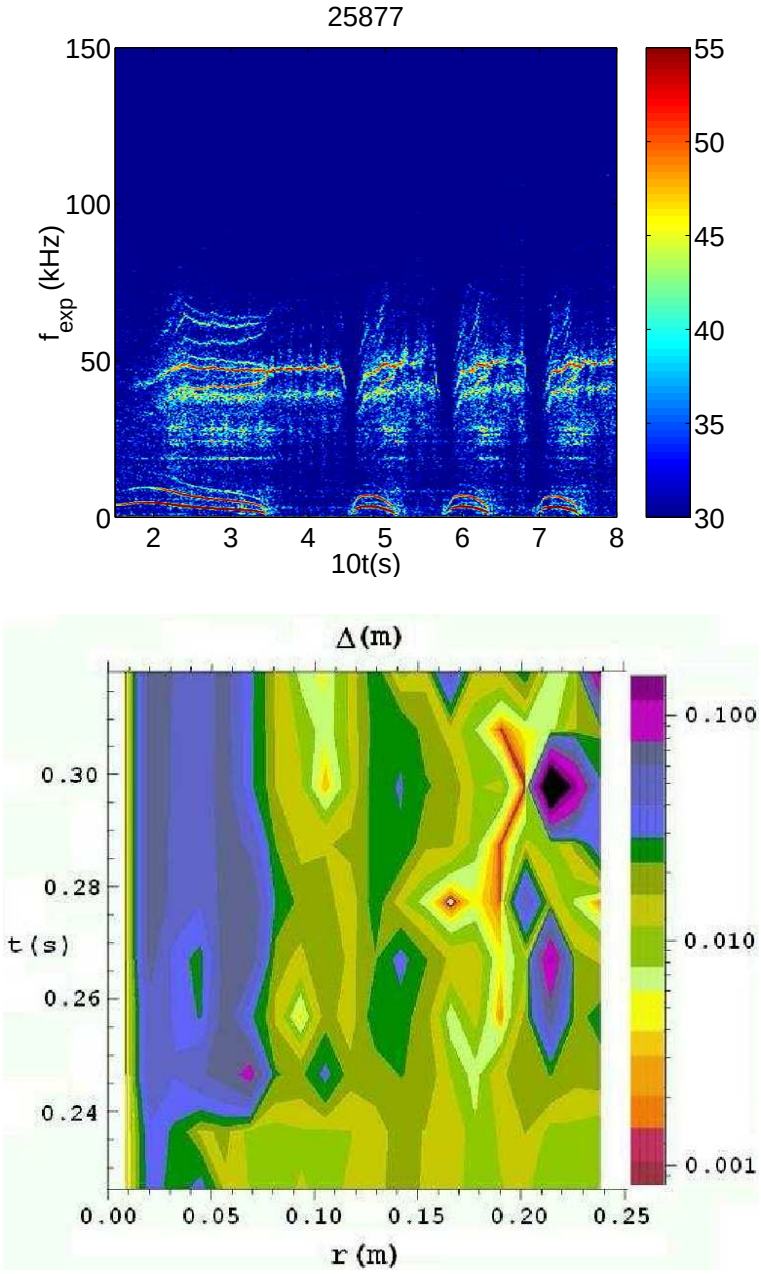

Figure 5.2:
Upper figure: Spectrogram (i.e. spectral amplitude versus time t and frequency $f_{\exp}$) of the signal from poloidal field Mirnov coils in FTU shot #25877.
Lower figure: Soft X-Ray tomography, showing the plasma displacement Δ versus time and radial position. At $q = 2$ ($r = 14cm$), the displacement $\Delta \simeq 3cm$ corresponds to a magnetic island half width of $W_{isl} = 1.5cm$. These experimental data are taken from reference [47].

5.5 Interpretation of the experimental data

In section 5.4, we have presented data relative to experimental observations of BAE in FTU plasma shot #25877, in the presence of a magnetic island [47]. The BAE frequencies have a clear dependence on the magnetic island size, starting from $f \simeq 34$ kHz for vanishing island and reaching $f \simeq 45$ kHz when the island is saturated at $B_{isl}/B_{pol} \simeq 3.5 \cdot 10^{-3}$ (corresponding to $\Delta = 2W_{isl} \simeq 3cm$ if we take $s = 0.6$). This scaling is consistent with Eq. 5.5, where the BAE theoretical frequency is given as a function of W_{isl}/r_0. During the island growth, the observed mode frequency increases roughly linearly, in the early phase, when the island is small (consistently with Eq. 5.6). In order to calculate the BAE frequency with Eq. 5.5, we first estimate the Alfvén frequency and the BAE-CAP frequency. The Alfvén frequency can be calculated by knowing that $R_0 = 93$ cm, and $B_0 = 5.8 \cdot 10^4 G$, obtaining $f_A = 1.2 \cdot 10^3$ kHz. The BAE-CAP frequency can be estimated as $f_{BAE-CAP} \simeq 68$ kHz, consistently with JETTO data of temperatures oscillating at $T_e = T_i = 0.6 - 0.7$ keV. The fact that observed mode frequencies fall below those of the BAE-CAP, confirms the interpretation of these fluctuations as BAE nonlinearly interacting with the magnetic island [32].

The magnetic shear is the parameter which is estimated with more uncertainty. Here, by knowing that the saturated island is $3cm$ wide, we have rescaled the magnetic field values obtained at the Mirnov coils, consistently with this magnetic island width, and assuming $s = 0.6$. With the same assumption, we have calculated the theoretical BAE frequency with Eq. 5.5. The comparison of experimental data and theoretical prediction is given in Fig. 5.3. We see that a good agreement is found, for this value of magnetic shear, at low magnetic island amplitudes. On the other hand a discrepancy is found at magnetic island amplitude with $B_{isl}/B_{pol,0} > 2 \cdot 10^{-3}$. Therefore, we can state that the perturbative theory gives consistent results only for low magnetic island amplitudes. For vanishing island amplitudes, the theoretical prediction approaches the value of $f_{BAE,0} \simeq 34$ KHz. It is worthwhile noting here, that BAE are detected in this FTU shot, only above the threshold of $B_{isl}/B_{pol,0} = 0.7 \cdot 10^{-3}$. This means that the available free energy can balance the damping (due to ion Landau damping), only above a certain magnetic island size. Some attempts of modeling the drive mechanism have been made recently [36]. Nevertheless a model predicting at the same time this value of threshold and the shift in frequency of BAE does not exist at the moment. This problem is out of the scope of this dissertation, and will be treated in a dedicated paper.

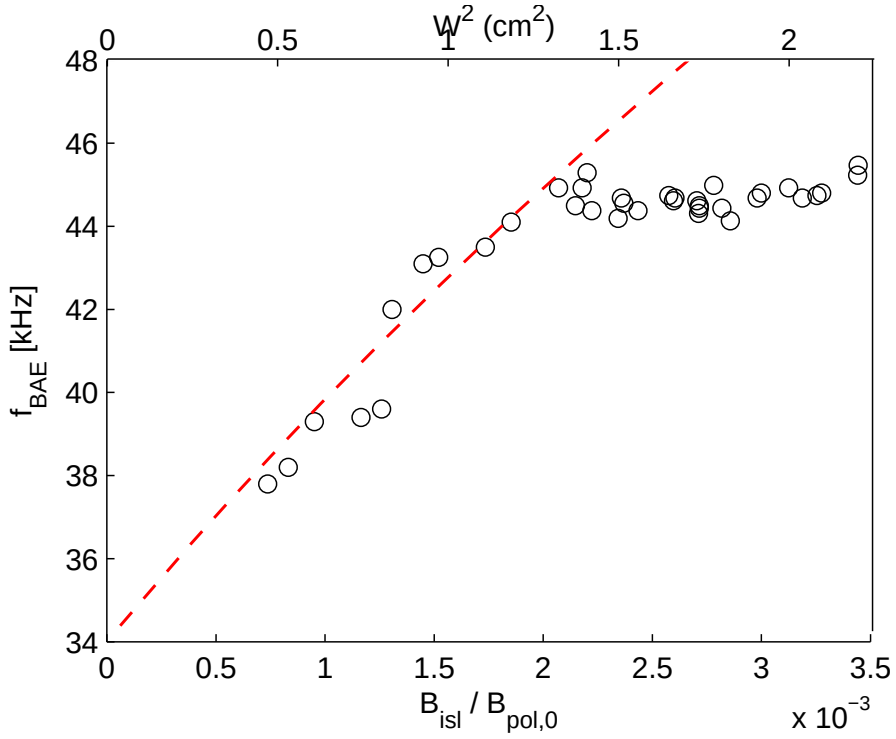

Figure 5.3: BAE frequency versus magnetic island amplitude, for the first f_{exp} increase displayed in FIG. 5.2. The circles are experimental data, as obtained by Mirnov coil measurements of perturbed magnetic field, and the red dotted line is the theoretical prediction given by Eq. 5.5, obtained by choosing $s = 0.6$. The upper x-axis is the magnetic island half width square, and the lower x-axis is the ratio of island and poloidal magnetic fields. For this shot, BAE are detected only above a certain threshold in magnetic island amplitude: $B_{isl}/B_{pol,0} = 0.7 \cdot 10^{-3}$. Note that the theoretical prediction, which is derived for perturbatively small magnetic island, is in agreement with the experimental data for the lowest values of island amplitude, whereas there is a divergence at higher island amplitudes. These experimental data are taken from reference [47].

5.6 Summary

In Chapter 3, we have shown that the SAW continuous spectrum of a finite-beta tokamak plasma in the presence of a magnetic island still presents the beta-induced gap at low-frequencies, and that the gap width is changed by the presence of the island. This window in the Alfvén continuum, namely $0 < f < f_{BAE-CAP}$, allows BAE to grow free of continuum damping in the proximity of the BAE continuum accumulation point [14, 22, 23, 44, 49]. We have also shown that new local structures of the SAW continuum are formed due to the presence of the magnetic island and that new continuum gaps (MiAE gaps) arise at higher frequencies. At frequencies $f > f_{BAE-CAP}$ new eigenmodes could grow inside the magnetic island, in the presence of a suitable driving free energy source. The substantial difference between these two frequency windows is given by the radial continuum structure. In fact, a mode with frequency inside the beta-induced gap can extend radially outside the separatrix without resonantly exciting the SAW continuum. On the other hand, a mode inside the MiAE gap is localized inside the magnetic island.

At frequencies lower than the BAE-CAP, we have seen that modes named BAE can grow and extend outside the island, and therefore be detected by Mirnov coils diagnostics located outside the tokamak. The linear dispersion relation of BAE was calculated recently in the framework of gyro-kinetic theory, in the limiting case of vanishing magnetic island. Here, we have calculated the nonlinear frequency shift due to the presence of the island, by adopting a perturbative theory where the magnetic island is supposed to be thin with respect to the BAE radial size. The theoretical BAE frequency has been compared with experimental data of BAE observed in FTU. The agreement of theoretical and experimental data has been found at low magnetic island amplitudes, whereas a discrepancy has been found at higher magnetic island amplitudes. Moreover, the observations show that BAE are detected only above a certain threshold in magnetic island amplitude. This suggests that the drive mechanism depends on the magnetic island amplitude, and balances the damping mechanism only above a certain threshold in the magnetic island size. The problem of BAE drive is not treated here, and will be faced in a dedicated paper.

Chapter 6

Conclusions

6.1 Motivations

In this dissertation, we have considered the dynamics of Aflvén modes in an equilibrium with a quasi-static magnetic island. Continuum modes and global modes have been considered both inside and outside the magnetic island. Continuum modes are singular structures that form when a shear Alfvén wave (SAW) in a nonuniform plasma approaches a resonance surface. Global Alfvén modes (AE, also called discrete Alfvén modes, because they have a discrete frequency), are modes with finite radial size and are eigenstates of the system.

The spectrum of continuum resonances is named continuous spectrum. Understanding the radial structure of the SAW continuous spectrum is one of the main aims in facing the MHD stability property of a tokamak equilibrium. In fact, continuum damping is one of the main damping mechanisms of shear Alfvén instabilities, and occurs at the resonant flux surfaces where the mode frequency is resonant with the continuous spectrum frequency. Therefore, a mode is not affected by continuum damping and can more easily grow unstable if its frequency lies in a gap of the continuous spectrum.

Global Alfvén modes are plasma instabilities whose characteristic frequency is of the same order of magnitude of energetic particles transit frequency. Energetic particles are present in the plasma as a product of fusion reactions, or as an effect of external plasma heating. Global Alfvén modes can resonantly interact with energetic particle populations, causing loss of confinement. For this reason, understanding the continuous spectrum structure and the stability of global Alfvén modes is one of the crucial problems, if one faces the stability problem of a tokamak plasma

and its potential impact on reaching the ignition condition.

6.2 Shear Alfvén wave continuous spectrum

The radial structure of the continuous spectrum of SAW is calculated in this dissertation in an equilibrium inside and outside a magnetic island flux tube. The equilibrium is considered to be static, due to the time scale separation between the magnetic island dynamics and the faster SAW dynamics. The flux tube is considered to be straight, in order to focus on the effects of the non-circularity of the cross section. Curvature effects are retained only in the formation of the BAE gap in the low frequency part of the continuous spectrum. A linear MHD model is adopted for finite-beta tokamak plasmas. A generalized safety factor is defined inside the magnetic island flux tube, giving information on the rational flux surfaces where different modes couple to create gaps in the SAW continuous spectrum. The linearized SAW equation is solved with a shooting method code inside a finite-size magnetic island and the result compared with the SAW continuous spectrum calculated in tokamak equilibria.

We have studied modes with the same helicity as that of the magnetic island, and modes with different helicity from that of the magnetic island. When considering modes with different helicities from that of the magnetic island in the region inside the magnetic island, we have found that there exists a SAW continuous spectrum, similar to that calculated in tokamak equilibria. For the limit of vanishing eccentricity of the flux surfaces, modes with different poloidal numbers are not coupled and therefore, the branches of the continuous spectrum intersect and there is no formation of gaps. This is shown to occur inside a magnetic island with very large (unrealistic) width, near the O-point, where the flux surfaces are nearly circular. On the other hand, a typical size magnetic island is shown to have wide gaps in the continuous spectrum, due to the strong eccentricity of the flux surfaces. This is analogous to the formation of EAE gaps in tokamaks, but is found here inside the magnetic island equilibrium.

When considering modes with the same helicity as the magnetic island, we have found that the BAE continuum accumulation point (BAE-CAP) is shifted in space from the rational surface of the island, to the separatrix flux surface position. Moreover, we have shown that the nonuniformity of the magnetic field intensity along the field lines generates a splitting between the frequency branches of the modes with even and

odd structures. The frequency of this splitting has a relevant value inside the island, and is negligible outside the island, for typical island sizes. Inside the magnetic island, we have found that the continuum frequency branches converge at the O-point to several magnetic island induced CAP (MiO-CAP). At the separatrix, the frequency of the BAE-CAP is splitted in two values. The continuum branch correspondent to the first odd eigenfunction inside the island converges to the original BAE-CAP, with same frequency as in absence of a magnetic island, and the other branches converge to a nonlinearly modified BAE-CAP, with a higher frequency. Outside the magnetic island, all continuum branches converge at the separatrix to the nonlinearly modified BAE-CAP.

We have also shown that new local structures of the SAW continuum are formed due to the presence of the magnetic island. The most remarkable novel feature is the presence of a continuous spectrum inside the island, very similar to that of a tokamak. In particular, gaps are present in the continuum inside the magnetic island, which correspond to regions free of continuum damping. These gaps are due to the ellipticity of the magnetic island flux surfaces.

6.3 Global Alfvén Eigenmodes

We have studied the existence of global AE, namely AE with a discrete frequency and a finite radial width, inside the magnetic island. We have focused on the main mechanism of formation of AE inside the island: namely eccentricity of the flux surfaces. Moreover, we have studied the existence of AE due to the effect of finite Larmor radius. The case of small eccentricity of the flux surfaces has been considered, for this is the case affordable with analytical techniques. The eigenvalue equation has been derived and solved analytically with a technique of solution matching. As a result, we provide the dispersion relation of ellipticity induced MiAE (or MiEAE). Their frequency lies inside the ellipticity induced gap, therefore they take the name of gap-modes. Moreover, the contribution of FLR terms was found to be crucial to create another potential well for AE. These modes with characteristic length scale of the order of the ion Larmor radius, have been identified as kinetic MiAE (or MiKAE). Their frequency is predicted to be above the MiAE ellipticity gap. They have been described as localized in a region close to the rational surface, and their perturbed field is predicted to be vanishing outside this region.

Here, we emphasize the analogy between the equilibrium inside a

magnetic island and the tokamak equilibrium, and, consequently, the analogies between AE within the magnetic islands (MiAE) and the well-known AE in tokamaks. Given that plasma equilibrium non-uniformities and wave resonant interactions with energetic particles provide, respectively, frequency range and mode drive [2, 3], the MiAE peculiarity resides in the corresponding SAW continuous spectrum dependence on the magnetic island size. Due to this strong similarity between an equilibrium inside a magnetic island and a tokamak equilibrium, we expect to find all kinds of Alfvénic instabilities inside a magnetic island, and not only instabilities ellipticity-MiAE. For instance, toroidicity-MiAE could grow inside a gap due to the flux tube toroidicity effects, which are not studied here and can be treated in a dedicated paper.

We have also shown that the SAW continuous spectrum of a finite-beta tokamak plasma in the presence of a magnetic island still presents the beta-induced gap at low-frequencies. This window in the Alfvén continuum, namely $0 < f < f_{BAE-CAP}$, allows BAE to grow free of continuum damping in the proximity of the BAE continuum accumulation point [14, 22, 23, 44, 49].

The substantial difference between MiAE and BAE is given by the radial continuum structure. In fact, a mode with frequency inside the

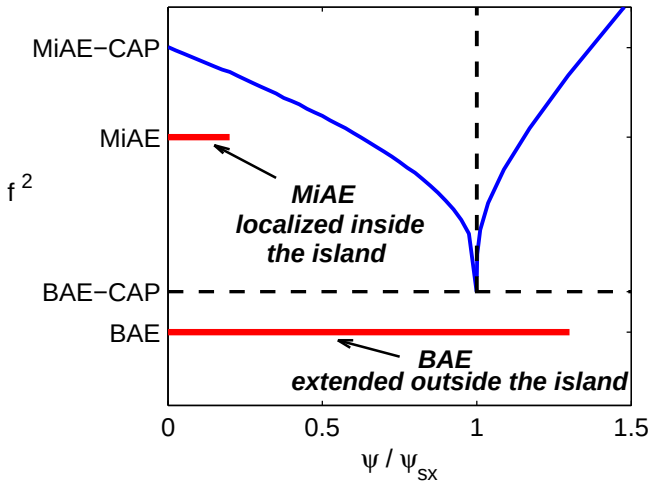

Figure 6.1: MiAE and BAE relative frequency and localization. The MiAE has a frequency higher than the nonlinearly modified BAE-CAP and is localized inside the island. The BAE has a frequency below the nonlinearly modified BAE-CAP and is more extended in space.

beta-induced gap can extend radially outside the separatrix without resonantly exciting the SAW continuum. This implies that a localized plasma eigenmode can exist inside the magnetic-island induced gap only if its fluctuating field vanishes sufficiently fast (exponentially) at the continuum position (see FIG. 6.1). If the fluctuating field is finite at the continuum position, its radial structure is characterized by the logarithmic singularity typical of continuum resonance and absorption and could be excited only as EPM above a critical drive threshold [11]. This argument gives us precise information on the radial structure of the new MiAE with respect to gap-modes like BAE. In fact, we can state that, if a BAE can extend over a radial range not limited by the island size, on the contrary a MiAE is very localized and positioned at the center of the island.

6.4 Future work

In this dissertation, a theory for the dynamics of Alfvén modes in the presence of a magnetic island has been developed, in the framework of linear ideal MHD. The continuous spectrum has been calculated and new gaps in the continuous spectrum have been found. Moreover, the frequency of the BAE continuum accumulation point has been calculated and its dependence on the magnetic island size has been made explicit. Inside the continuum gaps, the theory of global Alfvén modes (MiAE) due to the eccentricity of the section of the magnetic island flux tube has been developed in the limiting case of small eccentricity magnetic island. Moreover, the nonlinear modification of the BAE frequency has been calculated in the framework of a perturbative theory in the magnetic island size.

One of the next steps in the theory of global modes inside a magnetic island, is the implementation of numerical simulations where a magnetic island flux tube is considered as the equilibrium. In numerical simulation, the limiting case of small eccentricity of the magnetic island flux tube can be abandoned, and furthermore, the curvature and the helicity of the magnetic island flux tube can be restored, modeling in a more realistic way typical magnetic islands present in tokamak plasmas. Therefore, we expect to be able to calculate the frequency of MiAE with numerical simulations, and to compare them with the transit frequency of energetic particles.

A tokamak equilibrium modified by the presence of quasi-static magnetic island has analogies with a stellarator equilibrium, where Alfvén modes are present like in a tokamak [50]. The magnetic island O-point

plays the role of the helical magnetic axis for stellarators and the plasma inside the separatrix topologically corresponds to the whole stellarator plasma. A simplification in our case is given by the fact that the island (plasma) cross section has fixed shape while moving along the helical symmetry direction, while this is not the case in stellarator plasmas. In fact, magnetic islands in tokamaks are radially localized and the effect of the 1/R dependence of the equilibrium B-field on its shape is negligible at the lowest order; meanwhile, there are no effects from external coils to be considered, which are dominant in the case of stellarators. With these considerations in mind, some analogies may be drawn between the problem analyzed here and those considered in stellarators (see, e.g. Ref. [50]). The more fundamental connection between SAW in nonlinear tokamak equilibria with helical structures, such as magnetic islands, and in stellarators emerges when considering resonant excitation of these fluctuations, which naturally bring in new invariants of particle motions and the corresponding intrinsic frequencies, which have obvious consequences not only on the mode drive, but on the nonlinear saturation and related transport processes as well. These problems are far beyond the scope of the present paper and will be addressed elsewhere. As stated above, this work addresses radial (in magnetic flux coordinate) singular structures of the SAW continuous spectrum with the same symmetry as the nonlinear plasma equilibrium within a finite size magnetic island.

The model of MiAE has to be reformulated in the framework of a gyrokinetic theory, if one wants to take into account wave-particle resonances and finite Larmor radius effects. In order to calculate the growth rate of MiAE inside a magnetic island in a tokamak, a further study of driving and damping mechanisms is also required, taking into account resonances with thermal and energetic particles. We expect the driving mechanism to be given mainly by energetic particles radial nonuniformities.

Experimental investigations of MiAE can also be performed. As we have discussed in last section, MiAE magnetic perturbations are very localized inside the magnetic island, and as a consequence, a MiAE cannot be easily detected by a diagnostic system which measures the fluctuating field outside the tokamak, such as Mirnov coils. However, we expect that we could observe these modes with ECE or soft X-ray diagnostics.

MiAE could nonlinearly interact with energetic particles and affect their redistribution in the proximity of the magnetic island rational surface. This process would add on the redistribution of fast ion population near a magnetic island rational surface, caused in part by the radial magnetic field due to the magnetic island itself [51]. Therefore, adding the ef-

fect of MiAE can help understanding better fast particle dynamics in the presence of a magnetic island and explaining the possible discrepancies between measured fast ion redistributions and theoretical predictions.

The analytic theory of BAE has been developed in this dissertation in the case of perturbatively small magnetic island. The next step in the modeling of BAE is the nonlinear reformulation of the BAE dispersion relation in gyrokinetic theory, developed in Ref. [23, 32] in the framework of a linear theory. A crucial role in the driving mechanism is expected to be played by the magnetic island pressure nonlinearity, as suggested by Ref. [36].

In this dissertation, the frequency of MiAE and BAE has been calculated as a function of the magnetic-island width (see Eq. 4.30 and Eq. 5.5). This suggests the possibility of using the MiAE and BAE frequency scalings as a novel magnetic-island diagnostics in a fashion similar to other commonly used Alfvén spectroscopy techniques [52, 53, 54]. Unlike in the BAE case, the radial MiAE localization at the center of the island makes them difficult to detect by external measurements, and makes the use of internal fluctuation diagnostics, such as electron cyclotron emission and soft x rays, necessary. By detecting MiAE and BAE and measuring their frequency, one has indirect information on the magnetic-island size.

Chapter 7

Appendix

7.1 Coordinate metric

7.1.1 Notation for general curvilinear coordinates

Let $\{x^1, x^2, x^3\}$ be an orthonormal set of coordinates in R^3, with basis vectors $\{\hat{\boldsymbol{e}}_1, \hat{\boldsymbol{e}}_2, \hat{\boldsymbol{e}}_3\}$. All vectors with symbol $\hat{}$ on top are meant to be of unitary length, with length measured in this original coordinate system. Now let $\{q^1, q^2, q^3\}$ be a curvilinear set of coordinates in the same space, with basis vectors $\{\boldsymbol{g}_1, \boldsymbol{g}_2, \boldsymbol{g}_3\}$, defined as $\boldsymbol{g}_i = (\partial x^j/\partial q^i)\hat{\boldsymbol{e}}_j$ (the Einstein summation convention is always adopted, when an index appears twice in a term, unless explicitly stated). The basis vectors $\boldsymbol{g}_i$ are defined aligned with coordinates, and take the name of *co-variant* basis. Similarly, we can introduce a basis of vectors perpendicular to the co-variant basis vectors, named *contra-variant* basis vectors $\boldsymbol{g}^i$, defined as $\boldsymbol{g}^i = \boldsymbol{\nabla} q^i$, where the gradient is always meant to be calculated in the original coordinate system $\{x^i\}$. The contra-variant vectors are related to the co-variant vectors by the relations $\boldsymbol{g}^i \cdot \boldsymbol{g}_j = \delta^i_j$, where the scalar products are calculated in the original coordinate system, and δ^i_j is the Kronecker delta. Any vector can be written in terms of these basis vectors as $\boldsymbol{V} = V^i \boldsymbol{g}_i = V_i \boldsymbol{g}^i$, where V_i and V^i are named respectively co-variant and contra-variant components. Any vector can also be written as $\boldsymbol{V} = V^i_{ph} \hat{\boldsymbol{g}}_i$, where we call V^i_{ph} *physical* components of the vector, $V^i_{ph} = V^i |\boldsymbol{g_i}|$, with no summation on the index i here.

The metric tensor is defined as $g_{ij} = \boldsymbol{g}_i \cdot \boldsymbol{g}_j$, and can be used to calculate the infinitesimal line element of the set $\{q^i\}$ (also called *1-form* of the set $\{q^i\}$): $ds^2 = g_{ij}\, dq^i\, dq^j$. This is a generalization of the Pythagorean theorem, and in 2-D reduces to the theorem for triangles: $ds^2 = (dq^1)^2 + (dq^2)^2 - 2\cos\alpha\, dq^1\, dq^2$, where dq^1 and dq^2 are two sides

of the triangle and $\alpha = \pi/2 - \hat{\boldsymbol{g}}_1 \cdot \hat{\boldsymbol{g}}_2$. In the same way, the matrix g^{ij} is defined as $g^{ij} = \boldsymbol{g}^i \cdot \boldsymbol{g}^j$. The matrices g^{ij} and g_{ij} are one the inverse of the other: $g^{im} g_{mj} = \delta^i_j$. They can be used to calculate the contravariant components of a vector, knowing the co-variant ones, and viceversa: $V^i = \boldsymbol{g}^i \cdot \boldsymbol{V} = \boldsymbol{g}^i \cdot V_j \boldsymbol{g}^j = g^{ij} V_j$ and $V_i = g_{ij} V^j$. The determinant of g_{ij} is named g. The differential operators are defined in the set $\{q^i\}$ as:

$$\begin{aligned}
(\boldsymbol{\nabla} f)^i &= \partial^i f = g^{ij} \partial_j f \\
\boldsymbol{\nabla} \cdot \boldsymbol{V} &= \frac{1}{\sqrt{g}} \partial_i (\sqrt{g} V^i) \\
\nabla^2 f &= \frac{1}{\sqrt{g}} \partial_i (\sqrt{g}\, g^{ij} \partial_j f) \\
\boldsymbol{\nabla} \times \boldsymbol{V} &= \frac{1}{\sqrt{g}} \epsilon^{ijk} \boldsymbol{g}_i \partial_j V_k
\end{aligned}$$

Here the partial derivatives are defined as $\partial^i = \partial/\partial q_i$ and $\partial_i = \partial/\partial q^i$, and ϵ^{ijk} is the Levi-Civita tensor.

7.1.2 Coordinates outside a magnetic island

The domains of the coordinates (ρ, u, ζ), describing the region outside the island, are $\rho_{sx} = W_{isl} < \rho < \infty$, $0 < u < 2\pi$ and $0 < \zeta < 2\pi$, where ζ is the coordinate of translational symmetry for both the equilibrium and the perturbations, and periodicity in u is assumed for the perturbations. The gradients of these coordinates are:

$$\begin{aligned}
\boldsymbol{\nabla} \rho &= L/x\, \hat{\boldsymbol{q}} - \sqrt{1-e} \sin u/(2x)\, \hat{\boldsymbol{u}} = P/x\, \hat{\boldsymbol{\rho}} \\
\boldsymbol{\nabla} u &= \hat{\boldsymbol{u}}/\rho_0 \\
\boldsymbol{\nabla} \zeta &= \hat{\boldsymbol{\zeta}}/Z_0
\end{aligned}$$

where we use the notation $\hat{\boldsymbol{V}} = \boldsymbol{V}/V$ for a unitary length vector. Here $P = \sqrt{L^2 + (1-e)(\sin^2 u)/4}$, $L = \sqrt{x^2 - (\cos u + 1)/2}$ and $x = \rho/\rho_{sx}$.

A covariant basis $(\boldsymbol{g}_\rho, \boldsymbol{g}_u, \boldsymbol{g}_\zeta)$ can also be defined as orthogonal to the contra-variant basis $(\boldsymbol{g}^\rho = \boldsymbol{\nabla}\rho, \boldsymbol{g}^u = \boldsymbol{\nabla} u, \boldsymbol{g}^\zeta = \boldsymbol{\nabla}\zeta)$, namely satisfying: $\boldsymbol{g}^i \cdot \boldsymbol{g}_j = \delta^i_j$. The Jacobian for the coordinates outside the island, defined as the determinant of the metric tensor $g_{ij} = \boldsymbol{g}_i \cdot \boldsymbol{g}_j$, is $g_{out} = \rho_0^2 Z_0^2 x^2 / L^2$. With these definitions, the laplacian of a function f for perpendicularly localized modes, can be written in the coordinates (r, u, ζ) as:

$$\nabla^2_{out} f \simeq \frac{1}{\sqrt{g_{out}}} \frac{\partial}{\partial \rho} \Big(\sqrt{g_{out}}\, g^{\rho\rho} \frac{\partial f}{\partial \rho} \Big) \simeq \frac{1}{\rho^2_{sx}} \frac{P^2}{x^2} \frac{\partial^2 f}{\partial x^2} \tag{7.1}$$

where we have used $g^{\rho\rho} = \boldsymbol{g}^\rho \cdot \boldsymbol{g}^\rho = P^2/x^2$.

7.1.3 Coordinates inside a magnetic island

Here, we calculate the differential operators in the set of coordinates inside the magnetic island (ρ, θ, ζ). The domains of these coordinates are $0 < \rho < \rho_{sx} = W_{isl}$, $0 < \theta < 2\pi$ and $0 < \zeta < 2\pi$, where ζ is the coordinate of translational symmetry, and periodicity in θ and ζ is assumed for the perturbations. The gradients of these coordinates are:

$$\begin{aligned}
\boldsymbol{\nabla}\rho &= \sin\theta\,\hat{\boldsymbol{q}} - \cos\theta\sqrt{1-e}F\,\hat{\boldsymbol{u}} = \sqrt{a}\,\hat{\boldsymbol{\rho}} \\
\boldsymbol{\nabla}\theta &= (\cos\theta\,\hat{\boldsymbol{q}} + \sin\theta\sqrt{1-e}F\,\hat{\boldsymbol{u}})/\rho = \sqrt{b}\,\hat{\boldsymbol{\theta}}/\rho \\
\boldsymbol{\nabla}\zeta &= \hat{\boldsymbol{\zeta}}/Z_0
\end{aligned}$$

Moreover we have the relation $\boldsymbol{\nabla}\rho\cdot\boldsymbol{\nabla}\theta = c/\rho$. Here $F = \sqrt{1-(\rho\cos\theta/\rho_{sx})^2}$, and:

$$\begin{aligned}
a &= \sin^2\theta + \cos^2\theta(1-e)F^2 \\
b &= \cos^2\theta + \sin^2\theta(1-e)F^2 \\
c &= \cos\theta\sin\theta\,(1-(1-e)F^2)
\end{aligned}$$

The length of the co-variant basis vectors is $g_\rho = \sqrt{b/(1-e)}/F$, $g_\theta = \rho\sqrt{a/(1-e)}/F$, and $g_\zeta = Z_0$.

Now we calculate the differential operators, which are needed to solve explicitly the equation for the shear Alfvén wave dynamics in this set of coordinate. The metric tensor g^{ij} is given by:

$$g^{ij} = \begin{pmatrix} a & c/\rho & 0 \\ c/\rho & b/\rho^2 & 0 \\ 0 & 0 & 1/Z_0^2 \end{pmatrix}$$

and the Jacobian for the coordinates inside the island, is $g_{in} = \rho_{sx}^2 Z_0^2 x^2/(F^2(1-e))$. With the explicit value of g^{ij} and g, we can calculate the differential operators:

$$\boldsymbol{\nabla} f = \sqrt{a}\frac{\partial f}{\partial\rho}\hat{\boldsymbol{\rho}} + \frac{\sqrt{b}}{\rho}\frac{\partial f}{\partial\theta}\hat{\boldsymbol{\theta}} + \frac{1}{Z_0}\frac{\partial f}{\partial\zeta}\hat{\boldsymbol{\zeta}} \tag{7.2}$$

$$\boldsymbol{\nabla}\cdot\boldsymbol{V} = \frac{1}{Z_0}\frac{\partial V_{ph}^{\zeta}}{\partial\zeta} + \frac{\sqrt{1-e}\,F}{r}\Big(\frac{\partial}{\partial\rho}\Big(\frac{\rho V_{ph}^{\rho}}{\sqrt{b}}\Big) + \frac{\partial}{\partial\theta}\Big(\frac{V_{ph}^{\theta}}{\sqrt{a}}\Big)\Big) \tag{7.3}$$

$$\begin{aligned}
\nabla^2 f = {} & \frac{F}{\rho}\frac{\partial}{\partial\rho}\Big(\frac{\rho}{F}\Big(a\frac{\partial f}{\partial r} + \frac{c}{\rho}\frac{\partial f}{\partial\theta}\Big)\Big) + \\
& + \frac{F}{\rho}\frac{\partial}{\partial\theta}\Big(\frac{1}{F}\Big(c\frac{\partial f}{\partial\rho} + \frac{b}{\rho}\frac{\partial f}{\partial\theta}\Big)\Big) + \frac{1}{Z_0^2}\frac{\partial f}{\partial\zeta^2}
\end{aligned} \tag{7.4}$$

$$(\boldsymbol{\nabla}\times\boldsymbol{V})_\rho = \frac{\sqrt{b}}{\rho}\frac{\partial V^z_{ph}}{\partial\theta} + \frac{1}{F\sqrt{1-e}}\Big(\frac{c}{Z_0}\frac{\partial V^\rho_{ph}}{\partial\zeta} - \frac{\sqrt{a}\sqrt{b}}{Z_0}\frac{\partial V^\theta_{ph}}{\partial\zeta}\Big) \quad (7.5)$$

$$(\boldsymbol{\nabla}\times\boldsymbol{V})_\theta = -\sqrt{a}\frac{\partial V^z_{ph}}{\partial\rho} + \frac{1}{F\sqrt{1-e}}\Big(\frac{\sqrt{a}\sqrt{b}}{Z_0}\frac{\partial V^\rho_{ph}}{\partial\zeta} - \frac{c}{Z_0}\frac{\partial V^\theta_{ph}}{\partial\zeta}\Big) \quad (7.6)$$

$$(\boldsymbol{\nabla}\times\boldsymbol{V})_\zeta = \frac{F}{\rho}\Big(\frac{\partial}{\partial\rho}\Big(-\frac{\rho c V^\rho_{ph}}{F\sqrt{b}} + \frac{\rho\sqrt{a}V^\theta_{ph}}{F}\Big) + \frac{\partial}{\partial\theta}\Big(\frac{\sqrt{b}V^\rho_{ph}}{F} + \frac{cV^\theta_{ph}}{F\sqrt{a}}\Big)\Big) \quad (7.7)$$

It is straightforward to see that, in the case $e \simeq 0$ and in proximity of the O-point ($F = a = b = 1$, $c = 0$), these differential operators reduce to the known differential operators in cylinder geometry.

Using these definitions, and the fact that $g^{\rho\rho} = \boldsymbol{g}^\rho \cdot \boldsymbol{g}^\rho = a$, we can write the laplacian for perpendicularly localized modes in the coordinates (ρ, θ, ζ) in the approximate form:

$$\nabla^2_{in} f \simeq \frac{a}{\rho^2_{sx}}\frac{\partial^2 f}{\partial x^2} \quad (7.8)$$

7.2 Notation for the linear BAE dispersion relation

In this appendix, we define the functions used in section 5.2, for the linear theory of BAE [23, 44].

$$\begin{aligned} F_{BAE}(x) &= x(x^2+3/2)+(x^4+x^2+1/2)Z(x) && (7.9)\\ G_{BAE}(x) &= x(x^4+x^2+2)+(x^6+x^4/2+x^2+3/4)Z(x) && (7.10)\\ N_{BAE}(x) &= \Big(1-\frac{\omega_{*ni}}{\omega}\Big)[x+(1/2+x^2)Z(x)] \\ &\quad -\frac{\omega_{*Ti}}{\omega}[x(1/2+x^2)+(1/4+x^4)Z(x)] && (7.11)\\ D_{BAE}(x) &= \Big(\frac{1}{x}\Big)\Big(1+\frac{1}{\tau}\Big)+\Big(1-\frac{\omega_{*ni}}{\omega}\Big)Z(x) \\ &\quad -\frac{\omega_{*Ti}}{\omega}[x+(x^2-1/2)Z(x)] && (7.12)\end{aligned}$$

where $\tau = T_e/T_i$ and $Z(x)$ is the plasma dispersion function:

$$Z(x) = \pi^{-1/2}\int_{-\infty}^{+\infty}\frac{e^{-y^2}}{(y-x)}dy \qquad (7.13)$$

The function S_{BAE} is defined by:

$$\begin{aligned} &S_{BAE}(\omega) = \\ &= \frac{q^2}{2}\Big(\frac{\omega_{ti}}{\omega}\Big)^2\Big[\Big(1-\frac{\omega_{*ni}}{\omega}\Big)\Big(L-2L_{1/2}-\frac{2N}{D}(H-2H_{1/2})+\frac{N^2}{D^2}(F-2F_{1/2})\Big) \\ &\qquad -\frac{\omega_{*Ti}}{\omega}\Big(M-2M_{1/2}-\frac{2N}{D}(I-2I_{1/2})+\frac{N^2}{D^2}(G-2G_{1/2})\Big)\Big] \\ &+\frac{q^2}{D_{1/2}}\Big(\frac{\omega_{ti}}{\omega}\Big)^2\Big[\Big(1-\frac{\omega_{*ni}}{\omega}\Big)(F_{1/2}-F)-\frac{\omega_{*Ti}}{\omega}(G_{1/2}-G)-\frac{N}{D}(N_{1/2}-N)\Big]^2 \\ &+\Big(1-\frac{\omega_{*ni}}{\omega}\Big)\Big(T-\frac{2N}{D}V+\frac{N^2}{D^2}Z\Big)-\frac{\omega_{*Ti}}{\omega}\Big(U-\frac{2N}{D}W+\frac{N^2}{D^2}(V-Z/2)\Big) \end{aligned} \qquad (7.14)$$

where, in this appendix, the functions L, H, M, I, T, V, U, W are defined as:

$$\begin{aligned} L(x) &= x^7+(5/2)x^5+(19/4)x^3+(63/8)x \\ &\quad +(x^8+2x^6+3x^4+3x^2+3/2)Z(x), && (7.15)\\ H(x) &= x^5+2x^3+3x+(x^6+(3/2)x^4+(3/2)x^2+3/4)Z(x), && (7.16)\end{aligned}$$

$$
\begin{aligned}
M(x) &= x^9 + 2x^7 + (11/2)x^5 + (25/2)x^3 + (201/8)x \\
&\quad +(x^{10} + (3/2)x^8 + 4x^6 + (15/2)x^4 + 9x^2 + 21/4)Z(x), \qquad (7.17)\\
I(x) &= x^7 + (3/2)x^5 + (7/2)x^3 + (27/4)x \\
&\quad +(x^8 + x^6 + (9/4)x^4 + 3x^2 + 15/8)Z(x) \qquad (7.18)\\
T(x) &= x^3 + (5/2)x + (x^4 + 2x^2 + (3/2))Z(x) \qquad (7.19)\\
V(x) &= x + (x^2 + 1)Z(x) \qquad (7.20)\\
U(x) &= x^5 + 3x^3 + (13/2)x \\
&\quad +(x^6 + (5/2)x^4 + (9/2)x^2 + (15/4))Z(x) \qquad (7.21)\\
W(x) &= x^3 + 2x + (x^4 + (3/2)x^2 + 3/2)Z(x). \qquad (7.22)
\end{aligned}
$$

Bibliography

[1] ITER Physics Basis Editors, ITER Physics Expert Group Chairs and Co-Chairs and ITER Joint Central Team and Physics Integration Unit (1999) *Nucl. Fusion* **39** 2137–74
Aymar R., Chuyanov V., Huguet M., Shimomura Y. (ITER Joint Central Team and Home Teams) 2001 ITER-FEAT-The future international burning plasma experiment overview (C&S Papers Series 8/C) IAEA CD-ROM file OV/1 presented at the 18th IAEA FEC (Sorrento, Italy, 410 October 2000) and http://www.iaea.org/programmes/ripc/physics/fec2000/html/node1.htm

[2] Zonca F *et al.* 2006 *Pl. Phys. Contr. Fusion* **48** B15

[3] Chen L and Zonca F 2007 *Nucl. Fusion* **47** S727-S734

[4] Hasegawa A and Chen L 1974 *Phys. Rev. Lett.* **32** 454

[5] Chen L and Hasegawa A 1974 *Phys. Fluids* **17** 1399

[6] Hain K and Lüst R 1958, Z. Naturforsch. **13a** 956

[7] Hasegawa A and Chen L 1976 *Phys. Fluids* **19**, 12, 1924–1934

[8] Grad H 1969 *Phys. Today* **22** December, 34

[9] Kieras C E and Tataronis J A 1982 *J. Plasma Physics* **28** 395

[10] Cheng C Z *et al.* 1985 *Ann Phys* **161** 21

[11] Chen L 1994 *Phys. Plasmas* **1** 1519

[12] R. Betti and J. P. Freidberg, *Phys. Fluids B* **3**, 1865 (1991).

[13] R. Betti and J. P. Freidberg, *Phys. Fluids B* **4**, 1465 (1992).

[14] Chu M S *et al.* 1992 *Phys. Fluids B* **4** 3713

[15] W.W. Heidbrink, Phys. Plasmas 9, 2113, (2002)

[16] R.R. Mett and S.M. Mahajan, *Phys. Fluids B* **4**, 2885 (1992)

[17] Walén C. 1944 Ark. Mat. Astron. Fys., 30A(15):1

[18] Alfvén H 1950 "Cosmical Electrodynamics", Clarendon Press, Oxford.

[19] Elsasser W M 1956 *Rev Mod Phys* **28** 135

[20] Hasegawa A and Sato T 1989 "Space Plasma Physics (Stationary Processes)" Vol. 1 (New York; Springer)

[21] Furth H P *et al.* 1963 *Phys. Fluids* **6** 459

[22] Turnbull A D *et al.* 1993 *Phys. Fluids B* **5** 2546

[23] Zonca F *et al.* 1996 *Pl. Phys. Contr. Fusion* **38** 2011

[24] Biancalani A, Chen L, Pegoraro F and Zonca F 2010, "2D continuous spectrum of shear Alfvén waves in the presence of a magnetic island", submitted to *Plasma Phys. Control. Fusion.*

[25] Biancalani A, Chen L, Pegoraro F and Zonca F 2010 *Phys. Rev. Lett.* **105** 095002

[26] Biancalani A, Chen L, Pegoraro F and Zonca F 2010, "Shear Alfvén wave continuous spectrum within magnetic islands", submitted to *Phys. of Plasmas.*

[27] Swartz K and Hazeltine R D 1984 *Phys. Fluids* **27** 2043

[28] Buratti P *et al.* 2005 *Nuclear Fusion* **45** 1446

[29] Sharapov S E *et al.* 2001 *Phys. Lett.* **A 289** 127

[30] Takechi M *et al.* 2002 *Proc. 19th Int. Conf. on Fusion Energy* (Lyon, 2002) (Vienna: IAEA 2002) CD-ROM file EX/W-6

[31] Botrugno, A. *et al.*, 2010, *37th EPS Conference, Dublin, Ireland* Poster P4.110, http://www.eps2010.com

[32] Annibaldi S V *et al.* 2007 *Pl. Phys. Contr. Fusion* **49** 475

[33] Wei C *et al.* 2010 *Journal of the Phys. Soc. Japan* **79** 044501

[34] Rutherford P H 1973 *Phys. Fluids* **16** 1903–1908

[35] Freidberg J P, 1987 "Ideal Magnetohydrodynamics", Springer.

[36] Marchenko, V.S. and Reznik, S.N. (2009) *Nucl. Fusion* **49** 022002

[37] Cheng, and Chance 1986, *Phys. Fluids* **29** 11, 3695

[38] Betti, R. PhD Thesis, Massachusetts Institute of Technology (1992)

[39] Rosenbluth, M.N. and Rutherford, P.H., 1975 *Phys. Rev. Lett.* **34** 1428

[40] Chavdarovski, I., and Zonca, F., 2009, *Pl. Phys. Contr. Fusion*, **51** 115001

[41] F.Zonca and L.Chen, 2008, EPL **83** 35001

[42] Fried, B.D. and Conte S.D., "The Plasma Dispersion Function" (Academic Press, New York NY, 1961.)

[43] Vlad, G., *et al.* 1999, "Dynamics of Alfvén waves in tokamaks", *La Rivista del nuovo Cimento* **22**.

[44] Zonca F *et al.* 1998 *Pl. Phys. Contr. Fusion* **40** 2009

[45] Pegoraro, F. and Schep, T.J., 1986, *Plasma Phys. Control. Fusion* **28** 647

[46] M. Abramowitz, I.A. Stegun, Handbook of Mathem. Funct., page 17.

[47] A. Biancalani, L. Chen, F. Pegoraro, F. Zonca, S.V. Annibaldi, A.Botrugno, P. Buratti and P. Smeulders, 2008, *22nd IAEA Fusion Energy Conference, 13-18 October, Geneva* Poster Th/P3-5, http://www-pub.iaea.org/MTCD/Meetings/fec2008pp.asp

[48] Cenacchi, G., Taroni, A., "JETTO: a free boundary plasma transport code", (1988) ENEA Report RT/TIB/88/5.

[49] Zonca F, Chen L, Dong J Q and Santoro R A 1999 *Phys. Plasmas* **6** 1917

[50] Watari T *et al.* 2006 *Phys. Plasmas* **13** 062504

[51] Brüdgam M 2010 "Nonlinear Effects of Energetic Particle Driven Instabilities in Tokamaks", PhD thesis, TU München, Germany

[52] S. D. Pinches *et al.*, Plasma Phys. Contr. Fusion **46**, B187 (2004).

[53] Breizman B N *et al.* 2005 *Phys. Plasmas* **12** 112506

[54] F. Zonca *et al.*, Nucl. Fusion **49**, 085009 (2009).